Novel lipoparticles for the synergistic chemo-photodynamic therapy of the cancer cells

Dissertation

zur

Erlangung des Doktorgrades

der Naturwissenschaften

(Dr. rer. nat.)

dem

Fachbereich Pharmazie der

Philipps-Universität Marburg

vorgelegt von

Sajid Ali

aus **Lahore, Pakistan**

Marburg/Lahn **2019**

Erstgutachter:	**Prof. Dr. Udo Bakowsky**
Zweitgutachter:	**Prof. Dr. Frank Runkel**
Eingereicht am:	**07.01.2020**
Tag der mündlichen Prüfung am:	**25.02.2020**
Hochschulkennziffer:	**1180**

EIDESSTATTLICHE ERKLÄRUNG

Ich versichere, dass ich meine Dissertation

“Novel lipoparticles for the synergistic chemo-photodynamic therapy of the cancer cells”

selbständig ohne unerlaubte Hilfe angefertigt und mich dabei keiner anderen als der von mir ausdrücklich bezeichneten Quellen bedient habe. Alle vollständig oder sinngemäß übernommenen Zitate sind als solche gekennzeichnet.

Die Dissertation wurde in der jetzigen oder einer ähnlichen form noch bei keiner anderen Hochschule eingereicht und hat noch keinen sonstigen Prüfungszwecken gedient.

Marburg, den .....

.....

(Sajid Ali)

Acknowledgments

First and foremost, I would like to express my deepest and earnest gratitude towards my advisor Prof. Dr. Udo Bakowsky for providing me the prospects to carry out this project under his kind supervision with his immense knowledge, ideas, and patience, throughout my candidature. Besides the invaluable guidance in the studies, he had been a mentor for me to maturate my vision and blossom the personality. His continuous endeavors helped me transform this goal into actualization. I'm obliged to have his immense assistance for taking me to the right path as a torchbearer.

Besides my advisor, I feel highly privileged in thanking my group leader and co-supervisors Dr. Jens Schäfer and Dr. Jarmila Jedelská for their insightful and emanate discussions throughout my research work. I am sincerely grateful to them for sharing their truthful and illuminating views on a number of issues related to the project. Their aspiring guidance, continuous encouragement, and invaluably constructive criticism made it possible for me to carry out my course of work.

I am highly indebted to Dr. Shashank Reddy Pinnapireddy and Dr. Jana Brüßler for their tremendous support, precious advice and willingness to help during my lab work. My sincere thank goes also to Mrs. Eva Maria Mohr for her support and expertise during the cell culture experiments. I am very much grateful to Dr. Farhan Sohail for his help during the in vivo studies. I greatly appreciate the assistance extended by my fellow lab mates especially Muhammad Umair Amin, Imran Tariq, Muhammad Yasir Ali, Ghazala Ambreen and Uzma Ali for their utmost help and massive support during the whole course of my doctoral studies.

My Sincere thank goes to my colleagues at the research group A.G. Bakowsky especially Dr. Gihan Mahmoud, Dr. Konrad Engelhardt, Dr. Lili Duse and Nathalie Goergen for helping me out in my research. A very special thanks to Julia Michaelis for her patience and guidance in every official and administrative work. My sincere thanks to Dr. Christian Wölk and Dr. Gerd Hause (Martin Luther University Halle-Wittenberg) for helping me out in TEM studies.

I offer my regards to Deutscher Akademischer Austauschdienst (DAAD) and the Higher Education Commission of Pakistan (HEC) for providing me the scholarship and make it possible for me to get higher education.

Last but not the least, the exceptional gratitude to my family: my parents and to my brothers and sisters for supporting me spiritually throughout doctoral work and my life in general, whose inspiration and vision brought me where I am today.

Die vorliegende Arbeit entstand auf Anregung und unter Leitung von

Herrn Prof. Dr. Udo Bakowsky

am Institut für Pharmazeutische Technologie und Biopharmazie
der Philipps-Universität Marburg

TABLE OF CONTENTS

LIST OF FIGURES

LIST OF TABLES

LIST OF ABBREVIATRIONS

aPTT	Activated partial thromboplastin time
AFM	Atomic force microscopy
ALP	Alkaline phosphatase
ALT	Alanine aminotransferase
AST	Aspartate aminotransferase
ATCC	American type culture collection
Ca2+	Calcium
CAM	Chorioallantoic membrane model
CFU	Colony forming units
CH	Cholesterol
$CHCl_3$	Chloroform
CLSM	Confocal laser scanning microscopy
DCF	Dichlorofluorescein
DLS	Dynamic light scattering
DMEM	Dulbecco's modified Eagle's minimum essential medium
DMSO	Dimethyl sulfoxide
DOPE	1,2-dioleoyl-sn-glycero-3-phosphoethanolamine
DOTAP	1,2-dioleoyloxy-3-trimethylammonium propane
DPBS	Dulbecco's phosphate-buffered saline
DPPC	1,2-dipalmitoyl-sn-glycero-3-phosphocholine
DPPE-$MPEG_{5000}$	N-(methoxypolyethylene glycol 5000 carbamoyl)-1,2-dipalmitoyl-sn-glycero-3-phosphatidylethanolamine
DPPG	1,2-dipalmitoyl-sn-glycero-3-phosphoglycerol
EBSS	Earl's balanced salt solution
EDD	Egg development day
EDTA	Ethylenediaminetetraacetic acid
EE	Encapsulation efficiency
EPR	Enhance permeability and retention
EtOH	Ethanol
FBS	Fetal bovine serum
FDA	Food and drug administration
H & E	Hematoxylin and Eosin

H2DCFDA	2,7-dichlorofluorescin diacetate
Hb	Hemoglobin
HCT	Hematocrit
HeNe	Helium Neon
IC_{50}	Half maximal inhibitory concentration
IMDM	Iscove's modified Dulbecco's medium
LCNPs	Lipid coated nanoparticles
LDA	Laser doppler anemometry
LED	Light-emitting diode
LFTs	Liver function tests
LMA	Low melting agarose
MCH	Mean corpuscular Hemoglobin
MCHC	Mean corpuscular hemoglobin concentration
MCV	Mean corpuscular volume
MDR	Multidrug resistance
MeOH	Methanol
MHB	Mueller Hinton broth
Mg2+	Magnesium
MLVs	Multilamellar vesicles
MPV	Mean platelet volume
MTT	3-(4,5-dimethylthiazolyl-2)-2,5-diphenyltetrazolium Bromide
NEA	Non-essential amino acids
NMA	Normal melting agarose
OD	Optical density
PBS	Phosphate buffer saline
PDI	Polydispersity index
PDT	Photodynamic therapy
PLGA	Poly (lactic-co-glycolic acid)
PLT	Platelets
PVA	Poly(vinyl alcohol)
PS	Photosensitizer
RBCs	Red blood cells
RFTs	Renal functions tests
RH	Relative humidity

RFU	Relative fluorescence units
ROS	Reactive oxygen species
S.D	Standard deviation
SK-OV-3	Human ovarian adenocarcinoma cell line
SUVs	Small unilamellar vesicles
TBHP	Tert-butyl hydroperoxide
TEL	Tetraether lipid
TEM	Transmission electron microscopy
T_g	Glass transition temperature
WBCs	White blood cells

Chapter I: Introduction

1.1 Introduction

1.1.1 Background

Nanomedicine can be defined as the molecular scale interventions for the diagnosis, prevention, and treatment of the disease using novel carrier systems that can deliver the drugs to the disease site. The nanomedicine is currently a rapidly growing filed as much of the interest has been taken in the use of nanomedicine for the diagnosis and treatment of cancer [1]. According to the World Health Organization (WHO), cancer is the second leading cause of deaths worldwide and is responsible for an estimated 9.6 million deaths in 2018. Globally about 1 out of 6 deaths are caused by cancer. The successful treatment of cancer depends on the several capabilities that can be uniquely addressed via nanomedicine. These capabilities include the smaller size, ability to load multiple therapeutic moieties, increased bioavailability, larger surface area, increased circulation time, passive targeting of the disease site using enhanced permeability and retention effect (EPR), the active targeting by conjugating different targeting ligands on their surface as well as the safety. The ability of the nanocarriers to cofunctionalize with drug payloads and targeting moieties enables the synthesis of multimodal systems that may provide patients with improved treatment efficacy [1, 2].

1.2 Photodynamic therapy (PDT)

PDT has been developed over the past decades into a useful treatment for several types of solid cancers in man. It is a very simple and minimally-invasive therapeutic approach that is being widely used for the treatment of cancer. The principal of PDT is based on the combination of a light-sensitive molecule (photosensitizer), oxygen and light. After being administered, the photosensitizer compound can be preferentially localized into the tumor tissue. The tumor area is then illuminated by a light of specific wavelength to activate the drug molecule (photosensitization). This photochemical process results in the subsequent generation of the reactive oxygen species causing cell death [3]. The phototherapy has been known to the Chinese, Indians, and Egyptians for over 3000 years. Niels Rydberg was the first well known modern scientist in the field of phototherapy who performed phototherapy on about 800 patients. He was awarded a Nobel prize in 1903 for his work on the use of light in the treatment of skin tuberculosis [4]. The history of photodynamic therapy dates back to 1888, when Marccaci, in a brief finding concerned with the toxic effects of plant alkaloids, reported that quinine and cinchonamine were found to be more toxic to the enzymes, plants and frog eggs in the presence of the light as compared to the dark. Although he did not provide any experimental data, it was thought that

apparently, he did not recognize the essential nature and the importance of this observation. The photosensitizing effects on the biological systems were recognized two decades later [5]. The term "photodynamic" was first coined by Professor Hermann von Tappeiner und Jesionek in 1904 in Munich. One of the Von Tappeiner's Ph.D. student Oscar Raab found that apparent toxicity of acridine to the paramecium (protozoan) varied depending on the intensity of the sunlight. He also found that the low concentrations of acridine and other fluorescent compounds including quinine, eosin as well as methyl phosphine in the presence of light, sensitized the rapid killing of the paramecium. In his experiments, he demonstrated that these substances had no effect in the dark and also the light alone had no effect. Raab's observations were backed by the C. Ledoux-Lebards (1902) findings. His observations manifested that eosin killed paramecia more effectively in open flasks as compared to the closed bottles. On the basis of these observations, he postulated that the presence of oxygen was necessary for the photoinactivation of paramecia. These investigations triggered the discovery of many photosensitizing compounds such as tetrapyrroles including hematoporphyrin and chlorophyll, xanthenes, thiazines, and anthracenes, etc. All of these discovered compounds were fluorescent and needed the presence of oxygen for their action. It was also investigated that a variety of biological organisms or systems such as enzymes, toxins, proteins, viruses, protozoa, bacteria, fungi and cells of higher animals can be destroyed by sensitization using light [5, 6].

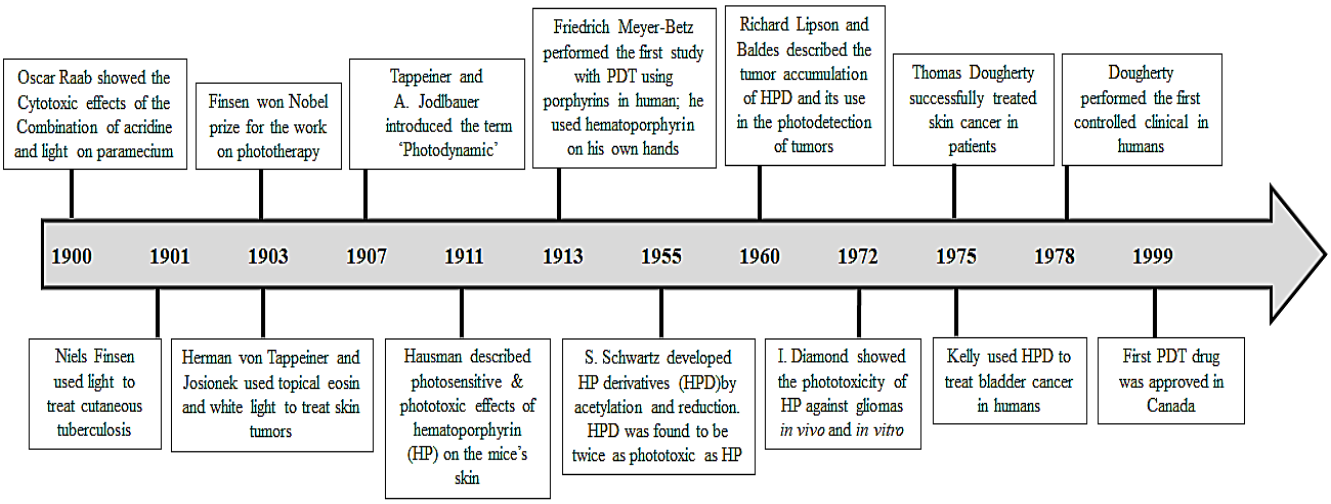

Figure 1. Historical developments of photodynamic therapy (1900-present) [7].

1.2.1 Mechanism of photodynamic therapy:

The photodynamic therapy typically consists of two processes including light absorption and the energy transfer. Generally, the photosensitizer (PS) in the ground state contains two electrons

having an opposite spin in the low energy molecular orbital. This ground state is termed as a singlet state. When irradiated by the light of a specific wavelength, one of the electrons after absorption of the light in the form of photons, is excited into a higher energy orbital. The electron keeps its spin in this high energy orbital and is termed as an excited singlet state. This is a very short-lived state (usually nanoseconds) during which the excited electron (species) can lose its energy by internal conversion into heat or by emitting light in the form of fluorescence. The excited singlet state may also undergo intersystem crossing resulting in the inversion of the electron spin. This state is relatively long-lived (microseconds) and is termed as an excited triplet state in which both the electron spin in a parallel confirmation. This PS excited triplet state may then undergo two kinds of reactions.

Type I reaction involves the direct reaction of the PS with substrates such as cell membrane or any molecule within the cell thereby transferring a proton or an electron to form an anion or cation radical respectively. These radicals then further react with the tissue oxygen to produce reactive oxygen species (ROS).

Type II reactions involve the transfer of energy from excited triplet PS state directly to the molecular oxygen causing the formation of excited singlet oxygen state [8].

Type I reactions mostly involve the transfer of the electron from the excited triplet PS to molecular oxygen (monovalent reduction) resulting in the initial production of superoxide anion. These superoxides do not cause so much oxidative damage to the cells as they are not reactive to the biological systems. These superoxides may act one of either ways or all of them simultaneously:

A) These superoxides may react themselves in the presence of superoxide dismutase (SOD) to form hydrogen peroxide (H_2O_2) and oxygen. This hydrogen peroxide is necessary for the functioning of the cellular enzymes. This hydrogen peroxide (H_2O_2) can readily cross the cell membranes and cannot then escape the cell. Inside the cell, it acts as reducing agents for the production of hydroxyl radical ($OH^{\cdot}$**)**. This process is called a Fenton reaction and is explained below.

B) The superoxide also causes the reduction of metal ions (e.g. ferric ion Fe^{3+}) by donating one electron. These reduced metal ions then act as a catalyst for the conversion of intracellular H_2O_2 into the hydroxyl radical ($OH^{\cdot}$) by causing the breakage of the oxygen-oxygen bond of hydrogen peroxide (H_2O_2) thus producing a hydroxyl radical ($OH^{\cdot}$) and hydroxide ion (OH).

C) The superoxide may also simultaneously react with hydroxyl radical ($OH^{\cdot}$) to form singlet oxygen.

D) Alternatively, the superoxide may also react with nitric oxide radical (NO^{-}) to produce peroxynitrite ($OONO^{-}$), a highly reactive oxidizing molecule [9].

Due to very short half-life and high reactivity of the singlet oxygen and free radicals produced during ROS production, the cell structures and the molecules in their close proximity are directly affected and subsequently destroyed by PDT. Both of these reactions can occur simultaneously. The ration between the processes is mainly dependent on the type of PS used, the amount of tissue oxygen and the concentration of the substrate involves.

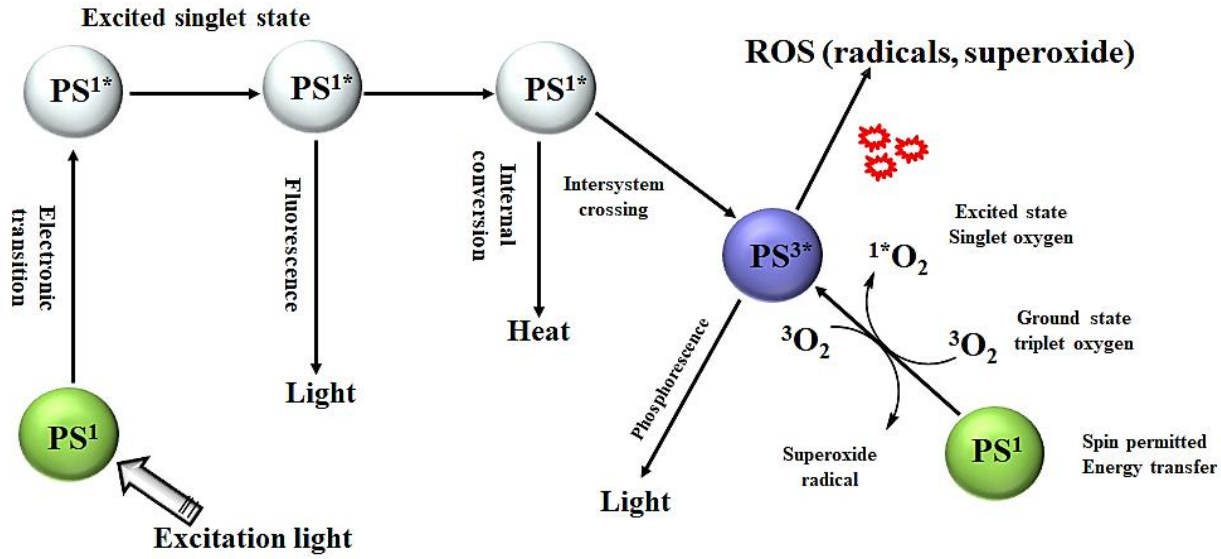

Figure 2. Schematic representation of photochemical and photophysical mechanisms of PDT [8].

1.2.2 Characteristics of ideal photosensitizer

The characteristics of an ideal photosensitizer have been discussed by various authors in the literature. Briefly,

1. They should have a low level of dark toxicity to both human and experimental animals and should have a low incidence of administrative toxicity.
2. They should absorb light in the red or infrared wavelengths in order to penetrate the tissue as the absorption bands at shorter wavelengths have less tissue penetration and are more likely to lead to skin photosensitivity (the power in the sunlight drops off at $\lambda > 600$nm) while the absorption bands at wavelength (> 800nm) means that the photons will not have sufficient energy for the PS triplet state to transfer energy to the ground state oxygen molecule to excite it to the singlet state.
3. They should have relatively high absorption bands (> 20,000-30,000 $M^{-1}cm^{-1}$) to minimize the dose of photosensitizer needed to achieve the desired effect.
4. They should have high selectivity for the tumor tissue as compared to the healthy tissue.

5. The synthesis of the PS should be relatively easy and the starting materials readily available to make large scale production feasible.
6. The photosensitizer should be a pure compound with constant composition and stable shelf life and be ideally water-soluble or soluble in the harmless aqueous solvent mixture. It should not aggregate in the biological environment as this reduces its photochemical efficiency.
7. The pharmacokinetic elimination from the patient should be rapid. i.e. less than one day to avoid the necessity for post-treatment protection from light exposure and prolonged skin sensitivity.
8. A short interval between injection and illumination is desirable to facilitate outpatient treatment that is both patient-friendly and cost-effective [10, 11].

1.2.3 Photodynamic therapy to the tumor cells:

The effects of the reactive oxygen species produced in the tissues depend on the type and concentration of the photosensitizer used, the conditions of irradiation, concentration of the oxygen in the tissue as well as the type of cancer cell. Since the half-life of the highly reactive singlet oxygen in biological systems is less than 40 ns and thus has a radius of action of only about 20 nm, the location of the PS within the cell determines which cell compartment is primarily damaged. This has a significant impact on the efficiency of PDT and the nature of cell death. Damage to structures such as mitochondria, lysosomes, endoplasmic reticulum (ER), plasma membrane or nucleus can lead to apoptosis, necrosis or autophagocytosis via various signal transduction pathways. Before the PS can be taken up by the tumor cells after intravenous administration, it first has to be distributed in the intravascular space and through the vessel walls into the tumor interstitium. Depending on the "drug-light interval" (distance between the application of the PS and the radiation), the PS is still in the vessels or it has already migrated into the interstitial space. Depending on the time of irradiation, in addition to the cells, the tumor vessels may also be the target structure of PDT. This leads to the destruction of endothelial cells of the vessel wall as well as to rheological changes such as increasing the viscosity resistance or the intravascular pressure. The consequences are thrombosis by activation of platelet aggregation, increased permeability of the vessels, bleeding, vessel constriction or blood stasis. The lack of oxygen and nutrients can, therefore, lead to necrosis of the tumor tissue. Furthermore, PDT is the trigger for a local inflammatory response that results in an antitumoral immune response. PDT leads to the direct release of inflammatory mediators and cytokines, including interleukins (IL) such as IL-1β, IL-2, IL-6, IL-10 and tumor necrosis factor α (TNF-α). This is followed by the immigration of immune cells such as neutrophils, mast cells, and macrophages. In addition, tumor

antigens and so-called "damage-associated molecular patterns" (DAMPs) are released. These act as immune stimulators as soon as they are expressed or released on the surface of damaged cells, and activate both the innate and adaptive immune systems. The antigen-presenting dendritic cells (DC) are activated and migrate to the local lymph nodes. There they lead to the activation of T helper cells and cytotoxic T cells. As a result, the immune response not only reaches the irradiated lesion but also tumor metastases. These three mechanisms of action of PDT, the direct cytotoxicity, the thromboembolic effect, and the immune response are mutually dependent.

1.3 Nanocarriers for cancer therapy

The nanocarriers are the nanosized materials usually with a diameter ranging from 1-1000nm that can carry multiple drugs or/and imaging agents. Due to their high surface area to volume ratio, it is possible to achieve high ligand density on the surface for targeting purposes. Nanocarriers can also be used to increase the local drug concentration by carrying the drug within and controlling its release when attached to the targets. Currently, natural and synthetic polymers, as well as lipids, are typically used materials for the construction of drug delivery vehicles. Generally speaking, the family of the nanocarriers includes lipid-based nanocarriers such as micelles and liposomes, carbon nanotubes, polymeric nanoparticles, polymer conjugates as well as the gold nanoparticles including nanoshells and nanocages. These nanocarriers have been explored for a number of therapeutic applications such as imaging, drug delivery, photothermal ablation of tumors, detection of apoptosis and radiation sensitizers [12].

1.3.1 Polymeric nanoparticles

Polymers are the most widely explored materials for the preparation of nanoparticles-based drug delivery systems. Nanoparticles have become an important area of research in the pharmaceutical sciences as they are able to deliver a variety of drugs for sustained periods of time. The history of the nanoparticle dates back to 1979 when Couvreur and his co-researchers prepared the polyalkylcyanoacrylate nanoparticles and discussed the adsorption/attachment of the antineoplastic drugs (i.e. methotrexate and dactinomycin) on the nanoparticles. They also described the release kinetics of the drug from the nanoparticles and elaborated their distribution and efficacy in the tumor model. These studies served as the basis for further development of the nanoparticles-based delivery of the drugs. This was followed by the preparation and initial clinical testing of Doxorubicin loaded nanoparticles [12]. Different natural polymers such as proteins and polysaccharides (e.g. collagen, chitosan) and synthetic polymer are used for the preparation of the nanoparticles. Most widely used synthetic polymers include poly (glycolic acid)

(PGA), poly (lactic acid) (PLA) and their copolymers i.e. poly(lactide-co-glycolide) (PLGA). Nanoparticles prepared from these polymers are well known for their subcellular size, biocompatibility with the tissue and cells, and biodegradability through the natural body pathways. Apart from this, these nanoparticles are stable in the blood, non-toxic, non-inflammatory, non-thrombogenic, non-immunogenic and applicable to various molecules such as drugs, proteins, peptides or nucleic acid [13]. These polymeric nanoparticles also give the advantage of manipulating the rate of drug release by varying the polymer ratio during the preparation process. The drug release occurs in a controlled manner through swelling followed diffusion through the polymer matrix, through surface or bulk erosion or in response to the local environment. The polymeric nanoparticles have been synthesized using various methods depending upon the type of drug to be encapsulated and the need for its application. The most commonly used method for the preparation of polymeric nanoparticle is the emulsion-solvent evaporation technique. This method has been successfully employed for the entrapment of hydrophobic drugs but shows poor results for the encapsulation of bioactive compounds that are hydrophilic in nature. Briefly, the solvent evaporation is carried out by dissolving the polymers and drug into a common organic solvent. Most commonly dichloromethane, acetone and ethyl acetate are used for PLGA copolymers. Then emulsion is then prepared by adding the aqueous phase containing a surfactant into the polymeric solution. The formation of the nanosized polymer droplets is then induced by sonication or high shear homogenization. In the end, the nanoparticles are then collected by centrifugation or by lyophilization [13, 14].

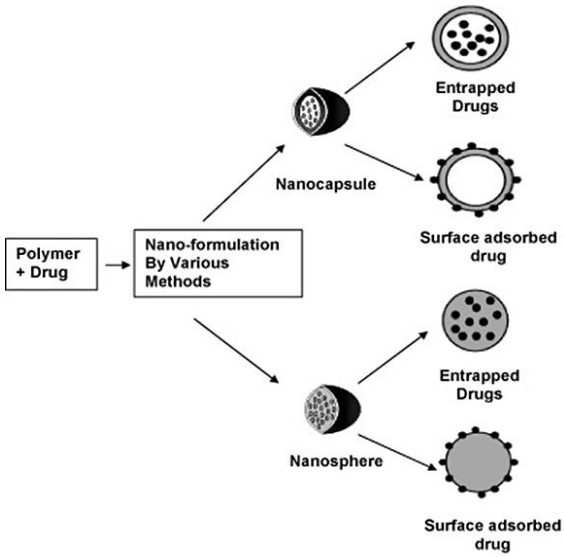

Figure 3. Different types of biodegradable nanoparticles. Based on the structure, they can be classified as nanocapsules or nanospheres. The manufacturing methodology varies according to

the type of nanoparticles. The bioactive compounds can be entrapped within the polymer matrix or can be absorbed on the surface [13].

1.3.2 Liposomes as drug carriers

The word liposomes have been derived from the Greek words; 'Lipos' means fat and 'Soma' means body. Liposomes are the concentric bilayer vesicular structures composed of phospholipids and formed when these lipids are exposed to an aqueous environment. Liposomes were first accidentally discovered in 1964 by a British hematologist Dr. Alec Bangham at the Babraham institute of Cambridge. The liposomes were discovered when Dr. Bangham and his co-worker Dr. Horne were testing a new electron microscope at the institute by adding a negative stain to the dry phospholipids leading to swollen phospholipid system. Investigations of their workgroup laid the stone of a new horizon for the development of new lipid-based drug delivery systems [15]. Within a dew year, a variety of enclosed lipid bilayer structures, initially described as 'Banghasomes' and later on 'liposomes' were prepared. Liposomes are the novel carrier systems that have been investigated more than any other delivery system as a result of their various forms. Glycerophospholipids are the most prominent lipids used for the preparation of liposomes. These lipids generally consist of a glycerol backbone esterified at C1 and C2 with two fatty acid chains with 10-24 carbon atoms. Each fatty acid chain may also contain 0-6 double bonds. The chain length and the degree of unsaturation determine the permeability and phase behavior of the lipids. These fatty acid chains form the hydrophobic part of the lipid molecule. At C3 the glycerol is esterified with alcohol via a phosphodiester linkage to form the hydrophilic part of the lipid. When dispersed in an aqueous medium, these lipids form spherical, vesicle-like structures by aligning themselves in such a way that the polar head (hydrophilic) group faces the aqueous region while non-polar part (hydrophobic tails) face each other and is shielded by the polar fraction. The unfavorable interactions between lipid-lipid and/or lipid-water molecules and large free energy between hydrophilic and hydrophobic environment leads to the formation of bilayer vesicular structure in order to achieve a thermodynamic equilibrium and minimum surface tension in the aqueous phase [16].

The liposomes can be classified in a number of ways. Generally speaking, they can be classified on the basis of the size as well as the number of bilayers. They are classified as small unilamellar vesicles (SUVs), large unilamellar vesicles (LUVs), multilamellar vesicles (MLVs) and multivesicular system (MVS). Based on the composition of the lipid used they can be classified as conventional liposomes (CL), cationic liposomes, pH-sensitive liposomes, thermosensitive liposomes, immunoliposomes, and long-circulating liposomes. They can also be classified on the

basis of the method of preparation as reverse-phase evaporation vesicles (REVs), ether injection vesicles (EIVs), French press vesicles (FPVs) and dehydrated rehydrated vesicles (DRVs).

The unique ability of the liposomes to entrap both the lipophilic and hydrophilic drugs enables a wide range of compounds to be encapsulated by these vesicles. The hydrophilic compounds are encapsulated into the aqueous core while the lipophilic molecules are entrapped into the lipid bilayer membrane. Additionally, the presence of the large aqueous core and the biocompatible nature of the phospholipid surface, these vesicles can also be used for the delivery of large macromolecules such as proteins, imaging agents as well the DNA. As nanocarriers, the liposomes offer several advantages including biocompatibility, ability to carry drug payloads, the capacity of self-assembly and a wide range of physicochemical and biophysical properties that can be modified to control their biological characteristics. They also protect the encapsulated compound from pre-mature inactivation and degradation. Liposomes are generally considered to be non-toxic, pharmacologically inactive and mimic the normal plasma membrane characteristics [17]. One of the major drawbacks of conventional liposomes is the physical and chemical stability as well as the rapid clearance from the blood circulation due to the adsorption of the plasma proteins on their surface (opsonization). This can be avoided by the surface coating of the liposomes with a hydrophilic carbohydrate, polymer or a lipid derivative of polyethylene glycol (PEG). Also, the composition of the lipid can be modulated to obtain prolonged circulatory half-life (stealth liposomes) [15].

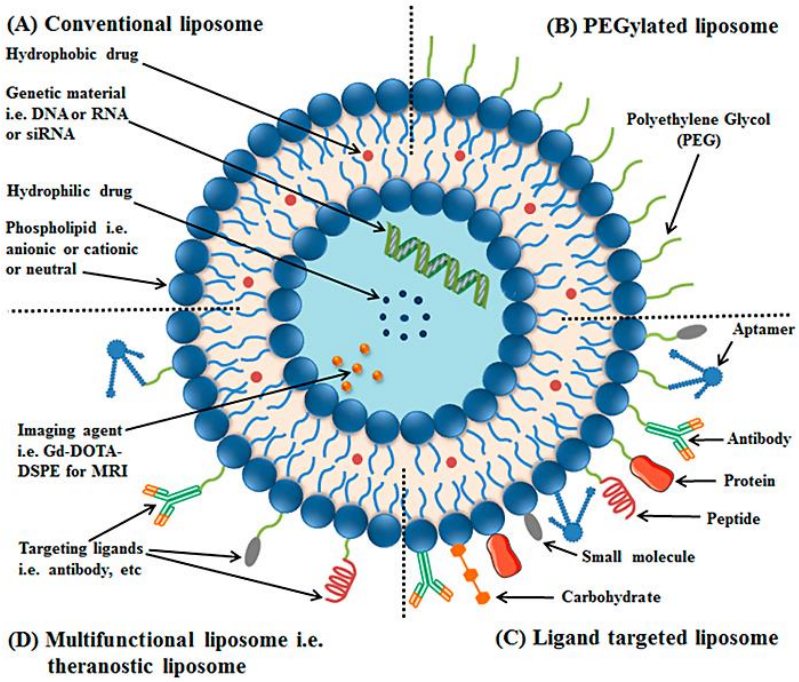

Figure 4. The structure and possible surface modifications of the liposomes [18].

1.3.3 Lipid coated polymeric nanoparticles

Lipid coated biodegradable nanoparticles (LCNPs) are the lipid-polymer hybrid systems comprising of polymeric nanoparticle core-shell enveloped by the single or multiple lipid layers thereby melding the biomimetic properties of long-circulating lipid vesicles as well as the mechanical advantages of the polymeric nanoparticles to enable an efficient drug delivery system. These nanoscopic architectures use the single nanocarrier system to combine the multiple therapeutic modalities delivering the payload at the desired tumor site and giving rise to a synergistic effect. These hybrid systems are advantageous over conventional carrier systems in terms of controllable size, tunable drug release properties, high drug loading, surface functionality as well the serum stability [19]. These lipid-polymer hybrid nanoparticles (LPHNs) as termed as lipoparticles are the superior delivery systems because these novel systems can mitigate the limitations associated with the conventional delivery systems (i.e. liposomes and polymeric nanoparticles).

Structurally, these lipoparticles are solid, submicron particulate systems consisting of at least two components. i.e. polymer and the lipid. The first building block is polymeric core, generally composed of a biodegradable hydrophobic polymer, that acts as carrier for poorly water-soluble drugs and imparts controlled drug release properties to the system. The commonly used polymers include the polylactide-co-glycolide (PLGA), polycaprolactone (PCL), dextran and albumin. These polymers are the most common choices because of their biocompatibility, nontoxicity, biodegradability, as well as their previous use in the various FDA, approved products. The second component is the shell or outer corona that uniformly surrounds the polymeric core. Commonly used lipids for the outer shell include, cationic, anionic and zwitterionic lipids such as 1,2 -dipalmitoyl -sn-glycero-3-phosphocholine (DPPC), 1,2 -dioleoyl-sn-glycero-3-phosphoethanolamine (DOPE), 1,2-dioleoyloxy-3-trimethylammonium propane (DOTAP), 1,2 -dipalmitoyl -3 -trimethylammonium -propane (DPTAP), lecithin as well as the hydrophilic substrates such as PEG-lipid conjugates. This layer allows the LPHNs to evade the uptake by the immune system and also imparts the long-circulating characteristics [20]. Various bioactive compounds such as drugs, proteins, genes, and different targeting legends can be entrapped, absorbed or covalently attached to the hybrid system. Additionally, a lipid monolayer can be deposited at the interface of the core and shell as a third component. This layer reduces the water penetration of the water and diffusion of the drug from the core. This, in turn, increases the encapsulation efficiency and alters the rate of drug release.

The Lipoparticles are generally prepared simply by mixing the polymeric nanoparticles and liposomes together in order to form lipid-polymer complexes in which a phospholipid bilayer (shell) completely covers the surface of the polymeric nanoparticle (core). The space between the core and shell is occupied by the water or aqueous buffer. Oppositely charged phospholipids are used to promote the electrostatic interactions between the polymeric core and lipid shell. Other than the two-step method for the preparation of lipoparticles, some other methods include the single-step method, modified solvent extraction/evaporation method and modified nanoprecipitation method [19, 21].

Some of the major advantages of the lipoparticles include the synergistic delivery of multiple biomolecules, improved encapsulation of hydrophobic drugs, tunable drug release profiles, mechanical stability, biocompatibility, narrow size distribution, serum and storage stability over the prolonged time periods as well as the high specific surface area [1].

1.4 Aims and objectives

The present study was aimed at the development of a novel integrated system comprising of lipid enveloped biodegradable nanoparticles (lipoparticles) for the combined chemo-photodynamic therapy. The developed lipoparticles were capable of delivering two pharmacologically active moieties simultaneously to the cancer cells. This multi-drug therapy is advantageous over the conventional therapies because a single nanocarrier system can be used to co-localize the different therapeutic moieties in the cancer cells thereby increasing the treatment efficacy, potentially overcoming the drug resistance and reducing the side effects to the neighboring tissues.

The key aspects covered in this work are divided into following parts:

1. Temoporfin (mTHPC) is a lipophilic compound that exhibits very poor water solubility as well as low permeability through the biological membranes (BCA class IV). In addition to these, poor bioavailability is an additional challenge to its applications in cancer therapeutics. The initial part of the work would be focused on the development of different liposomal formulations using a broad range of lipid combinations encapsulating mTHPC to enhance the liposomal stability, prolonged circulation time and to compare the photodynamic effect in Ovarian carcinoma cells (SK-OV-3).
2. The second part of the work would be directed towards the preparation of PLGA nanoparticles encapsulating Pirarubicin (THP) as a model anticancer drug. Being the potent hydrophobic molecule, the pharmacokinetic parameters of THP can be modified by encapsulating it into a nanoparticulate system thus reducing the side effects and increasing

the efficacy of the system Two different size nanoparticles would be prepared to evaluate their differential parameters.

3. Based on the preliminary studies, the later part of the studies would be aimed at the surface modification of the THP nanoparticles by coating the best performing mTHPC loaded liposomes over them thereby combining two different therapeutic modalities within a single nanocarrier.
4. Optimizations and detailed physicochemical evaluations of the prepared formulations by established techniques including size and charge distribution measurements. Comprehensive structural and morphological characterizations by different microscopic techniques including atomic force microscopy and electron microscopic studies.
5. Establishing the *in vitro* cell culture studies including ROS, intracellular uptake, comet assay as well as stability studies. In ovo studies using the CAM model as alternative in vivo model would be employed for establishing the efficacy of the prepared liposomes.
6. Acute in vivo cytotoxicity assessment to evaluate the biocompatibility of the system

Chapter II: Materials and Methods

2.1 Materials

2.1.1 List of materials and devices:

Materials and Devices	Source
AFM Probes; NSC14/Al BS & NSC16/Al BS	Mikromasch, Tallinn, Estonia
Ampicillin	Sigma Aldrich Chemie GmbH, Taufkirchen, Germany
Atomic force microscope; NanoWizard® 3	JPK Instruments AG, Berlin, Germany
Autoclave, Tuttnauer 3850 ELC	Tuttnauer GmbH, Linden, Germany
Bath sonicator; Transonic Digital S	Elmasonic P30H Schmidbauer GmbH, Singen, Germany
Cell counter R1	Olympus Corporation, Tokyo, Japan
Cell counting slides R1-SLI	Olympus Corporation, Tokyo, Japan
Cell culture lysis reagent	Promega GmbH, Mannheim, Germany
Centrifugation machine II	Centurion Scientific, Chichester, UK
Centrifuge 5418	Eppendorf AG, Hamburg, Germany
Chitosan	Sigma-Aldrich, Taufkirchen, Deutschland
Cholesterol	Sigma Aldrich Chemie GmbH, Taufkirchen, Germany
Chlorpromazine	Alfa Aesar GmbH & Co. KG., Karlsruhe, Germany
Coagulation analyzer	TECO GmbH, Neufahrn, Germany
CO_2 incubator, HeraCell	Heraeus GmbH & Co. KG, Hanau, Germany
Confocal laser scanning microscope; LSM 700	Carl Zeiss Microscopy GmbH, Jena, Germany
Constant power supply LKB 2197	LKB Bromma, Bromma, Sweden
Disposable folded capillary cell; DTS1060	Malvern Instruments Ltd, Malvern, UK
DMEM	Capricon Scientific, Ebsdorfergrund, Germany
DMSO; ≥ 99%	Carl Roth GmbH & Co. KG, Karlsruhe, Germany
DOPE, DOTAP, DPPC, DPPE-$mPEG_{5000}$, And DPPG	Gift samples from Lipoid AG, Steinhausen, Switzerland
Electrophoresis chamber	Thermo Electron GmbH, Ulm, Germany

Ethanol	Carl Roth GmbH & Co. KG, Karlsruhe, Germany
Ethyl acetate	VWR International, Darmstadt, Germany
Extruder; Avanti Mini	Avanti Polar Lipids Inc., Alabaster, USA
Female BALB/c, mice	National Institute of Health, Islamabad, Pakistan
Fetal bovine serum	Capricon Scientific, Ebsdorfergrund, Germany
Fertilized eggs	Mastkükenbrüterei Brormann, Rheda-Wiedenbruck, Germany
Filipin III	Sigma Aldrich Chemie GmbH, Taufkirchen, Germany
Formaldehyde	Carl Roth GmbH & Co. KG, Karlsruhe, Germany
Fluorescence microscope I CKX-53	Olympus Corporation, Pennsylvania, USA
Fluorescence microscope II	EVOS FL cell imaging system, Thermo Scientific, San Diego, USA
Freeze drier; Christ Beta I	Martin Christ Gefriertrocknungsanlagen GmbH, Osterode am Harz, Germany
H2DCFDA	Sigma Aldrich Chemie GmbH, Taufkirchen, Germany
Hatching incubator; Ehret KMB 6	Dipl. Ing. W. Ehret GmbH, Emmendingen, Germany
Hematology analyzer	Icon-3, Norma Instruments, Budapest, Hungary
Heparin sodium salt	Thermo Fischer Scientific, Dreieich, Germany
IMDM	Capricon Scientific, Ebsdorfergrund, Germany
Antibiotic/antimycotic solution	Capricorn Scientific GmbH Ebsdorfergrund, Germany
Laminar flow hood; Labogene	LMS GmbH &Co.KG, Brigachtal, Germany
LED device (prototype)	Lumundus GmbH, Eisenach, Germany
Liquid CO_2	Praxair Deutschland GmbH, Düsseldorf, Germany
Low melting agarose	Carl Roth GmbH & Co. KG, Karlsruhe, Germany
Microplate reader FLUOstar® Optima	BMG Labtech, Ortenberg, Germany
Magnetic stirrer; MCS 66	CAT Scientific, Paso Robles, USA
Megafuge 1.0 R	Thermo Fischer Scientific, Dreieich, Germany
Mounting medium; FluorSave™	Calbiochem Corporation, San Diego, USA
MTT dye	Sigma Aldrich Chemie GmbH, Taufkirchen, Germany
Microscopy Slides	Carl Roth GmbH & Co. KG, Karlsruhe, Germany
Nano-100 Micro-spectrophotometer	Hangzhou Instruments Co., Ltd, Hangzhou, China
Normal melting agarose	Carl Roth GmbH & Co. KG, Karlsruhe, Germany
Orbital shaker KS4000 IC	IKA Werke GmbH & Co. KG Staufen, Germany

Petri dishes; Tissue culture grade	Sarstedt AG & Co., Nümbrecht, Germany
Pirarubicin; THP (≥ 99%)	Selleckchem, Munich, Germany
PLGA Resomer® RG 503H	Evonik Nutrition & Care GmbH Essen, Germany
Pneumatic egg puncher	Schuett Biotech, GmbH, Göttingen, Germany
Polycarbonate membranes	Whatman plc, Buckinghamshire, UK
PURELAB flex II dispenser	ELGA LabWater, High Wycombe, UK
PVA; Mowiol® 4-88	Kuraray Europe GmbH Frankfurt, Germany
Rotary evaporator; Laborota efficient 4000	Heidolph Instruments GmbH & Co. KG, Schwabach, Germany
Serum biochemical marker analyzer	Micro lab 300, Merck, Germany
Shaking incubator; IKA KS4000 IC	IKA Werke & Co. KG, Staufen, Germany
SK-OV-3 cell line	ATCC®, Manassas, USA
Stereomicroscope	Stemi 2000-C, Carl Zeiss GmbH, Germany
Sodium acetate (> 98.5%)	Carl Roth GmbH + Co. KG Karlsruhe, Germany
Sodium chloride (> 99.8%)	Carl Roth GmbH + Co. KG Karlsruhe, Germany
SYBR® safe DNA gel stain	Thermo Fischer Scientific, Dreieich, Germany
Temoporfin; mTHPC (≥95%)	Cayman chemicals, Hamburg, Germany
TEClot aPTT-S Kit	TECO GmbH, Neufahrn, Germany
Trypsin-EDTA,	Capricorn Scientific GmbH Ebsdorfergrund, Germany
Triton™ X-100	Sigma Aldrich Chemie GmbH, Taufkirchen, Germany
Transmission electron microscope;	(TEM) JEM-1400, JEOL Ltd., Tokyo, Japan
Uranyl acetate	Sigma Aldrich Chemie GmbH, Taufkirchen, Germany
Vacuum pump; SC 920	KNF Neuberger GmbH, Freiburg, Germany
Water bath	Kottermann GmbH & Co. KG, Hänigsen, Germany
Zetasizer Nano ZS	Malvern Instruments Ltd, Malvern, UK
0.2 µm PES syringe filters	Sarstedt AG & Co. KG, Nümbrecht, Germany
15 mm cover slips	Gerhard Menzel B.V. & Co. KG, Braunschweig, Germany
6-well plates; TC Standard. F	Sarstedt AG & Co. KG, Nümbrecht, Germany
12-well plates; Nunclon Delta	Nunc GmbH & Co. KG, Wiesbaden, Germany
96-well microtiter plates, Nunclon Delta	Thermo Fischer Scientific, Dreieich, Germany
5 ml glass vials	Schott AG Müllheim, Germany

2.1.2 Solvents

All the solvents were of HPLC or analytical grade and were used without any further modifications. Ultrapure water from PURELAB flex -IV equipped with a point of use biofilter (ELGA LabWater, UK) was used for all the experiments. The phosphate-buffered saline (PBS: pH 7.4) with and without Ca^{2+}/ Mg^{2+} were prepared in the lab, sterile filtered and stored at 4 ºC for further use.

2.1.3 Cell culture

A wild type human ovarian adenocarcinoma (SK-OV-3) cell line was procured from American type culture collection (ATCC®, Manassas, USA). The cells were cultivated at 37°C and 7% CO_2 under humid conditions in a high glucose DMDM supplemented with 10% FCS and MEM-non-essential amino-acids (Gibco™, Thermo-Fischer). The cells were grown as a monolayer and passaged to 80 % confluency.

2.1.4 Chorioallantoic membrane

The chick chorioallantoic membrane (CAM) assay was conveniently used as an alternative *in-vivo* model. For this purpose, specific pathogen-free fertilized chicken eggs each weighing 50-60 g were used.

2.1.5 Lipids

2.1.5.1 DPPC

DPPC (1,2-dipalmitoyl-sn-glycero-3-phosphocholine) is a saturated, amphiphilic phospholipid molecule consisting of two non-polar palmitic acids (fatty acid) chains attached to a phosphocholine polar head group. It has a molecular weight of 734.039 g/mol. It is found in solid/gel phase at 37 $^{\circ}$C (human body temperature) but exists as a liquid phase at a glass transition temperature (T_g) of 41 $^{\circ}$C. For a free-floating fully hydrated DPPC, four distinguished phases can be described as subgel, gel, ripple and fluid phase. Based on the polar-non polar interactions, it can arrange itself from a planner bilayer structure to a spherical bilayer (i.e. liposomes) or unilayer (i.e. micelles) vesicular structure. DPPC is zwitterionic in nature because of the presence of negative charge on the phosphate group and positive charge on the quaternary ammonium group. It is the most widely found lipid in the pulmonary surfactants, eggs and lipid bilayer making up the plasma membranes [22, 23]. For this study, DPPC with a purity of 99%, was used as a major

vesicle forming lipid. The lipid was dissolved in a mixture of chloroform: methanol (2:1 v/v) to get a stock solution of 10mg/mL of the lipid and stored at -20 ˚C until further use.

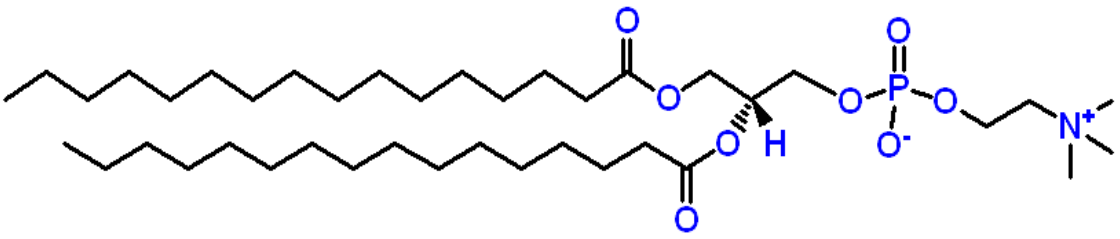

Figure 5. Chemical structure of DPPC

2.1.5.2 DPPE-mPEG5000

DPPE-mPEG$_{5000}$ (1,2 -dipalmitoyl- sn- glycero-3-phospho ethanolamine-N [methoxy (polyethylene glycol)- 5000] is a saturated lipid having a covalent bond between the phospholipid and linear PEG chain. DPPE-mPEG5000 has a molecular weight of 5745.030 g/mol with a phase transition temperature (Tm) of 63 ºC. The inclusion of the PEG-PE conjugates in the drug carrier systems results in the drastically prolonged circulation times. This is due to the increase stearic repulsion of the PEG-coated particles leading to the particle-particle interaction, therefore causing the inhibition of the adsorption of various opsonins. This in turn also increases the biological stability of PEG conjugated carrier systems [24]. The PEG-PE lipid when added at higher molar ratios (above the bilayer saturation concentration) in the formulations, induce the formation of mixed micelle structure. Depending on the lipid composition of the sample, these micelles may adopt either a discoidal or threadlike shape [25]. For this study, DPPE-mPEG5000 with a purity of 99%, was used. The lipid was dissolved in a mixture of chloroform: methanol (2:1 v/v) to get a stock solution of 10mg/mL of the lipid and stored at -20 ˚C until further use.

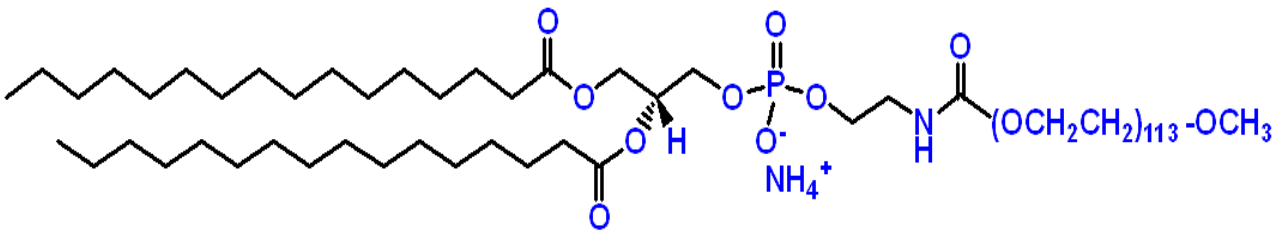

Figure 6. Chemical structure of DPPE-mPEG5000

2.1.5.3 DOTAP

DOTAP (1,2-dioleoyl-3-(trimethylammonium)-propane) is an unsaturated, synthetic cationic lipid composed of a quaternary amine as a head group attached to the two oleoyl tail chains with

a molecular weight of Mw= 698.542 g/mol. The racemic mixture of the DOTAP has a phase transition temperature (Tm) of less than 5 °C [26]. Because of its cationic nature, it is a widely used lipofection agent in liposomal transfection studies. The incorporation of unsaturated lipids (i.e. DOTAP) could also accelerate light-triggered drug release via liposomal carrier systems [27]. It is also generally observed that increasing DOTAP share causes an increase in membrane fluidity, which peaks at 75% DOTAP content and then slightly decreases again [28]. A ≥ 90% pure DOTAP was used for this study. The lipid was dissolved in a mixture of chloroform: methanol (2:1 v/v) to get a stock solution of 10 mg/mL of the lipid and stored at -20 °C until further use.

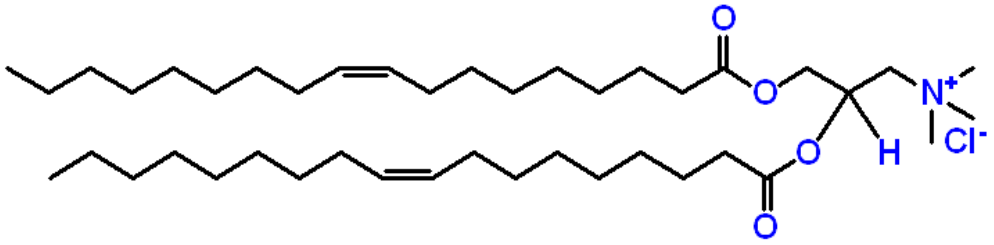

Figure 7. Chemical structure of DOTAP

2.1.5.4 DPPG

1,2-dipalmitoyl-sn-glycero-3-phosphoglycerol (DPPG) is an anionic, saturated phospholipid comprising of two palmitoyl chains attached to a glycerol backbone. DPPG has a molecular weight of 744.952 g/mol with a glass transition temperature of 41 °C (Similar to the DPPC). DPPG in combination with other lipids is used to increase the intracellular uptake of the drug-loaded nanocarrier systems. In our study, DPPG with a purity of 99% was used was generously donated by Lipoid (Steinhausen, Switzerland). A stock solution of 10 mg/mL lipid was prepared by dissolving it in a mixture of chloroform: methanol (2:1). The stock solution was preserved at -20 °C stored in a glass vial until further use.

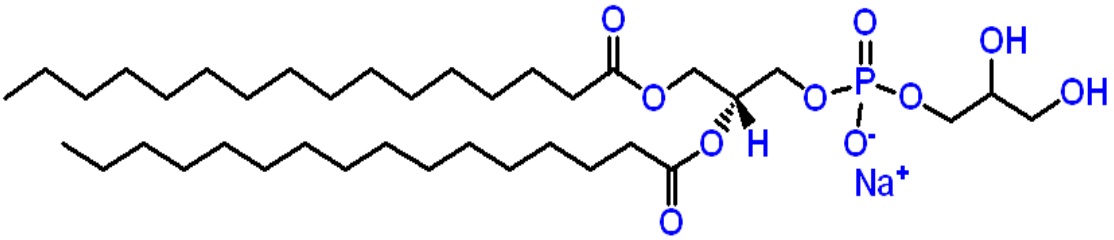

Figure 8. Chemical structure of DPPG

2.1.5.5 TEL

The plasma membrane of the archaea is rich in tetraether lipids (TELs) and diphytanylgylcerol diether, also known as archeols [29]. TELs are the basic building blocks of the cell membrane of the archaea of the genus Sulfolobus acidocaldarius and Thermoplasma acidophilus. The special structure of the tetraether lipids shields the cell interior from the external influences and ensures increased rigidity of the cell membrane. Archaeal TELs (polar lipid fraction E; PLFE) isolated from Sulfolobus acidocaldarius is a mixture of two lipids, 90% glycerol dialkyl nonitol tetraether (GDNT/ calditolglycerocaldarchaeol) and 10% glycerol dialkyl glycerol tetraether (GDGT/ caldarchaeol). These two basic types of TELs consist of two biphytanyl chains (C40), each of which is attached via ether bonds to a glycerol molecule. Both carry at one end a phosphatidyl myo inositol group. At the other end, GDNT has an annular nonitol group (calditol group) linked to β-D glucose, while GDGT has a β-D galactosyl-D glucose group [30]. The phytanyl hydrocarbon chains (C40) contains cyclopentane rings in their structure. As the number of cyclopentane rings is increased, it results in the tightening of the membrane packing. The bipolar tetra-lipids form monolayers within cell membranes, by completely traversing the membrane rather than being a double membrane, as in conventional lipids. It is believed that the presence of a hydrogen network between the head groups in the TELs and presence of higher molar fractions of the TELs in the membranes results in the greater rigidity and increased temperature. These extraordinary stability characteristics of the TEL against a variety of physical and biochemical stressors have provided the basis for using these lipids to develop various technological applications e.g. stable liposomal formulations, nanoparticles for targeted imaging and therapy [31].

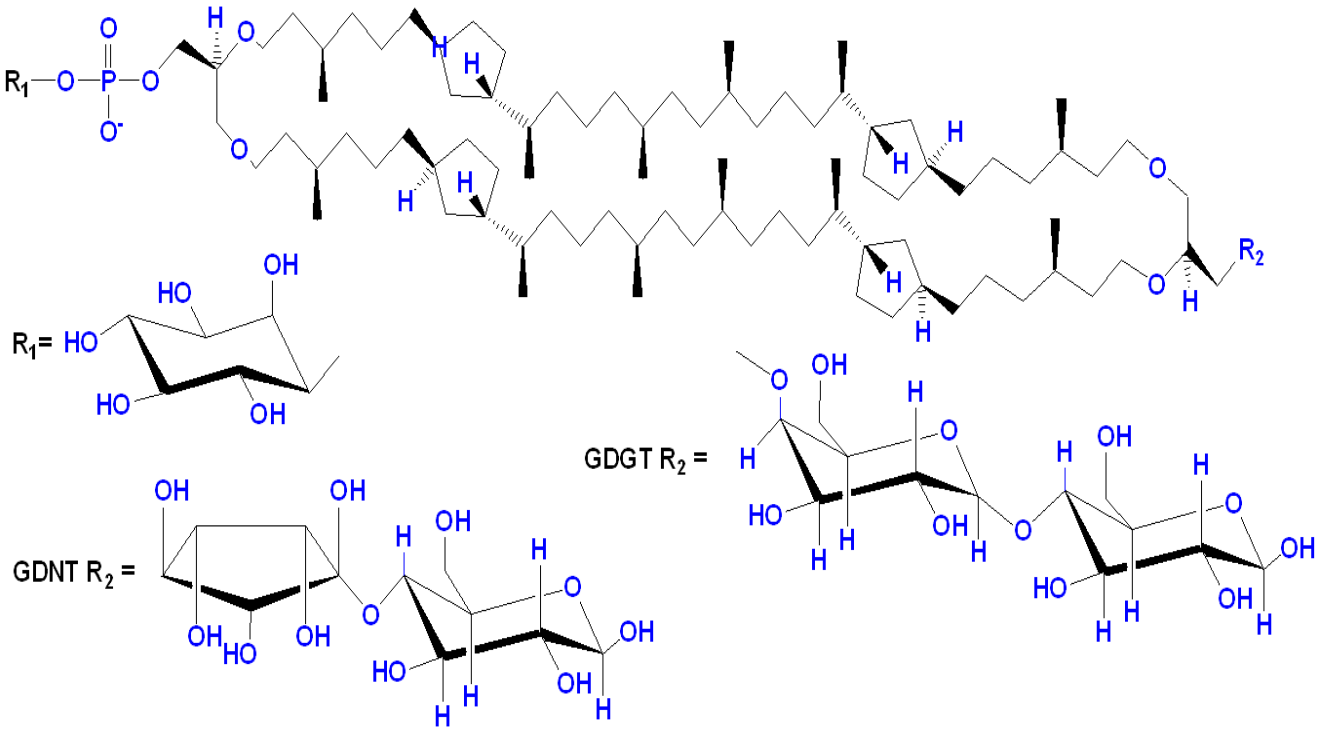

Figure 9. Chemical structure of GDGT (caldarchaeol) and GDNT (calditolglycerocaldarchaeol) present in polar lipid fraction E (PLFE). The bipolar tetraether lipids in the PLFE were isolated from S. acidocaldarius [32].

2.1.5.6 Cholesterol

Sterols are the vital constituents of neutral membranes playing a critical role in the regulation of membrane fluidity. Cholesterol is the most common sterol in the mammalian cell membrane, being present in the several liposome-based therapies approved by FDA. The cholesterol molecules are natural phospholipids with a tricyclic ring having a double bond at the position 5, 6 and 3 beta-hydroxy groups [33]. It has a molecular weight of 386.654 g/mol. Cholesterol acts to maintain transfection in the presence of serum by improved binding and uptake by the cells. Inclusion of the cholesterol in the liposomes also tends to increase the stability and half-life of the neutral and anionic liposomes in the blood circulation by causing changes in the fluidity of the membrane. This is attributed to the fact that less protein became bound to the cholesterol containing liposomes which in turn reduced the liposomal uptake by the reticuloendothelial system (RES) [34]. It also reduces the leakage of water-soluble drugs in the liposomal membrane by reducing the permeability of the membrane [35]. A stock solution of 10 mg/mL was prepared by dissolving the cholesterol in chloroform: methanol (2:1; v/v) and stores at -20 $^{\circ}$C till the further use.

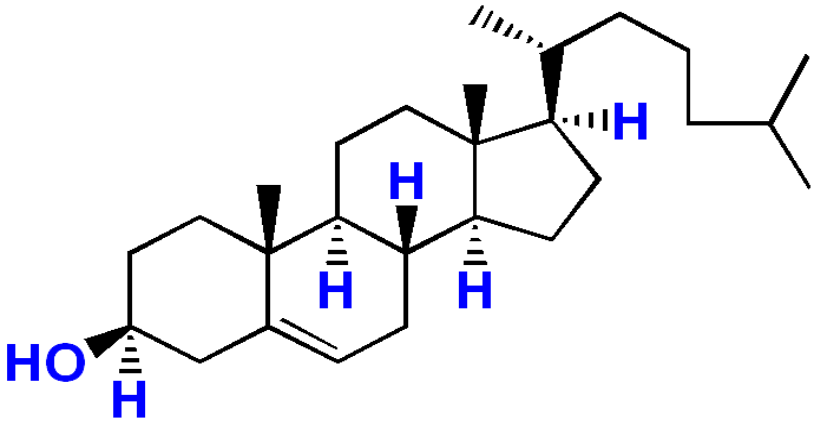

Figure 10. Chemical structure of Cholesterol

2.1.6 Polymers

2.1.6.1 PLGA

PLGA (Resomer® RG 503 H; Poly(D,L-lactide-co-glycolide) 50:50) are the most widely used polyester-based synthetic biodegradable co-polymers, currently considered best biomaterial by the United States Food and Drug Administration (FDA) for the drug delivery due to their excellent biocompatibility, biodegradability, mechanical strength and controlled released properties. PLGA is synthesized via the ring-opening polymerization of two different monomeric units namely polylactic acid (PLA) and polyglycolic acid (PGA). During this process, these successive monomeric units are linked together by ester linkages, resulting linear aliphatic polyester products. The degradation products (i.e. lactic acid and glycolic acid) are readily eliminated from the body through body's citric acid cycle and do not require the surgical procedures from their removal from the body [36, 37]. The release from the drug-loaded PLGA nano or microparticles can be controlled by varying its monomeric ratio (lactide: glycolide). It is estimated that time required for the hydrolytic degradation of PLGA is dependent on different factors including (1) co-polymer ratio, (2) end group (ester or free carboxyl group), (3) molecular weight, (4) glass transition temperature (5) viscosity of the polymer, (6) solubility of the drug, (7) pH of the biodegradation media, (8) temperature, (9) drug loading, and (10) porosity. In General, presence of the higher glycolide contents, low molecular weight, amorphous nature, presence of free carboxylic end group and smaller nanoparticle size leads to the faster degradation and drug release [38, 39]. In our study, acid terminated PLGA (Resomer® RG 503 H) with lactide to glycolide ratio in 50:50 and a molecular weight of 24,000-38,000 g/mol was used for the preparation of PLGA nanoparticles. Resomer 503 H has the fastest degradation time of less than 3 months as compared to all other PLGA grades with a viscosity of 0.32- 0.44 g/dL and a transition temperature (Tg) of

44- 48 °C. A stock solution of 20 mg/mL of the polymer was prepared in the ethyl acetate, filtered using a 0.2 µm Nylon syringe filter and stored at -20 °C until further use.

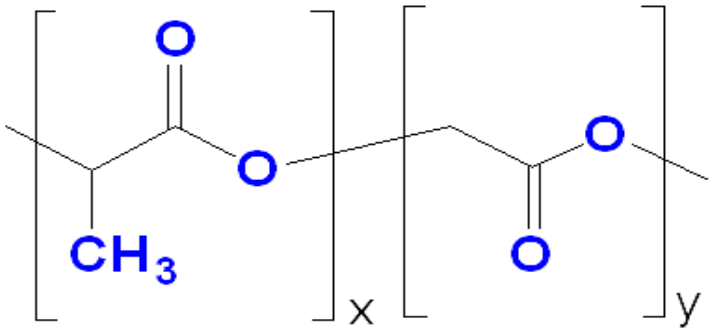

Figure 11. Chemical structure of PLGA; Resomer RG 503H. Where 'x' and 'y' represents the successive monomeric units of lactic acid and glycolic acids respectively

2.1.6.2 Chitosan

Chitosan ((1→4),2-amino-2-deoxy-ß-D-glucan) is semi-synthetic polysaccharide obtained from the deacetylation of the naturally occurring polymer chitin. Chitin is one of the most abundant polysaccharides in nature and is the major constituent of the exoskeleton of the arthropods such as crabs, shrimps, lobsters, and insects. Several billion tons of the chitin is produced every year by the marine copepods alone. Chitosan molecule is a copolymer in which N-acetylglucosamine (2-acetylamino-2-deoxy-D-glucopyranose) and glucosamine units are linked together through 1→4 glucosidic bonds. where the glucosamine content is more than 90%. Chitosan is relatively insoluble in water but soluble in acid. Chitosan has been used in variety of biochemical applications such as hemodialysis membrane, tissue engineering, artificial skin, wound healing, and drug delivery systems. It also shows antibacterial (bacteriostatic, bactericidal) and anti-yeast (candidacidal) properties in vitro [40, 41]. Being a biodegradable and biocompatible biomolecule, it has used in the regenerating blood/ tissue interface. It has a similar structural property of that of glucosamine-glycans and seems to mimic their functional behaviour. It can be degraded into the by the lysozymes into N-acetyl glucosamine, which can be used in the synthesis of glycoproteins or can be excreted out as carbon dioxide after further degradation [42]. In the recent study, ultrapure chitosan from shrimp shells with a molecular weight of 150 KDa and viscosity (η) of ≤ 200 mPa.s was used.

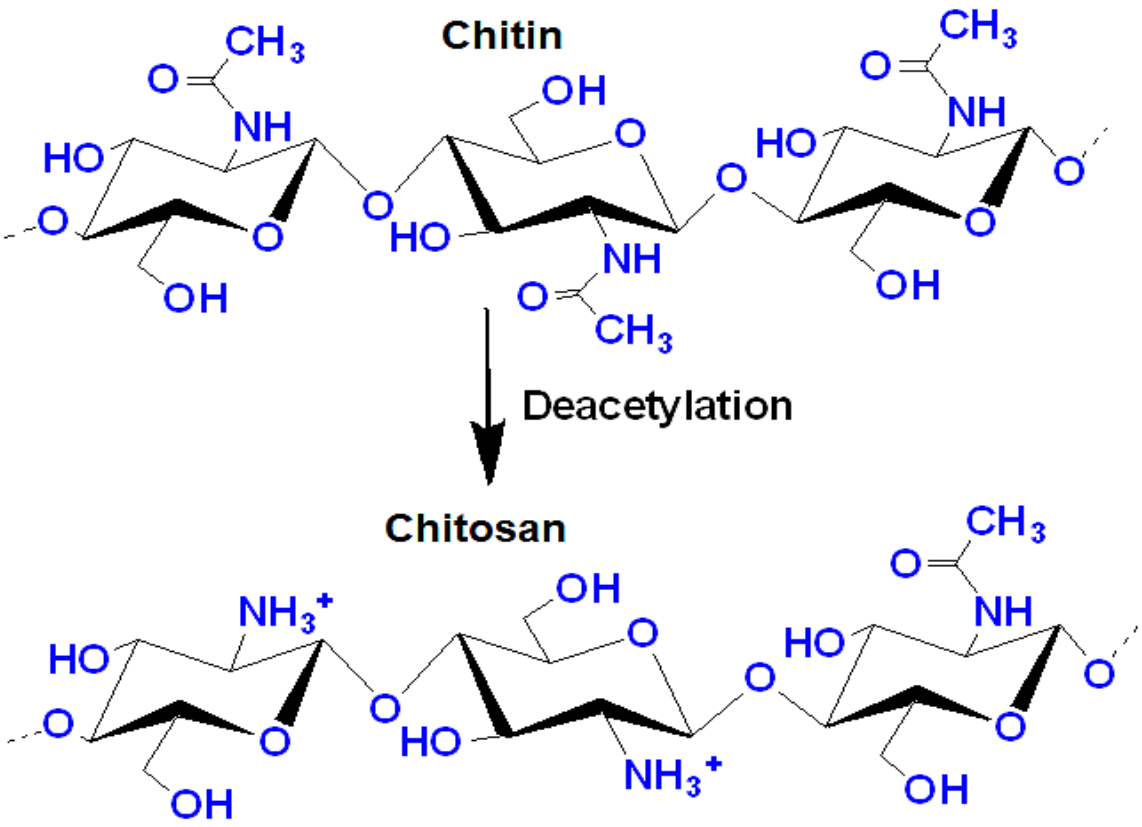

Figure 12. Chemical structure of Chitin and Chitosan [43]

2.1.6.4 PVA

Polyvinyl alcohols (PVA) are the synthetic polymers used in a large number of commercial, food, industrial and biomedical applications. Based on the method of preparation, it is divided into two categories, fully hydrolyzed and partially hydrolyzed. Its physical characteristics depend on the method of preparation from the hydrolysis of polyvinyl acetate (PVAc). PVA is found to have very low or no acute toxicity and mutagenic or clastogenic potential. It is poorly absorbed from the gastrointestinal tract and does not accumulate in the body [44, 45]. Based on all these properties, PVA is most commonly used emulsifier in the drug delivery systems e.g. polymeric nanoparticles, nanofibers, and orodispersible membranes, etc. In our study Mowiol 4-88 with a molecular weight of M_w ~31,000 with a viscosity of 3.5-4.5 mPa (4% in H_2O at 20 ºC) was used as a surfactant for the preparation of PLGA nanoparticles. It exists in the form of colourless to light yellow granules and is partly hydrolyzed with high adhesive power. A stock solution of 5% w/v was prepared in distilled water and stored at 4 °C until further use.

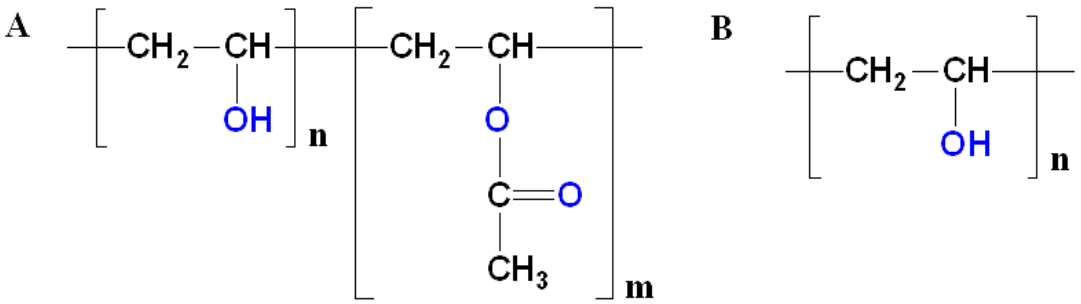

Figure 13. Chemical structure of A) partly hydrolyzed and B) fully hydrolyzed PVA

2.1.7 Drugs

2.1.7.1 Temoporfin

mTHPC (5, 10, 15, 20-Tetrakis (3- hydroxyphenyl) chlorine; Temoporfin) is one of the oldest yet most potent 2nd generation synthetic photosensitizers (PS) belonging to the family of chlorine photosensitizers. mTHPC is a non-polar compound with a molecular weight of 680.8 g/mol and is derived from the reduction of mTHPP (meso-tetra-hydroxyphenyl-porphyrin). mTHPC requires lower activation energies to produce an efficient photodynamic effect. Being a chlorine compound, it is activated with the red light at a longer wavelength of 650-652 nm and is indicated for the treatment of the different types of cancers i.e. head and neck carcinoma. Beside the clinical results, mTHPC is estimated to be 100-200 times more potent than Photofrin®. However, the hydrophobic mTHPC molecules tend to form aggregates in the aqueous media and bind strongly to serum proteins, leading to the limitation in its transportation within the biological media, tumor selectivity, limited bioavailability and hence in photodynamic therapy (PDT) [46, 47]. In the present study, mTHPC was encapsulated in different liposomal formulations in an attempt to increase its bioavailability, high tumor selectivity and to reduce the potential side effect (e.g. dark toxicity). A stock solution of 1 mg/mL was prepared by dissolving the pure drug (≥95%) in ethanol and stored at -20 °C until further use.

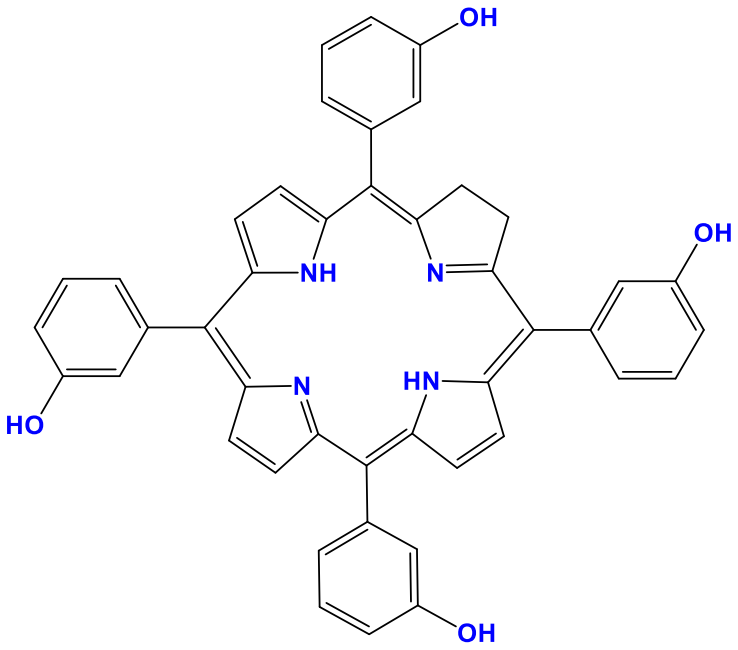

Figure 14. Chemical structure of Temoporfin (mTHPC)

2.1.7.2 Pirarubicin

Pirarubicin (2″ R)-4′-O-tetrahydropranyl doxorubicin; THP) is an anthracycline derivative that inhibits type II topoisomerase and DNA polymerase. THP has a molecular weight of 627.64 g/mol. It is a pyranyl derivative of doxorubicin and involve the generation of reactive oxygen spices (ROS). Due to the presence of the pyranyl group and its lipophilic properties, it exhibits a more potent anticancer activity and faster cellular uptake than doxorubicin [48]. It is used for the treatment of a variety of cancer such as head, neck, breast, and lymphoma. The limitation of the pirarubicin mediated chemotherapy is the indiscriminate distribution into normal the body tissues and organs before its delivery to the tumor thus causing adverse effects such as bone marrow suppression and cardiac and renal toxicity. All these adverse effects limit the use of THP in clinical settings [49]. The pharmacokinetic parameters of THP can be modified by encapsulating it into a nanoparticulate system thus reducing the side effects and increasing the efficacy of the system. Nanocarriers composed of PLGA have been investigated to carry the drugs to their designated site of action. Being biocompatible and biodegradable in nature, PLGA nanoparticles are interesting vehicles for the systemic delivery of THP. A stock solution of 1 mg/mL was prepared by dissolving the THP in ethyl acetate and stores at -20 ˚C till the further use

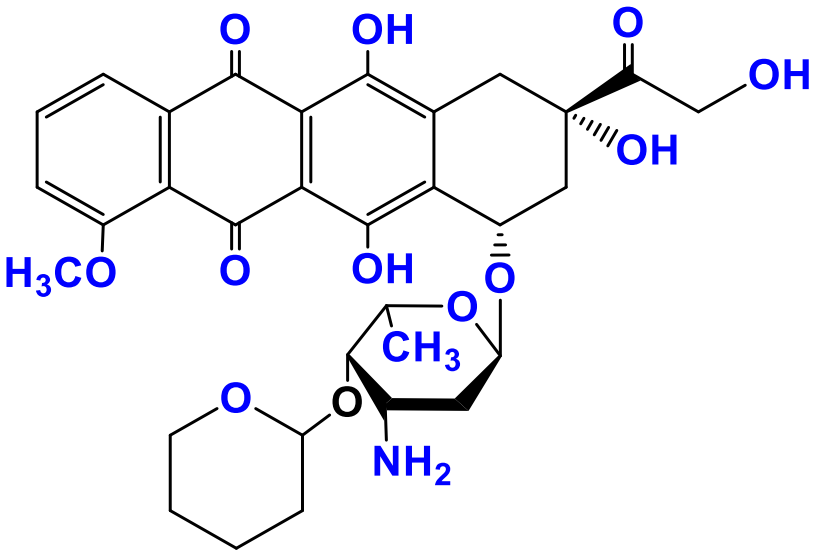

Figure 15. Chemical structure of Pirarubicin (THP)

2.2 Methods

2.2.1 Preparation of mTHPC loaded liposomes

Liposomes were formulated using the traditional thin-film hydration method [50]. Briefly, five different lipid compositions; DPPC/Cholesterol (90:10 molar ratio), DPPC/DPPE-mPEG$_{5000}$ (95:5 molar ratio), DPPC/TEL (90:10 molar ratio), DPPC/DOTAP (90:10) and DPPC/DPPG (90:10) were dissolved in organic solvent mixture (chloroform: methanol 2:1; v/v). The organic solvents were evaporated using a rotary evaporator (Heidolph Laborota 4000 efficient, Heidolph Instruments, Schwabach, Germany) equipped with a vacuum pump at 41°C. For drug-loaded liposomes, mTHPC was added to the lipid mixture in a ratio of 1:20. The film was then re-hydrated using 1 mL of PBS (pH 7.4) and thoroughly agitated to form 7.35×10^{-3} M mTHPC loaded liposomes. The pre-formed liposomes were then sonicated in a bath-type sonicator (Elmasonic P, Elma Schmidbauer, Singen, Germany) above the phase transition temperature (T_g) of the dominant lipid (i.e. DPPC=41˚C) for 15 min. The obtained multilamellar liposomes (MLVs) were then extruded 21 times using polycarbonate membrane filters (Nuclepore track-etch membrane, Whatman GmbH, Germany) first through 200 nm and subsequently from 100 nm using Avanti mini-extruder® (Avanti Polar Lipids, Alabama, USA) to obtain unilamellar liposomes. The extruded liposomes were stored at 4°C until further analysis [51].

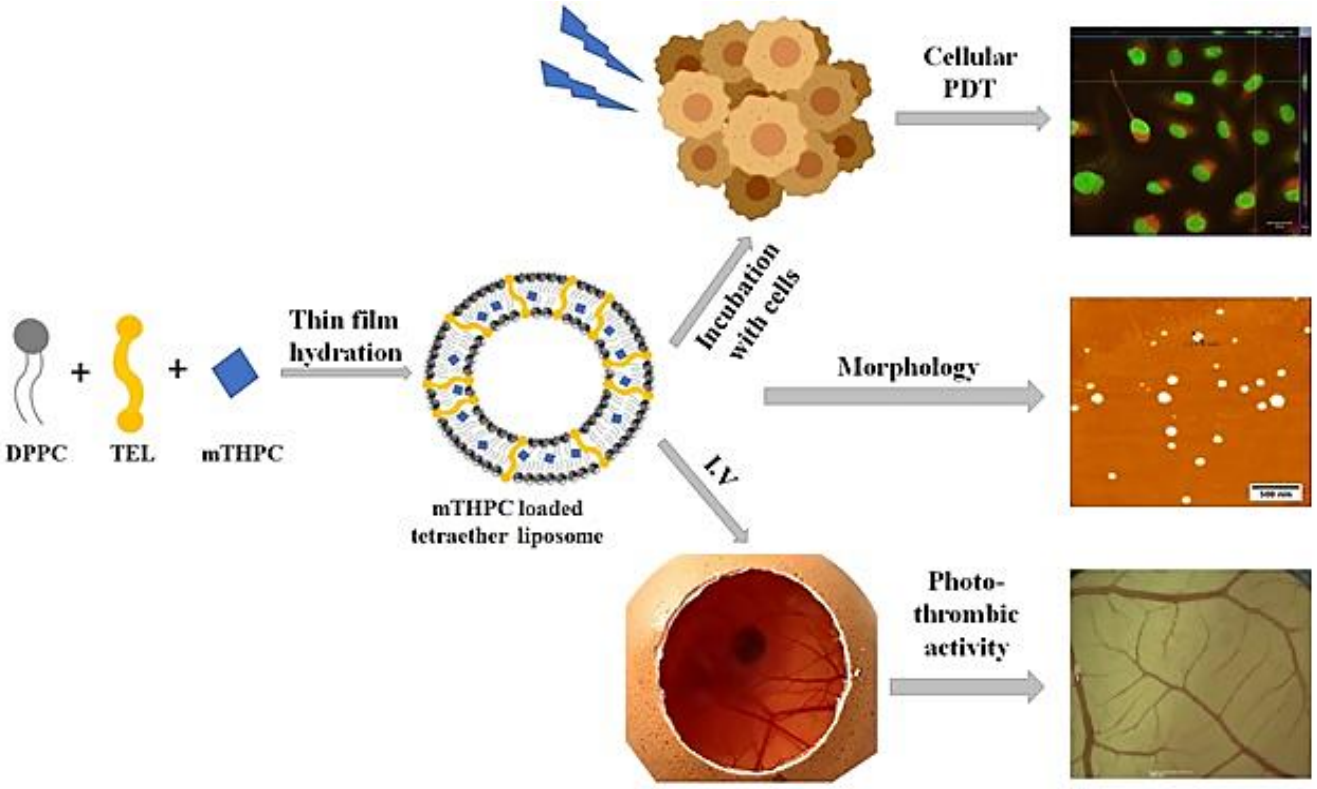

Figure 16. Schematic representation of photodynamic therapy (PDT) using mTHPC loaded tetraether (TEL) based liposomes illustrating the cellular photodynamic therapy, morphological characterization using atomic force microscopy and in-ovo photo-thrombic activity

2.2.2 Preparation of Pirarubicin loaded nanoparticles

THP loaded PLGA nanoparticles and unloaded (blank) nanoparticles were prepared using the emulsion solvent evaporation technique as described by Kumar et al [52]. Briefly, the THP stock solution was prepared by dissolving THP in ethyl acetate at a concentration of 1 mg/mL. 100 mg of PLGA was dissolved in 5 mL of ethyl acetate containing 2mg THP. The polymer-drug solution (organic phase) was then passed through a 0.2 µm Nylon syringe filter (Pall Corporation, New York, USA) and was then added dropwise into the 0.3% or 1% (w/v) PVA solution (aqueous phase). The formed o/w emulsion was then homogenized at 15000 rpm using Ultra-turrax with 18G stainless steel dispersing head (IKA-Werke, Staufen, Germany) for 10 min. 1 mL of chitosan (0.1% w/v chitosan) was added to the formed nano-emulsion. The nanoprecipitation was amplified by the addition of ultrapure water dropwise to make up the volume to 30 mL. The organic phase was allowed to evaporate overnight by continuous stirring at room temperature to form the nanoparticle suspension. The same procedure was followed to prepare the blank nanoparticles except for the addition of the THP stock solution. The following day, after the complete evaporation of the organic solvent, the nanoparticle suspension was centrifuged at 2000x

g for 45 s using Eppendorf centrifuge 4518 (Eppendorf, Hamburg, Germany) to remove any formed agglomerates. The resultant pellet was discarded and the supernatant was washed with water to separate the unentrapped drug from the nanoparticles. The washing of the nanoparticles was done twice at 16000x g for 20min. The nanoparticles suspension was then freeze-dried using an Alpha 1-4LSC lyophilizer (Martin Christ Gefriertrocknungsanlagen, Osterode am Harz, Germany) using 0.2% PVA as a cryoprotectant. The lyophilized nanoparticles were stored at 2-8 ºC until further analysis [53].

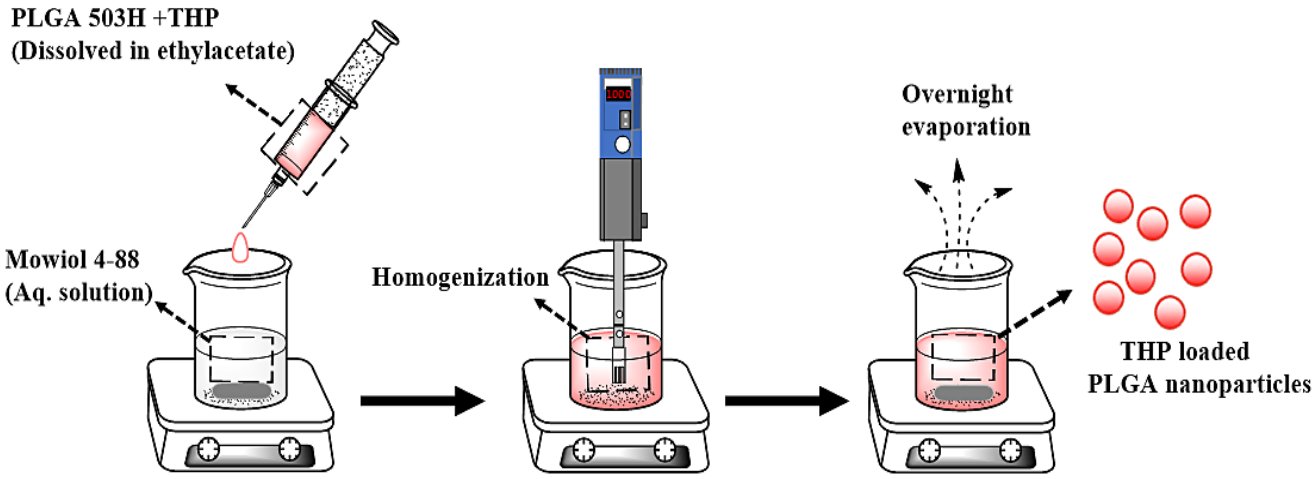

Figure 17. Schematic representation of THP loaded PLGA nanoparticles using emulsion solvent evaporation technique

2.2.3. Preparation of lipid enveloped nanoparticles:

The stoichiometry describes the relationship (typically a ratio) between the relative quantities of the substances taking part in a particular reaction or forming a compound. To optimize the stoichiometry of mTHPC loaded liposomes and THP loaded PLGA nanoparticles different Liposome: NP ratios were attempted and were then optimized to 1: 100. Consequently, to coat pre-formed liposomes over the pre-formed nanoparticles, an appropriate amount of mTHPC loaded liposomes was added to the THP loaded PLGA nanoparticle suspension and mixed thoroughly. The mixture was incubated and then sonicated for 20min, resulting in a self-organized lipid bilayer on the nanoparticle's surface [54, 55].

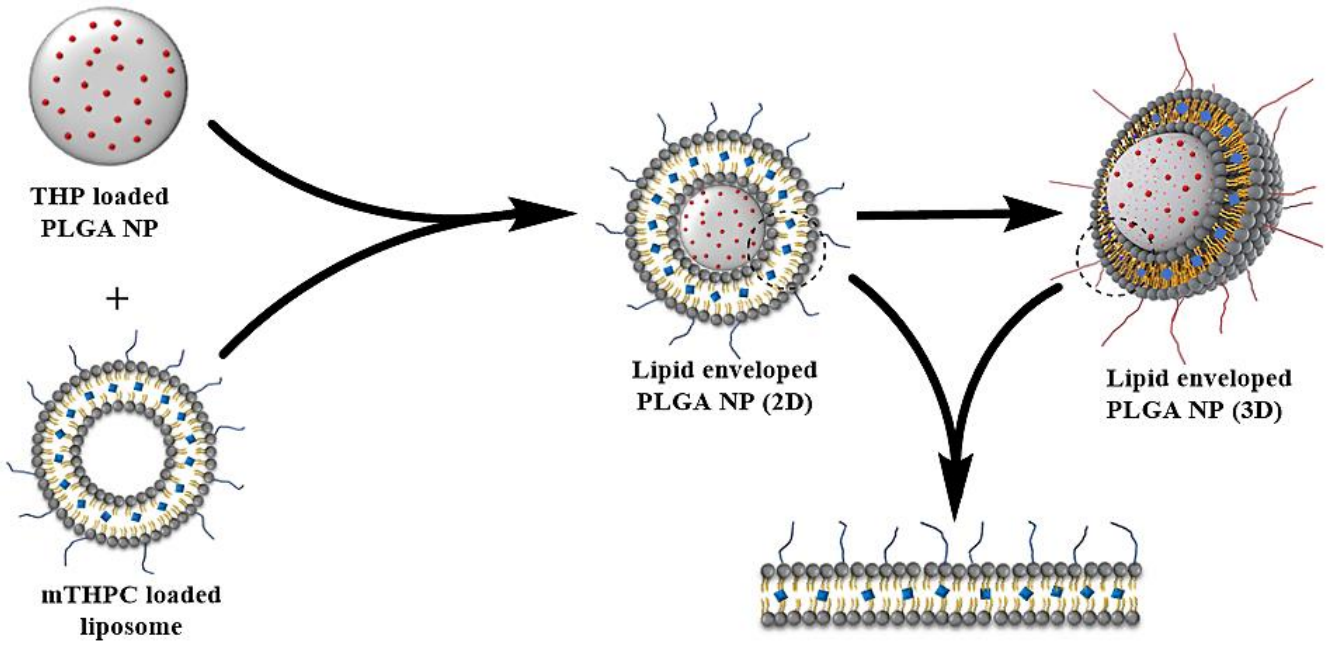

Figure 18. Schematic illustration of the preparation of lipid coated PLGA nanoparticles

2.2.4 Physicochemical characterizations

2.2.4.1 Photon correlation spectroscopy

The hydrodynamic diameter of the liposomes was measured by PCS using Nano ZS Zetasizer (Malvern Panalytical GmbH, Kassel, Germany), equipped with a 10 mW HeNe laser at a wavelength of 633 nm at 25°C and scattered light detection at 173°. Laser attenuation and measurement positions were automatically adjusted by the instrument with each measurement. The average particle diameter and polydispersity index (PDI) was always measured using disposable capillary cell (DTS1060, Malvern Instruments) for all the samples by diluting the liposomes (1:100) with purified water [56]. Data are expressed as mean ± standard deviation (SD) from the measurement of three independent samples (n=3) with each measurement comprising of 15 individual runs. All the results were expressed as the size distribution by intensity.

2.2.4.2 Laser doppler anemometry

The Zeta potential (ζ) of mTHPC loaded liposomes was performed with Nano ZS Zetasizer by measuring the electrophoretic mobility with LDV at 25°C and a scattering angle collection at 17°. A clear disposable folded capillary cell (DTS1060) was used for this purpose. Prior to measurement, the samples were subsequently diluted as described above. The values are expressed as mean ± SD for the measurement of three independent samples. Three individual

samples were measured for this purpose with every measurement having 15 - 100 runs, depending on the sample [57].

2.2.4.3 Encapsulation efficiency

2.2.4.3.1 Encapsulation efficiency of mTHPC loaded liposomes

The encapsulation efficiency (EE%) of mTHPC loaded liposomes was determined by the solvent extraction technique using air-driven ultracentrifuge Airfuge® (Beckman Coulter GmbH, Krefeld, Germany). Briefly, 200 µl of prepared liposomes were centrifuged for 90 min at 20 PSIG (60,000 rpm) using Beckman Polyallomer microcentrifuge tubes (Beckman Coulter GmbH, Krefeld, Germany). After centrifugation, the supernatant was separated and the pellet was resuspended using 200 µl of ethanol. Similarly, an equal amount of ethanol was added to the supernatant. Further centrifugation steps were carried out to remove and discard any undissolved lipids. The amount of mTHPC encapsulated was quantified from both solutions using Multiskan™ GO UV/VIS microplate spectrophotometer (Thermo Fischer Scientific GmbH, Dreieich, Germany). Liposomes having the same lipid composition without mTHPC were used as a blank. The calibration curve for mTHPC was constructed in both ethanol and ethanol/water (1:1) [58].

2.2.4.3.2 Encapsulation efficiency of THP loaded PLGA nanoparticles

The encapsulation efficiency from the THP loaded PLGA nanoparticles was determined also by the solvent extracting technique. Briefly, 1 mL of freshly prepared nanoparticle suspension was centrifuged at 16000x g for 20min using Eppendorf centrifuge 4518 (Eppendorf, Hamburg, Germany) to separate the unentrapped drug. The supernatant was withdrawn and an equal volume of acetonitrile was added to the supernatant. Similarly, the nanoparticle pellet was dissolved by the addition of 1 mL acetonitrile and sonicated for 15 min for the complete extraction of the drug. The absorbance from both of the solutions was determined using a UV/VIS spectrophotometer (UV mini 1240, Shimadzu, Japan) at 230 nm. Nanoparticles without drug were taken as blank control. The amount of drug encapsulated was quantified using the calibration curves constructed in the same solvent systems with known THP concentrations [53].

The EE% was determined using the following formula:

$$\mathrm{EE\%} = \frac{\text{Amount of drug encapsulated}}{\text{Total amount of drug added}} \times 100 \ldots\ldots \mathbf{Eq.}\,[\mathbf{1}]$$

2.2.4.4 *In vitro* drug release profile:

The release profile of pirarubicin loaded nanoparticles was carried out in PBS (pH 7.4) containing 1% tween 80 (v/v). Briefly, the freshly prepared nanoparticles were washed as described earlier. The nanoparticle pellet containing 0.5 mg of the drug was then resuspended in 5 mL of PBS (pH 7.4) with 1% tween 80 and placed in a shaking incubator (KS 4000 IC, IKA Werke, Staufen, Germany) at 100 rpm and 37 ºC. For the following days, 0.5 mL of the sample was withdrawn at specified time intervals. The sample was centrifuged at 15000x g for 10 min and the supernatant was separated. In order to assure the sink conditions, the pellet was resuspended in fresh PBS (pH 7.4) containing 1 % tween 80 and returned to the original nanoparticle suspension. The amount of THP in the supernatant was analyzed spectrophotometrically using US/VIS spectrophotometer (UV mini 1240, Shimadzu, Japan) at 230 nm. At the end of the experiment, the nanoparticle pellet was dissolved in the acetonitrile and the amount of drug remained in the nanoparticles was also determined. For all the measurements, a background subtraction with blank PLGA nanoparticles (without drug) processed in the same way was carried out [57].

2.2.5 Morphological characterizations

2.2.5.1 Atomic force microscopy (AFM)

A total of 50 µl of diluted sample dispersion (1:100 with purified water) was transferred to the silicon chip mounted on the glass slide and left to settle down for 15 min. The supernatant was then removed by aspiration using a lint-free tissue (KIMTECH Science, Kimberly-Clark Europe Limited) and the sample was allowed to dry. AFM was performed using vibration damped (i4 Series - Active Vibration Isolation, Accurion GmbH, Göttingen, Germany) NanoWizard®-3 NanoScience AFM system (JPK BioAFM, Bruker Nano GmbH, Berlin, Germany). Commercially available soft n-type silicon 1-lever cantilever tips HQ: NSC14/AL_BS (Mikromasch Europe, Wetzlar, Germany) with a resonance frequency of 160 KHz and nominal force constant of 5 N/m were used for the for the liposomes while HQ: NSC16/AL_BS (Mikromasch Europe, Wetzlar, Germany) cantilever tips with a resonance frequency of 190 KHz and force constant of 45 N/m were used for the measurement of THP loaded PLGA nanoparticles and lipid-coated nanoparticles. The scan speed was adjusted between 0.5-1.5 Hz. These measurements were performed using the intermittent contact mode in the air to avoid the sample disruption. The images were visualized using height measured, lock in-phase and lock in amplitude mode. The raw images were processed with JPK data processing software [59, 60].

2.2.5.2 Transmission electron microscopy (TEM)

For the transmission electron analysis (TEM) analysis, the samples were diluted to 1:50 with water. 15 µl of the diluted formulation was mounted on the 300 mesh formvar coated carbon supported 0.037 mm copper grids (Plano GmbH, Wetzlar, Germany). The sample was allowed to stand for 5 min. The supernatant was then removed and the samples were then negatively stained by adding 15 µl of 2% uranyl acetate on the copper grid (for contrast under the microscope) and allowed to incubate for 2min. After the incubation is over, the excess of uranyl acetate was removed using wet tissue. The samples were then analyzed under the JEM-1400 Transmission Electron Microscope (Jeol Ltd; Tokyo, Japan). The TEM was equipped with a high-resolution retractable CCD camera (Gatan Inc., Pleasanton, USA) and was operated at an accelerating voltage of 120KV with a beam current of 75 µA [61].

2.2.5.3 Cryo-transmission electron microscopy (Cryo-TEM)

Cryo-TEM was performed as described by Janich et al [62]. The vitrified liposomal samples were examined using the blotting technique. The process was performed at room temperature in a humidity-controlled environmental chamber of an EM GP grid plunger (Leica Microsystems, Wetzlar, Germany). Briefly, 6µl of the sample was placed on a grid coated with an ultra-flat holey carbon film (C-flat, Protochips Inc., Raleigh, NC). The excess liquid was removed by blotting using a filter paper. The grids were plunge-frozen immediately by immersing in liquid ethane and maintained at a temperature below 108 K (-165.15 $^{\circ}$C). The frozen grids were transferred into a Libra 120 transmission electron microscope (Carl Zeiss Microscopy GmbH, Jena, Germany; acceleration voltage 120 kV) equipped with a Gatan 626 cryotransfer system. Images were taken with a BM-2k-120 dual-speed on-axis SSCCD camera (TRS, Moorenweis, Germany).

2.2.6 *In vitro* cell culture experiments

2.2.6.1 Cell line and culturing

A wild-type human ovarian adenocarcinoma (SK-OV-3) cell line was procured from ATCC (American type culture collection, Manassas, USA). The cells were cultivated at 37°C and 7% CO_2 under humid conditions in a high glucose DMDM supplemented with 10% FCS and MEM-non-essential amino-acids (Gibco™, Thermo-Fischer). The cells were grown as a monolayer and passaged to confluency [50, 58].

2.2.6.2 Light delivery to the cells

A prototype LED device containing light-emitting diodes (Generation-I LED irradiator, Lumundus GmbH, Eisenach, Germany) was used. The device was equipped with the function to change the irradiation time (s) and current (mA) as required. It was supplied with two different LEDs of 457 nm (blue) and 652 nm (red) wavelengths. The device was able to deliver irradiance of 22.4 Wm^{-2} at a current of 20 mA and wavelength of 652 nm. Similarly, 220.2 W/m^2 irradiance can be delivered at a current of 100 mA and a wavelength of 457 nm. The actual light dose (Jcm^{-2}) delivered to the cells seeded in 96 well plates is equal to irradiance (Wcm^{-2}) times the irradiation time.

2.2.6.3 Cytotoxicity studies

2.2.6.3.1 MTT assay

The cells were seeded in the clear flat bottom 96 well microtiter plates (Nunclon Delta, Thermo Fischer Scientific GmbH, Dreieich, Germany) at a seeding density of 10,000 cells/well (0.35cm^2) and allowed to adhere overnight. Post 24 h stabilization, the cells were incubated with 100 µL/well of THP loaded nanoparticles and free THP (dissolved in DMSO) in different concentrations ranging from 100 µM to 0.78 µM (appropriately diluted with the medium) and were incubated for 4 h. Post incubation, the samples were removed and fresh medium was added to the cells. The plates were then returned to the incubator and incubated overnight. After 24 h, the medium was replaced with the 200 µL of MTT appropriately diluted with medium (2 mg/mL) and incubated for 4 h. After the incubation, MTT dye was aspirated and formazan crystals were dissolved using 200 µL of DMSO. The plates were incubated on a shaking incubator (IKA KS4000 IC, Staufen, Germany) for 20 min. The absorbance was recorded at 570 nm using FLUOStar Optima plate reader (BMG Labtech, Ortenberg, Germany). The cell viability of the untreated cells was considered to be 100%. The cell viability was determined using the formula [63]:

$$\text{Cell Viability } \% = \frac{\text{Ab}_{\text{Sample}} - \text{Ab}_{\text{Blank}}}{\text{Ab}_{\text{Control}} - \text{Ab}_{\text{Blank}}} \times 100 \ldots\ldots \textbf{Eq.}\,[\mathbf{2}]$$

where Ab_{Sample} and $Ab_{Control}$ denote the treated and untreated samples respectively. While Ab_{Blank} indicates the well containing medium without any cells. The values are expressed as mean ± SD with all the experiments performed in triplicate.

2.2.6.3.2 *In vitro* irradiation and cytotoxicity synergism

The cellular photodynamic therapy (cPDT) for the mTHPC loaded liposomes and lipid-coated nanoparticles was performed using MTT assay as described above. For in vitro irradiation experiments, different concentrations of mTHPC loaded liposomes ranging from 5 µM to 0.05 µM (appropriately diluted with the medium) were used. The incubation time was optimized for 2 h after initial incubation for different times e.g. 1 h, 2 h, and 4 h. Post incubation, the liposomal formulations were replaced with fresh medium and the mTHPC taken up by the cells was irradiated at 652 nm (red) for 23, 223 and 446 S at a fluence of 22.4 Wm^{-2} (20 mA). This corresponds to 0.05, 0.5 and 1 Jcm^{-2} of the total light dose delivered respectively. Similarly, in other experiments, mTHPC was illuminated at 457 nm (blue) for 45, 227 and 455 sec at a fluence of 220.2 W/m^2 (100 mA) which corresponds to 1, 5 and 10 Jcm^{-2} of total light energy delivered. An unirradiated well plate treated similarly with liposomal formulations was considered as dark control. Free mTHPC dissolved in DMSO was taken as a standard control whereas cells without any liposomal formulation were considered as a negative control [50].

Based on the results obtained from the physicochemical characterizations and the cell viability assay, THP nanoparticles with an average hydrodynamic diameter of 200 nm were considered to be the optimal size for the further studies. Consequently, these nanoparticles were coated with mTHPC loaded DPP/DPPG/$mPEG_{5000}$-DPPE liposomes. The cell viability assay was also performed for the lipid-coated THP nanoparticles for the combined delivery of the mTHPC and THP to the cancer cells. For this purpose, the SK-OV-3 cells were incubated with similar concentrations of mTHPC loaded DPPC/DPPG/$mPEG_{5000}$-DPPE liposomes as well as lipid-coated THP nanoparticles (as described above) for 4 h. Post incubation, the medium was replaced and the cells were irradiated with different light fluences (i.e. 50 mJ/cm^2 and 350 mJ/cm^2) at a wavelength of 652 nm [64]. The next day, cell viability was determined using MTT assay.

2.2.6.4 Measurement of cellular reactive oxygen species (cROS)

The quantitative determination of ROS was performed using a free radical sensor and cell-permeable fluorescent dye DCFDA. The assay was performed according to the DCFDA cellular ROS detection protocol from Abcam with slight modifications. Briefly, SK-OV-3 cells were seeded in the dark, clear bottom 96 well microtiter plates at a density of 25,000 cells/well. Cells were allowed to adhere overnight. On the following day, the cells were washed with PBS (pH 7.4) supplemented with Ca^{2+} and Mg^{2+} and were then incubated with 25 µM of DCFDA, by incubation for 45 min at 37 ºC. After washing again with PBS, they were incubated with liposomes for 2 h.

50 µM of TBHP was used as a positive control. After the incubation, cells were irradiated at a radiation fluence of 1 Jcm^{-2} at 457 and 652 nm. The cells were then washed with PBS and the fluorescence was recorded at λ_{ex} 480 nm/λ_{em} 520 nm using FLUOStar Optima plate reader. Based on the results obtained from cPDT and measurement of cROS, the irradiation was done using 652 nm wavelength light for the further experiments [65].

2.2.6.5 Intracellular uptake studies

For intracellular uptake analysis of mTHPC encapsulated liposomes, SK-OV-3 cells were seeded onto the sterile cover glasses (15 x 15 mm) placed in 12 well cell culture plates (Nunclon Delta, Nunc GmbH & Co. KG., Wiesbaden, Germany) at a density of 90,000 cells/well. After 24 h, the medium was replaced by 5 µM of mTHPC loaded liposomes and incubated for 2 h at 37°C. After the incubation, the medium was aspirated and cells were washed twice with sterile ice-cold PBS (pH 7.4) supplemented with Ca^{2+} & Mg^{2+}. The cells were then fixed with 4% formaldehyde by incubating the cells for 20 min at room temperature. They were then washed again with PBS (pH 7.4). The cell nuclei were counterstained with 50nM of Sytox green™ nucleic acid stain (Thermo-Fischer Scientific GmbH, Dreieich, Germany) for 20 min. After washing twice with PBS (pH 7.4), the cover glasses were then removed from the well plate, mounted on glass slides and sealed with fluorescence free glycerol-based FluorSave™ reagent (Calbiochem, San Diego, USA). The stained cells were then observed under the LSM700 confocal laser-scanning microscope (Carl Zeiss Microscopy, Jena, Germany). The cellular uptake was then observed using fluorescence detection filters for Sytox green™ ($\lambda_{ex/em}$ 504⁄523 nm) and mTHPC ($\lambda_{ex/em}$ 420/652 nm) [65, 66].

2.2.6.6 *In vitro* genotoxicity assessment

The single-cell gel electrophoresis (Alkaline comet assay) was used to assess the DNA damage and genotoxicity induced by mTHPC encapsulated liposomes. All the procedures were performed in dark [67]. Briefly, 1,00,000 SK-OV-3 cells per well were seeded into a six-well plate and were allowed to adhere overnight. The following day the cells were incubated with 0.5 µM of mTHPC loaded liposomes, 20 µM of THP loaded nanoparticles and similar concentrations of lipid-coated PLGA nanoparticles for 4 h. After the incubation is over, the mTHPC liposomes were replaced with the fresh medium. Consequently, the cells were irradiated at an equitoxic light dose to produce 80% cell viability in order to avoid any false positive responses. The treated cells were then incubated overnight. The next day, the cells were trypsinized and centrifuged for 5 min at 1000 rpm to get the cell pellet. The obtained cell suspension was washed twice using sterile PBS

(pH 7.4) and cell density was adjusted accordingly. As a next step, 80,000 cells (25 µl) of the PDT treated cell suspension was mixed with 75 µl of 1% of prewarm low melting agarose (LMA) (Carl Roth GmbH, Karlsruhe, Germany). The mixture was applied on the superfrost glass slide previously precoated with of 1% standard normal melting agarose (NMA) and was immediately covered with coverslips. The glass slides were then placed on an ice block for 10 min until solidified and the coverslips were gently removed. The cell membrane lysis was done by submerging the slides overnight into the staining jar containing cold lysis solution (300 mM NaOH, 1.2 M NaCl, 2% DMSO and 1% Triton™ X-100). The slides were then transferred to the electrophoresis tank containing alkaline electrophoresis buffer (300 mM NaOH and 1mM EDTA) and were left in the buffer for 30min to allow the unwinding of DNA. Electrophoresis was performed for 30 min at 250 mA current and 25 V, resulting in the DNA unwinding and exposing the alkali labile sites. After the electrophoresis, the slides were neutralized by washing the slides with double distilled water. The cell fixation was then done by submerging the slides into the 70% ethanol for 20 min. After fixation, the slides were cells were stained with SYBR® safe DNA staining dye (1:10000 in PBS) for 20 min [68]. Finally, the slides were washed with double distilled water to remove any unbound stains. The comet analysis was done under a fluorescence microscope (CKX-53 Olympus, USA). Fifty individual comets were scored for each formulation.

2.2.6.7 Cellular uptake pathway analysis

In order to determine the liposomal uptake mechanism by the cells, the SK-OV-3 cells were seeded into a 96 well plate at a seeding density of 10,000 cells/well and were allowed to adhere overnight by maintaining at 37°C and 5% CO_2. The next day, the cells were washed with PBS (pH 7.4) supplemented with Ca^{2+}/Mg^{2+}. The cells were then pre-incubated with the inhibitors of the vesicular uptake pathway (i.e. Chlorpromazine 30 µM and Filipin-III 15 µM) for 1 h. After incubation is over, the nanoformulations (mTHPC-LP, THP-NP, LCNP as well as free drugs) were added to the cells and were again incubated for a total of 4 h. Post incubation, the samples were replaced by fresh medium and irradiation was performed at a light dose of 0.5 Jcm^{-2}. Subsequently, the cells were incubated again for 24 h. Un-irradiated plates were taken as the dark control. The following day, cell viability was determined using MTT assay as described previously [51].

2.2.6.8 Apoptosis assay using flow cytometry

The cell apoptosis assay was performed using flow cytometry APC annexin V (human vascular anticoagulant) according to the manufacturer protocol with slight modifications. Briefly, 90,000

SK-OV-3 cells per well were seeded in 12-well cell culture plates and were allowed to adhere overnight. Post stabilization, the cells were incubated with the nanoformulations at a concentration of 1.5µM of mTHPC loaded liposomes, 15µM of THP loaded nanoparticles and similar concentrations of the lipid-coated nanoparticles containing mTHPC and THP to get 60% cell viability. The cells were then incubated for 4 h. Post incubation, the formulations were replaced with the fresh medium. The cells were then irradiated with a light dose of 0.05 Jcm^{-2} at 652 nm (except for THP loaded nanoparticles and free THP). The cells without any treatment were taken as the negative control. The plates were then returned to the incubator for overnight. The following day, cells were trypsinized, washed with ice-cold PBS (pH 7.4) without Ca^{2+}/Mg^{2+} and resuspended in 1X binding buffer. 50µL of binding buffer supplemented with 1µL (10 µg/ ml) of APC annexin V were gently mixed with an equal volume of the cell suspension and incubated at room temperature for 15 min under dark conditions. After the incubation is over, a 300 µL of binding buffer containing 0.4 µL (5 mg/mL) of propidium iodide (PI) was added and placed in ice for 5 min. The apoptosis analysis was then conducted by flow cytometry (Guava® easyCyte™, Millipore Sigma, USA). The data was processed by FlowJo® v. 10.6 software.

2.2.6.9 Biocompatibility studies

2.2.6.9.1 *Ex-vivo* hemolysis assay

To evaluate the effect of mTHPC loaded liposomes on human blood, the *ex-vivo* hemolysis assay was performed as described by Raschpichler et al [69]. Briefly, 10 mL of fresh human blood was drawn into the EDTA tubes to prevent the coagulation and centrifuged at 500 × g for 5 min, resulting in separation of blood plasma from the human erythrocytes. The plasma was aspirated and erythrocyte pellet was washed three times with sterile PBS (pH 7.4) and diluted to 1:50 with PBS. mTHPC loaded liposomes (10X of the desired final concentration tested in cell culture experiments) were then incubated with erythrocytes in V-bottom microtiter plates for 1 h at 37°C in an orbital shaker KS4000 IC (IKA Werke, Staufen, Germany). The plates were then centrifuged and the supernatant was transferred into a clear flat bottom 96 well plate. The absorbance was measured at 540 nm using FLUOStar Optima plate reader. Sterile filtered PBS (pH 7.4) and 1% Triton™ X-100 were taken as negative and positive controls, respectively. The absorbance value from Triton™ X-100 was considered as 100% hemolysis. The assay was done in triplicate and the results were expressed as mean ±SD. The percentage of hemolysis was calculated using the formula [69]:

$$\textbf{Hemolysis}\ [\%] = \frac{\mathrm{Ab_{Sample}} - \mathrm{Ab_{Nc}}}{\mathrm{Ab_{PC}} - \mathrm{Ab_{Nc}}}\ \mathrm{X}\ 100\ \ldots\ldots\ \textbf{Eq}\ [\mathbf{3}]$$

2.2.6.9.2 Activated partial thromboplastin time test (aPTT)

In order to verify that the mTHPC loaded liposomes do not trigger the coagulation cascade upon intravenous administration, aPTT test was performed as described by Pinnapireddy et al [70]. The test was performed in the Coatron M1 coagulation analyzer (TECO GmbH, Neufahrn, Germany) using TEClot aPTT-S kit as described by the manufacturer's manual with slight modifications. Briefly, fresh blood was drawn in a citrate tube and centrifuged at 1500 × g for 15min to separate the blood plasma. 25 µl of the plasma was mixed with 25 µl of the sample, followed by the addition of 50 µl of aPTT reagent for the activation of coagulation factors. Finally, 0.025 M prewarm calcium chloride ($CaCl_2$) was added to the mixture to activate the coagulation of blood. Coagulation was confirmed spectrophotometrically, and the clotting time was recorded in seconds. The experiments were performed in triplicate and the results were expressed as mean ±SD [70].

2.2.6.9.3 Photo-thrombic activity of mTHPC liposomes (CAM assay)

Fertilized eggs weighing 50-60 g were purchased from Mastkükenbrüterei Brormann (Rheda-Wiedenbruck, Germany). After the delivery, the eggs were disinfected with ethanol (70%) and placed in a hatching incubator (Dipl. Ing. W. Ehret GmbH, Emmendingen, Germany) equipped with the automatic rotator at a temperature of 37°C and relative humidity of 65%. The intact chick CAM angiogenesis model was used as described by Tariq et al [71], with slight modifications. Briefly, on egg development day 4 (EDD 4), a 30 mm hole was made on the apical part of the egg with the help of pneumatic Egg Puncher (Schuett Biotech GmbH, Germany) at a pressure of about 2-3 bars to expose the premature CAM surface. The exposed surface was then covered with a small petri dish and placed back to the incubator in the static upright position until the CAM was fully developed. On EDD 12, 100 µl of the liposomal sample (200 µM) was injected intravenously *in-ovo* using a stereo-microscope (Stemi 2000-C, Carl Zeiss GmbH, Jena, Germany) and incubated for 60 min. After the homogenous distribution of the sample, a PVC ring (diameter 5 mm) was placed on a predefined treatment area. An image of the CAM surface was recorded prior to irradiation. Subsequently, the chosen area was irradiated using a red laser diode (652 nm, 40 mW) with Weber needle (Weber Medical GmbH, Lauenförde, Germany). The irradiation was performed for 2 min at an area of 3.1 mm^2 that corresponds to 4.8 Jcm^{-2} energy (optimized energy; data not shown). Vascular occlusion was recorded post-irradiation from 10 min to 48 h using

Stemi 2000-C stereo-microscope (Carl Zeiss GmbH, Jena, Germany) attached with a Moticam 5 CMOS camera (Motic Deutschland GmbH, Wetzlar, Germany). For each liposomal formulation, the experiment was performed in triplicate and images were recorded pre and post photodynamic treatment. Eggs treated with normal saline were considered as a negative control [72, 73].

2.2.6.10 Serum stability studies:

The stability studies of mTHPC encapsulated liposomes were conducted in simulated conditions. In order to simulate the physiological conditions, 0.2 mL mTHPC loaded liposomes were mixed with 1 mL of 60% FCS (diluted in PBS (pH 7.4) to get a volume ratio of 5. Similarly, 1 mL PBS (pH 7.4) was also mixed with 0.2 mL of mTHPC containing liposomes to get the same volume ratio of 5. Both of the mixtures were then incubated for 24 h in a shaking incubator at 100 rpm and 37ºC. In the control experiments, only PBS (pH 7.4) was mixed with FCS keeping the other parameters constant. The samples were withdrawn at specific time intervals, appropriately diluted with purified water and measured using Nano ZS Zetasizer. The results were obtained for, three independent formulations [74].

2.2.6.11 *In vivo* experiments

2.2.6.11.1 Animals

Healthy female albino (BALB/c) mice weighing 30-35 g with an age 8-10 weeks were obtained from the National Institute of Health, Islamabad. All the animals were provided free access to water and commercial laboratory food (ad libitum). They were housed in a controlled environment (Temperature: 22 ± 2 $^{\circ}$C, Humidity: 60 ± 10% with a 12 h light/ dark cycle). All the experiments were performed as per defined protocols approved by the Bio-ethical committee of Riphah Institute of Pharmaceutical Sciences, Riphah International University, Lahore, Pakistan.

2.2.6.11.2 In vivo acute toxicity assessment

In *vivo*, acute toxicity studies were determined in mice for 7 days as per the Organization for Economic Cooperation and Development (OECD) 425 guidelines [75]. Briefly, the animals were randomly assigned into 6 groups with each group comprising of 3 animals (n= 3). Group 1 and group 2 were administered with free mTHPC (dissolved in 0.1% DMSO) and mTHPC loaded liposomes respectively (mTHPC dose equivalent to 0.150 mg kg^{-1} body weight). Similarly, Group 3 and group 4 were treated with free THP (dissolved in 0.1% DMSO) and THP loaded nanoparticles respectively (THP dose equivalent to 5 mg kg^{-1} body weight). Group 5 was treated

with lipid-coated nanoparticles and group 6 was treated with normal saline (considered as the control group). The formulations were administered in two equally divided doses (viz day 1 and 3) intravenously via tail vein using a 21-gauge needle. The animals were kept under observation for 1-7 days for any sign of changes in the body weight, visual observations of mortality, behavioral patterns (e.g. skin and fur, eyes, salivation, respiration, consistency of feces, urine color, sleep patterns, convulsions and coma, etc.), any sign of illness throughout the study period. After 7 days of observations, the blood was withdrawn for blood biochemical analysis and the mice were euthanized for tissue histological studies [76, 77].

2.2.6.11.3 Blood biomarker assay

In an attempt to determine the toxicity of our formulations on the mice's blood, serum biochemical indexes were analyzed. After 7 days post-exposure, blood from each mouse was withdrawn under anesthesia into a sterile tube via thoracic puncture. In order to separate the plasma, the blood was centrifuged at 1200x g for 10 min, using the centrifuge (Centurion Scientific, Chichester, UK). The supernatant was removed carefully and stored at -20 $^{\circ}$C until further analysis. Serum biochemical markers including renal function tests (RFTs), liver function tests (LFTs) including, bilirubin level, creatinine level, blood urea, total protein, and cholesterol level were performed using serum biochemical marker analyzer (MicroLab 300, Merck, Germany).

Hematological investigations were conducted on the heparinized part of the blood. Complete blood screening including total erythrocyte count (TEC), hemoglobin concentration (Hb), mean corpuscular volume (MCV), hematocrit (HCT), mean corpuscular hemoglobin (MCH), mean corpuscular hemoglobin concentration (MCHC), total leucocyte count (TLC), platelet count as well as mean platelet volume (MPV) were performed using a hematology analyzer (Icon-3, Norma Instruments, Budapest, Hungary) [78].

2.2.6.11.4 Body visceral index

Body visceral index is a vital tool to evaluate any toxic effect of the nanoformulations on mice’s organs after their repeated administration. Change in body organ weight was determined at the end of the treatment (post 7 days). The animals were euthanized by cervical dislocation method and vital body organs (i.e. heart, kidney, liver, and lungs) were removed, washed carefully with sterile normal saline and weighed. The organ weights were then compared with the body organ weights of the control group to determine the organ body weight index using the formula [79, 80]:

$$\textbf{Body Visceral Index}\ [\%] = \frac{\text{Organ weight}}{\text{Body weight}} \text{X}\ 100 \ldots\ldots \textbf{Eq}\ [\mathbf{4}]$$

2.2.6.11.5 Erythrocyte adhesiveness test (EAAT)

The erythrocyte aggregation test is a simple test that indirectly reveals the presence and proportion of the inflammation. It is a commonly used screening test for high-risk individuals for myocardial infarction. For EAAT, the erythrocytes of the mice were separated from the other blood components and washed three times with sterile PBS by centrifugation at 5,000 g for 5 min. The RBC pellet was then re-suspended with PBS to make a final stock suspension of 2% (v/v). A 100 µl of the erythrocyte suspension was mixed with 100 µl of the nanoformulations containing 50 µM of mTHPC and 75 µM THP and were then incubated for 2 h at room temperature. After the incubation, 10 µl of the sample mixture was placed on a glass slide and observed under bright field microscopy [81].

2.2.6.11.6 Histopathological examinations

In order to examine any pathological changes (i.e. abnormalities or lesions) induced by our formulations, histopathological examinations were done as described. Briefly, after sacrificing the animal, the vital organs were removed and washed carefully with normal saline. The organs were immediately placed in 10% formalin solution. The organs were then embedded into the paraffin blocks and sliced carefully into 0.5 µm thin tissue sections using a rotary microtome (Hunan Kaida Scientific Instruments, Changsha, China). The sections were then fixed onto the glass slides and stained with hematoxylin-eosin periodic acid Schiff (PAS) stain (H-E stain). The slides were examined microscopically and photos were taken using a microscope (Olympus BX51M, Tokyo, Japan) [80].

2.3 Statistical analysis:

Non-linear curve fitting functions were applied on normalized dose-response cell viability data obtained from the MTT assay and the IC_{50} values were calculated. All the experiments were performed in triplicate unless otherwise stated and results are expressed as mean ± SD. Two-way analysis of variance (ANOVA) with Dunnett's test (multiple comparisons against a control group) was performed for the comparison of percentage viability obtained from cytotoxicity assays. One-way ANOVA with post hoc test (Dunnett's multiple comparisons against control) was performed on the rest of the data using Graph Pad Prism 5. Significance levels of $p<0.05$ were considered

for the rejection of the nulls hypothesis. Statistical significance is expressed as *p < 0.05, **p < 0.01, ***p < 0.001 and ****p < 0.0001.

Chapter III: Results and Discussion

3.1 mTHPC (Temoporfin) loaded liposomes

3.1.1 Physicochemical characterizations

Liposomal formulations not only facilitate the administration of the hydrophobic PS but also avoid their precipitation into aggregated form and result in increased bioavailability with higher accumulation of PS at the tumor site [82]. By assimilating the PS into the liposome, the fluidity of the system can be altered and hence delivery process of the PS can be modified. mTHPC being a hydrophobic molecule, tend to align itself in the non-polar region of the liposomal bilayer membrane where it contributes to strong hydrogen-bonding interactions with the polar heads of the phospholipids (e.g. DPPC). mTHPC acts as a hydrogen donor because of the strong electron-withdrawing effect of the aromatic ring of its phenolic constituents [83]. This drug-lipid interaction lowers the molecular motion of phospholipids giving rise to more rigid and stable systems. Physically these interactions are also responsible for higher loading capacity and reduced fluidity of the membrane [84, 85]. In the current study, five different liposomal formulations were used to study their effect on cellular uptake, serum stability, biocompatibility, and light-induced toxicity. The composition of prepared liposomes and their physicochemical properties are presented in Table 1. All the prepared liposomal formulations contained DPPC as major vesicle-forming lipid combined with other lipids in specified molar fractions. No significant modification of liposomal size and zeta potential was induced owing to the presence of different DPPC molar ratios in different liposome formulations. The hydrodynamic diameter of all the formulations was in nanometric range, ranging from 106.0 ± 5.5 nm to 132.5 ± 8.6 nm with a PDI of less than 0.2 for the formulation containing DPPC/Cholesterol and DPPC/DOTAP, which represents the narrow monomodal distribution of liposomal vesicles. The liposome containing TEL, DPPG and DPPE-mPEG5000 in small molar fractions exhibited a PDI of more than 0.2. This relatively higher PDI can be attributed to the presence of smaller rod and disc-shaped micellar structure as well as the large PEG chains present in a formulation that also gives a stealth effect to the liposome [25]. It is also attributed to the presence of some bi- or oligolamellar vesicles as confirmed morphological studies. All the liposomal formulation possessed an overall negative zeta potential ranging from -13.2 ± 2.0 to -6.6 ± 0.3 mV except for DOTAP containing liposome having a surface charge of 24.33 ± 12.2.

Table 1. Physicochemical properties of mTHPC loaded liposomes. Each liposome contains 0.5 mg of mTHPC in 10 mg of total lipid. Hydrodynamic diameter is expressed as a function of particle size distribution by intensity. Values are expressed as mean ± SD for three independent measurements (n=3).

Formulation (mol %)	Diameter (nm) ± SD	PDI ± SD	Zeta Potential (mV) ± SD
DPPC: Cholesterol (90:10)	106.00 ± 5.50	0.17 ± 0.02	-9.45 ± 2.58
DPPC: DPPE-mPEG$_{5000}$ (95:5)	117.80 ± 8.12	0.20 ± 0.03	-9.59 ± 1.86
DPPC: TEL (90:10)	111.00 ± 1.30	0.27 ± 0.03	-15.50 ± 3.55
DPPC: DOTAP (90:10)	107.53 ± 8.89	0.12 ± 0.02	+25.70 ± 7.85
DPPC: DPPG (90:10)	115.24 ± 9.33	0.15 ± 0.02	-14.20 ± 2.82
DPPC: Cholesterol (90:10)-mTHPC	109.60 ± 2.20	0.13 ± 0.03	-6.68 ± 0.39
DPPC: DPPE-mPEG$_{5000}$ (95:5)-mTHPC	129.40 ± 9.60	0.25 ± 0.03	-8.98 ± 2.00
DPPC: TEL (90:10)-mTHPC	120.20 ± 3.31	0.23 ± 0.02	-13.20 ± 2.09
DPPC: DOTAP (90:10)-mTHPC	132.56 ± 8.66	0.16 ± 0.02	+24.23 ± 12.2
DPPC: DPPG (90:10)-mTHPC	127.71 ± 7.45	0.23 ± 0.03	-13.18 ± 5.68

3.1.2 Encapsulation efficiency (EE%)

The encapsulation efficiency of mTHPC loaded liposomes was determined using the ultracentrifugation method. The results of mTHPC encapsulation in the lipid bilayer (Table 2) showed that more than 70% of mTHPC was encapsulated in all the liposomal formulations. DPPC/Cholesterol (90:10) liposomes showed the least amount of drug encapsulated i.e. 78.0 ± 4% which increased to highest in DPPC/TEL liposomes with an encapsulation efficiency of 90.40 ± 2.60%. This comparative higher encapsulation can be attributed to the fact that the liposomes made from the polar lipid fractions of *S. acidocaldarius* show a remarkable stability. This stability of the liposomes is due to the ability of TEL to preserve membrane integrity due to tight membrane packing that results in retaining the entrapped molecules with a very low leakage problem [72]. The overall high drug load in all the liposomes can be credited to the hydrophobic and intermolecular interactions (hydrogen bonding) between drug and lipid molecules [85].

Table 2. The encapsulation efficiency of mTHPC loaded liposomes (0.5 mg of mTHPC per 10 mg of total lipid). Values are expressed as mean ± SD for three independent formulations (n=3).

Liposome Formulation	Theoretical drug load (µg/mL)	Practical drug load (µg/mL) ± SD	% EE ± SD
DPPC: Cholesterol (90:10)-mTHPC	500.00	390.49 ± 20.02	78.09 ± 4.00
DPPC: DPPE-mPEG$_{5000}$ (95:5)-mTHPC	500.00	408.54 ± 14.84	81.70 ± 3.26
DPPC: TEL (90:10)-mTHPC	500.00	452.01 ± 19.05	90.40 ± 2.60
DPPC: DOTAP (90:10)-mTHPC	500.00	364.40 ± 20.33	72.98 ± 6.11
DPPC: DPPG (90:10)-mTHPC	500.00	423.48 ± 16.33	84.67 ± 2.96

3.1.3 Morphological characterizations using AFM and Cryo-TEM

Morphological interpretations of the mTHPC loaded liposomes were conducted using AFM and Cryo-TEM studies. For AFM studies, the images were acquired using intermittent contact mode (tapping mode). This intermittent tapping of the cantilever tip reduces the shear forces applied on the liposomes, which can deform or burst the vesicles. Depending on the vesicle composition, interactions between the sample and substrate surface (e.g. glass or silica), as well as the continuous oscillation of the tip, can induce the deformation of vesicles. Longer sample deposition times on the substrate may also lead to the formation of planner vesicles [86]. In our AFM studies, all the liposomes appeared to be round or slightly oval-shaped. The diameter of the particles resulting from the analysis of the AFM cross-sectional micrographs was found to be in good correlation with the hydrodynamic diameter obtained from PCS measurements (Table 1). The height measured view was used to analyze the liposomal size distribution parameters (Fig. 19). Some irregularly shaped liposomes also spread on the silicon surface like a sheet of lipid monolayer that might be due to the adsorption of the lipid layer the silica surface as well as the liposomal disruption during the preparation of samples [59].

Cryogenic transmission electron microscopy (cryo-TEM) is a significant tool for the visualization of delicate ultrastructure of colloidal drug delivery systems (e.g. liposomes). It is the most widely used technique to study the shape, size and the overall composition of these carrier systems as it permits the evaluation of colloidal dispersions in the vitrified frozen state. It has an advantage that the rapid cooling of samples ensures minimum perturbation of the original samples [87].

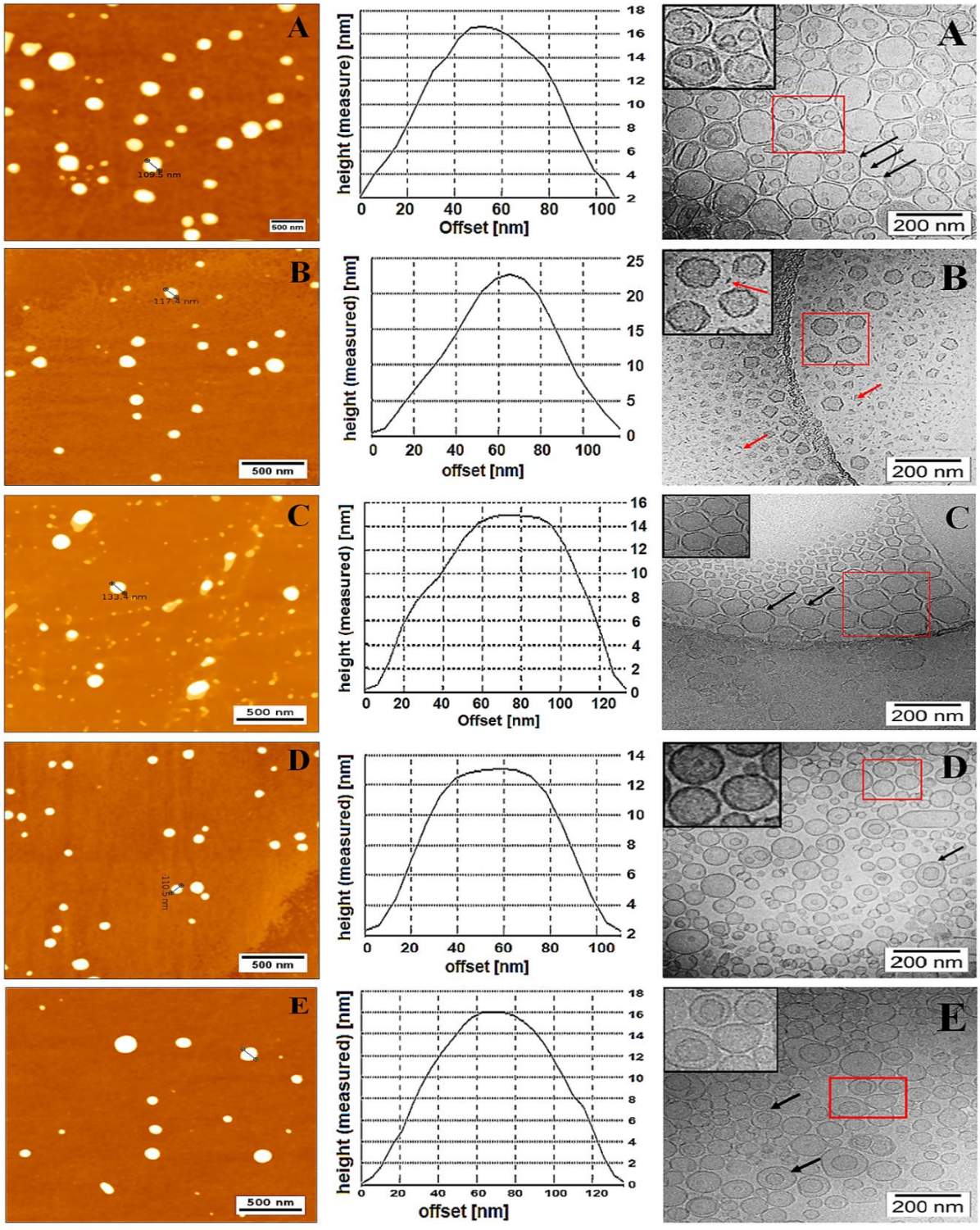

Figure 19. AFM micrographs (1st Row) and Cryo-electron tomographic images (3rd Row) showing the structural characteristics of mTHPC loaded liposomes. A) DPPC/Cholesterol B) DPPC/DPPE-mPEG5000 and C) DPPC/DOTAP D) DPPC/TEL E) DPPC/DPPG. For AFM studies, soft HQ: NSC14/AL_BS cantilevers were used to obtain the height measured images in trace direction. Middle pane (2nd Row) showing the cross-sectional profile of the liposomes along

the identified lines. The scale bar represents 500 nm scale for AFM images and 200 nm scale for Cryo-TEM images.

Fig. 19(A-E) (right pane) represents the typical cryo-TEM micrographs of mTHPC loaded liposomes. Preparation of liposomes by extrusion resulted in the population of mainly unilamellar vesicles but some fractions of bi- and oligolamellar vesicles, as well as multivesicular systems (black arrows in Fig. 19A, D & E), can also be observed. Liposomal formulation composed of DPPC/Cholesterol (90:10) has predominately shown the round and slightly elliptical structures (Fig. 19A). This can be attributed to the presence of cholesterol as well as the tight packing of the vesicles under the influence of which, the liposomes tend to appear oval-shaped [87]. For the formulations containing DPPE-mPEG$_{5000}$ in small molar fractions, disc-like associates (mixed micelles) can be assumed along with other vesicular structures (red arrows, Fig. 19B). These micelles appeared as small rods, disc or circular in shapes and can be credited to the presence of PEG chains in the formulation [88]. Nevertheless, the presence of discs needs more proof, because from the orientational point of view they should also appear as circular structures and ellipses. Liposomes also appeared somewhat circular and more or less polygonal in other formulations (Fig. 19C). This is because of the rigidity of the lipid bilayer that may influence the liposome shape, as the liposomes with a rigid lipid bilayer in the gel state often appear cubic or angular shaped particularly when the vesicles are small in size. In tetraether lipid-based formulation, liposomes also appeared circular or somewhat elongated (Fig. 19D). This is because of the rigidity of the lipid bilayer that may influence the liposome shape, as the TEL liposomes with a rigid membrane have the ability to preserve the membrane integrity by tight membrane packing of lipid molecules.

3.1.4 *In vitro* cell culture experiments

3.1.4.1 Cellular photodynamic therapy (cPDT)

The unirradiated and photo-destruction effect of mTHPC (free as well as liposome loaded) was investigated in the SK-OV-3 by assessing the percentage cell viability using MTT assay. It was carried out in the presence of different concentrations of mTHPC liposomes for 2 h in the dark followed by subsequent irradiation of the cells with red light (λ=652 nm). The initial 1 h incubation did not show any significant effect on the cell viability (data not shown), indicated the need for increased incubation time. Treatment of the cells with mTHPC (dissolved in 0.1% DMSO) without subsequent irradiation resulted in a dose-dependent reduction of cell viability inferred as dark toxicity. This dark toxicity was evident at the mTHPC concentration equal to or

above 2.5 μM (1.7 μg/mL) (Fig. 20). In contrast, mTHPC encapsulated in liposomal formulations did not show any dark toxicity. These findings were in line with the previous studies conducted by another working group [89]. The survival of SK-OV-3 cells, incubated with different mTHPC concentrations and irradiated with varying light fluences is represented in Figure 20. At the light dose of 0.05 Jcm^{-2}, the cell viability was reduced to less than 40% in the treated groups (except for DPPC/TEL and DPPC/DOTAP liposomes) as compared to untreated controls. The untreated control groups-maintained cell viability of 95-98% which confirms that the application of irradiation only, did not produce any significant cell destruction. For the formulation containing tetraether lipids, the cell viability was still recorded at about 60%. This could be due to the slower release of PS from the liposomal membrane, stabilized in the presence of tetraether lipids, while the lower effect produced by the DOTAP liposomes can be attributed to the slower uptake of the liposomes [72]. With increasing fluence, the cell viability continuously decreased in all the formulations, ending up at 18-20% at 1 $Jcm-^{2}$. Similar dose-response curves were obtained when the fluence was kept constant and the concentration of mTHPC was varied between 0.05 and 5 μM [90]. The half-maximal inhibitory concentration (IC_{50}) of the liposomes was also reduced proportionally, as the fluence or PS concentration into the cells was increased. The highest reductions of IC_{50} (Table 3) were recorded in the PEGylated and DPPG containing formulations. The statistical evaluation using two-way ANOVA with Dunnett's multiple comparisons showed that the PDT effect produced by different light fluences differed significantly ($p<0.0001$) to the unirradiated samples (dark control).

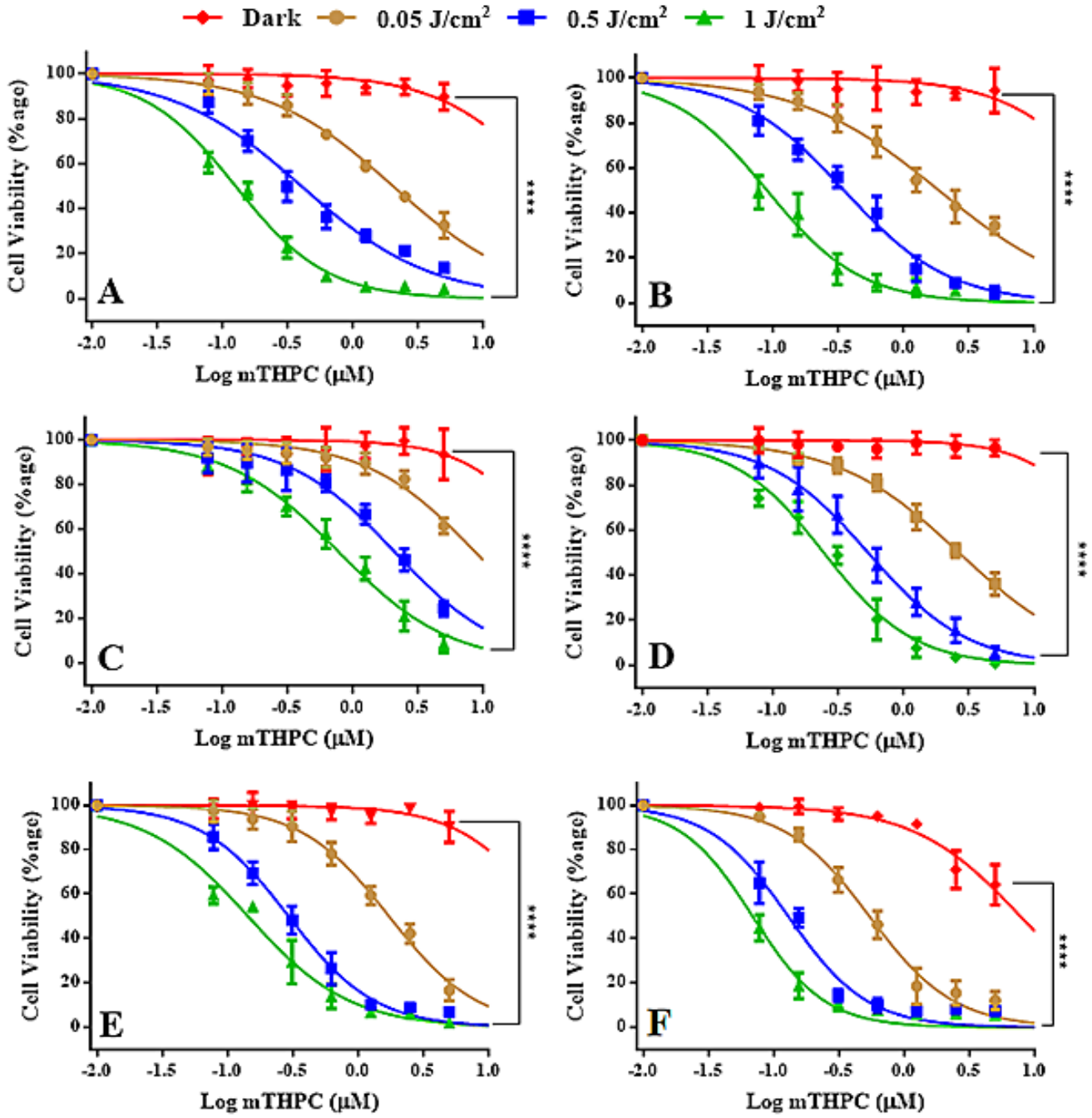

Figure 20. Dose-response nonlinear curves representing dark & photo-induced cytotoxicity to SK-OV-3 carcinoma cells. mTHPC formulations; DPPC/Cholesterol (A), DPPC/DPPE-mPEG5000 (B), DPPC/DOTAP (C), DPPC/TEL (D), DPPC/DPPG (E) and free mTHPC dissolved in 0.1% DMSO (F) were incubated for 2 h and then irradiated with series of light exposures of 0.05, 0.5 and 1 Jcm^{-2} with red light (λ=652 nm). Whereas dark represents the formulations without irradiation. Each value is represented as the mean ± SD for three independent experiments. For the statistical analysis, the comparison was done against the dark treatment. P values ($p<0.05$) were considered significant and denoted as '****' ($p<0.0001$) and '**' ($p<0.01$).

Table 3. The half-maximal inhibitory concentration (IC_{50}) values of the photo-cytotoxicity induced by the mTHPC loaded liposomes and free mTHPC (dissolved in DMSO) in SK-OV-3 cells. The IC_{50} values were calculated by non-linear curve fitting from the graphs and tabulated for the respective radiation doses (fluences).

Formulations	Red Fluence (J/cm^2) λ= 652nm	IC_{50} (µM)	Blue Fluence (J/cm^2) λ = 457nm	IC_{50} (µM)
DPPC/ CH.- mTHPC	0.05	2.66	1	14.3
	0.5	0.53	5	0.64
	1	0.24	10	0.26
DPPC/ DPPE-mPEG$_{5000}$-mTHPC	0.05	1.87	1	3.08
	0.5	0.35	5	0.28
	1	0.09	10	0.15
DPPC/ DOTAP- mTHPC	0.05	8.68	1	26.5
	0.5	2.10	5	2.65
	1	0.78	10	1.01
DPPC/ TEL-mTHPC	0.05	3.40	1	20.6
	0.5	0.80	5	1.46
	1	0.65	10	0.94
DPPC/ DPPG- mTHPC	0.05	0.17	1	6.03
	0.5	0.29	5	1.11
	1	0.14	10	0.40
mTHPC-Std	0.05	0.54	1	2.91
	0.5	0.13	5	1.11
	1	0.07	10	0.27

In order to evaluate the photodynamic effect produced by mTHPC after activation at a different wavelength, all the formulations were irradiated with a series of light fluences at a wavelength of λ=457 nm. Similar to previous studies, free mTHPC (dissolved in DMSO) produced dark toxicity but none of the liposomal formulations affected the cell viability without application of the fluence [90].

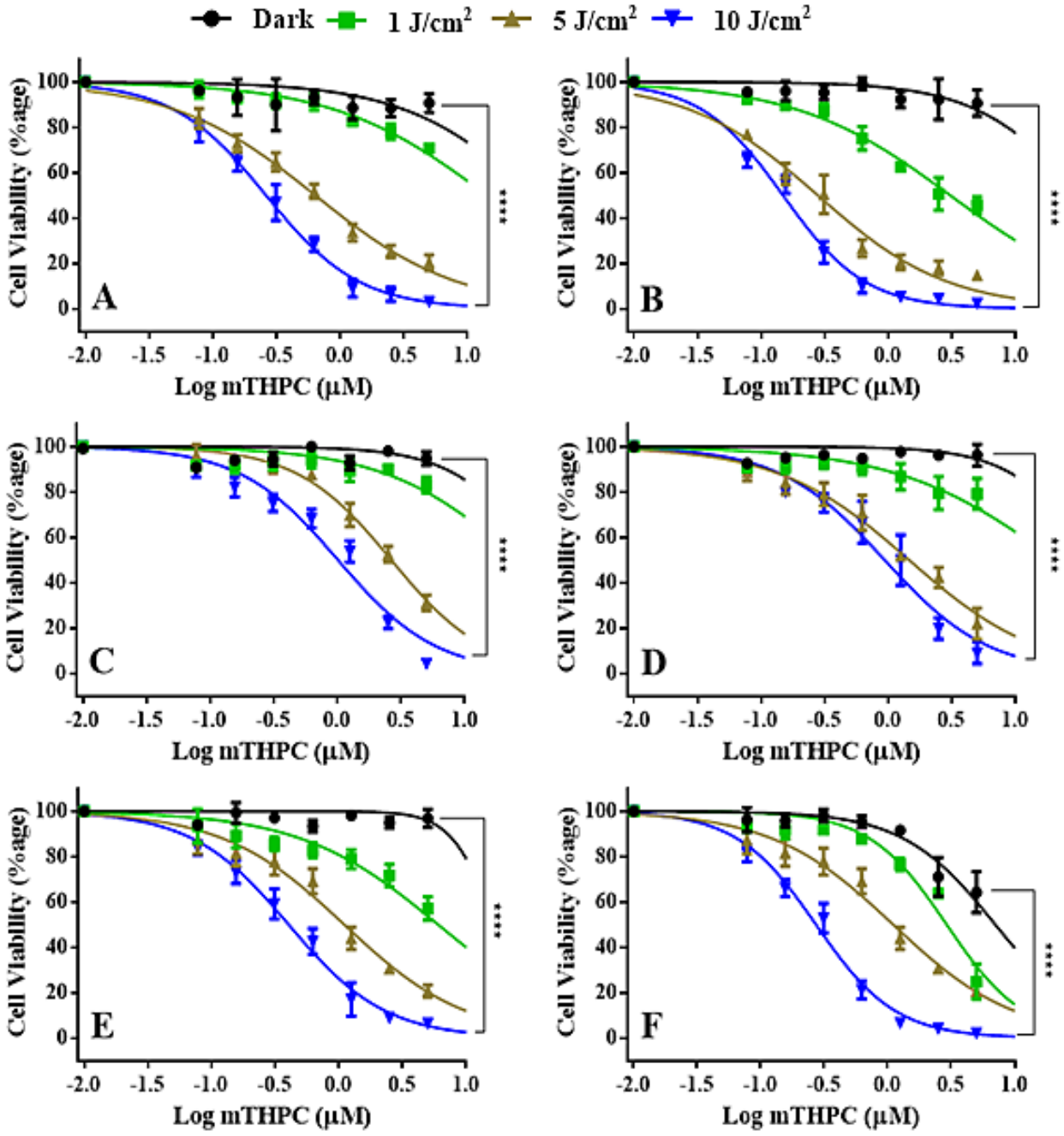

Figure 21. Dose-response nonlinear curves representing photo-induced cytotoxicity to SK-OV-3 carcinoma cells. mTHPC formulations; DPPC/Cholesterol (A), DPPC/DPPE-mPEG5000 (B), DPPC/DOTAP (C), DPPC/TEL (D), DPPC/DPPG (E) and free mTHPC dissolved in 0.1% DMSO (F) were incubated for 2 h and then irradiated with series of light exposures of 1 Jcm^{-2}, 5 Jcm^{-2} and 10 Jcm^{-2} with blue light (λ=457 nm). Whereas dark represents the treatments without irradiation. The half-maximal inhibitory concentration (IC_{50}) was calculated by non-linear curve fitting. Each value is represented as the mean ± SD for three independent experiments. For the statistical analysis, the comparison was done against the dark treatment. P values ($p<0.05$) were considered significant and denoted as '****' ($p<0.0001$) and '**' ($p<0.01$).

When irradiated with a light dose of 1 Jcm^{-2}, only liposome comprising DPPC/DPPE-$mPEG_{5000}$ was able to reduce the cell viability to 52% comparable to the photo-toxicity produced by free mTHPC. This could be attributed to the presence of mixed micelles and smaller liposomes in the formulation. These micelles are quickly taken up by the cells, the photosensitizer is release readily resulting in the immediate burst effect [25]. By further increasing the fluence level, the cell viability gradually decreased to 20% in all the formulations at a light dose of 10 Jcm^{-2} (Fig. 21). It was evident from the cell viability data obtained from photodynamic therapy, that in order to produce a comparable photo-destruction effect as produced by 1 Jcm^{-2} (when irradiated at 652 nm), a ten-fold higher fluence (i.e. 10 Jcm^{-2}) was required (when irradiated at 457 nm). This could be credited to higher light absorption, increased penetration depth (i.e. 2-3 mm as compared to 0.3 mm in blue light) as well as the higher quantum yield of light at longer wavelength region (i.e. red) as described by Kiesslich et al [91].

3.1.4.2 Determination of reactive oxygen Species (cROS)

In order to quantify the ROS generation and oxidative stress during the photodynamic treatment of the SK-OV-3 cells, the ROS assay was performed. It is based on cellular esterase-mediated hydrolysis of acetate group and intracellular oxidation of non-fluorescent H_2DCFDA (2`,7`-dichlorodihydrofluorescein) into green fluorescent DCF. The data obtained from the photodynamic mediated production of ROS is shown in Fig. 22 In our experiments, the irradiated liposomal formulations produced increased levels of intracellular ROS as compared to non-irradiated ones (dark). The highest amount of ROS was produced by PEGylated liposomes owing to the presence of mixed micellar structures in the formulation resulting in the higher uptake of the PEG-PE based micellar structures [25]. Because of their smaller size, they exhibit a spontaneous penetration into the interstitium of tumor vasculature due to enhanced permeability and retention effect. Diffusion and accumulation parameters of the drug carriers in tumors have been shown to be highly dependent on their cut off size. The higher uptake of these mixed structures, in turn, deliver increased quantities of the drug to the tumor resulting in higher cytotoxicity [92]. It indicates the liposomes containing DPPE-$mPEG_{5000}$ caused the highest damage to the cell as compared to other liposomes. Nevertheless, in both experiments, cells were irradiated at the same energy level with different wavelengths, but the amount of ROS produced was higher when irradiated with the red light. These results were also in line with our previous results obtained from the cell viability assay. It can be suggested that the production of ROS is very crucial for an effective photodynamic treatment of cancer cells.

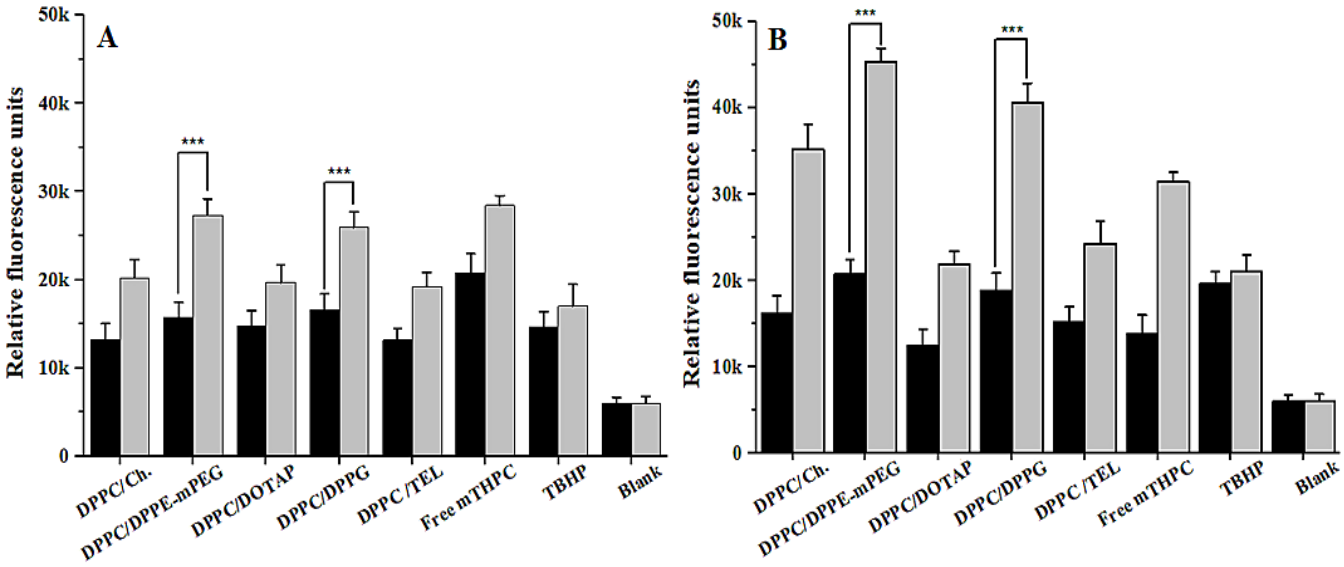

Figure 22. Production of reactive oxygen species after dark (black bars) and photodynamic treatment (light grey bars) of SK-OV-3 cells with mTHPC loaded liposomes. Following 2 h incubation, SK-OV-3 cells were irradiated at a light dose of 1 Jcm^{-2} at $\lambda = 457$ nm (A) and at $\lambda =$ 652 nm. TBHP (50 µM) was used as a positive control. All the measurements were performed in triplicate and values were expressed as mean ± SD (n=3)

3.1.4.3 Intracellular uptake studies

The cellular uptake and intracellular distribution of free and liposome-bound mTHPC were evaluated using CLSM (Fig. 33). Therefore, SK-OV-3 cells were incubated with the different liposomal formulations (5 µM) at 37ºC for 2 h. A considerable localization of mTHPC was observed in both dark and irradiated samples. The red fluorescence of mTHPC loaded liposomes could be readily detected as a diffuse signal throughout the cytoplasm with particularly intense localization in the perinuclear region. The fluorescence distribution of the intracellular mTHPC did not show any significant difference between the liposomal formulations and free mTHPC (dissolved in DMSO). The cells were counterstained with Sytox green™ (50 nM) and were observed as a green fluorescent signal in the nuclear region. The co-localization of red and green fluorescence in the merge channel showed no sign of mTHPC localization in the nucleus. From the CLSM micrographs, it was observed that PEG-PE based liposome showed a comparable intracellular localization as that of free mTHPC which can be attributed to higher uptake of the combination of micelles and liposomes present in PEG-PE based formulation. On the basis of these observations, it was inferred that intracellular activation of mTHPC leads to the destruction of subcellular organelles resulting in cell death. Confocal microscopy also proved that a comparable fluorescence was emitted from the individual cells, which indicated the uniform

uptake of mTHPC by the cells. This examination could be an important prerequisite for an effective PDT in tumor tissue, focusing on the complete destruction of cancer cells.

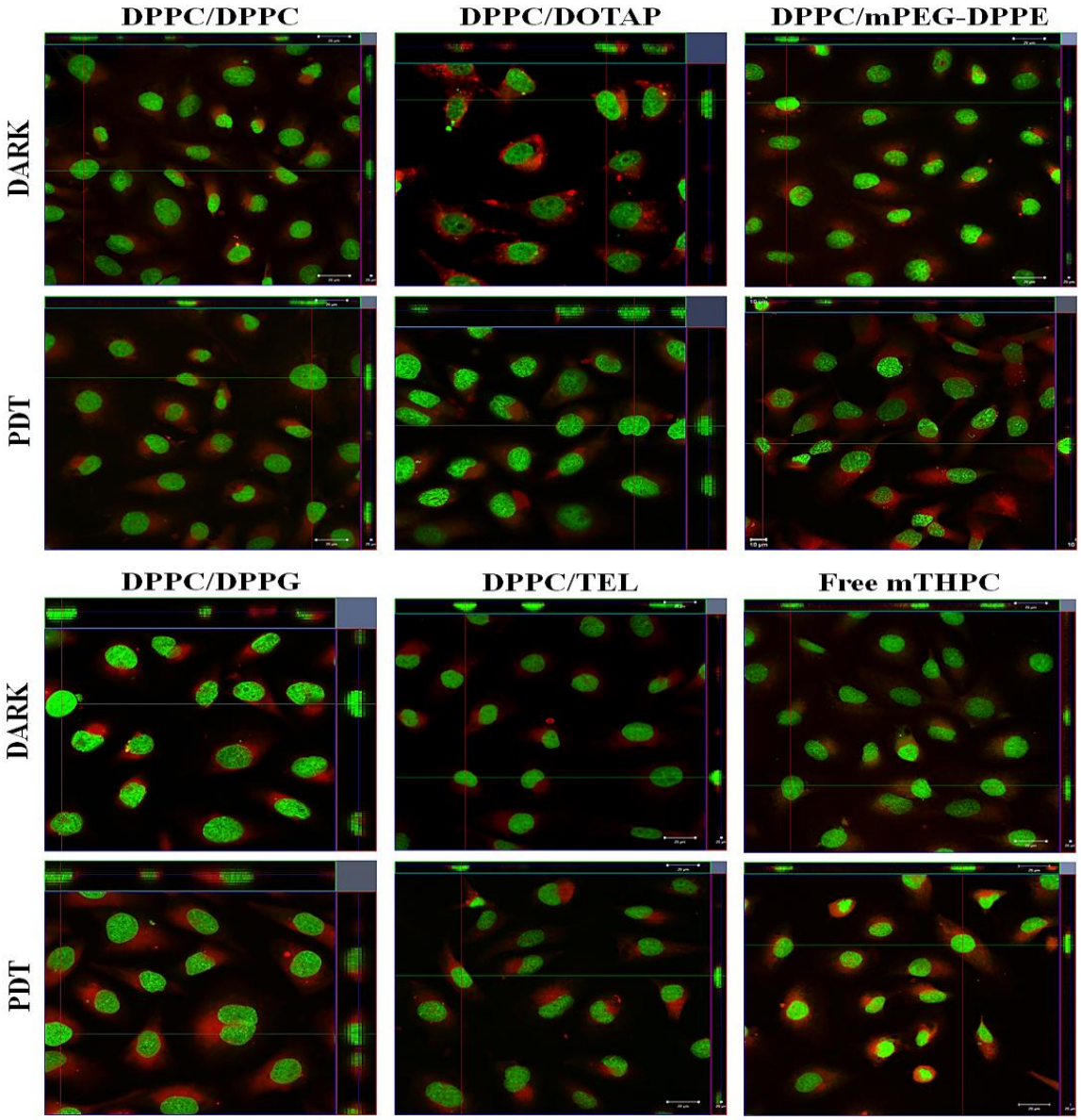

Figure 23. CLSM micrographs of SK-OV-3 cells incubated with 5 µM mTHPC loaded liposomes and free mTHPC (dissolved in DMSO) for 2 h at 37ºC. The cells were subsequently irradiated at 652 nm with a radiation fluence of 0.05 Jcm^{-2}. The untreated cells were taken as negative control (NC). The nucleus was counterstained using Sytox green™ (50 nM). The cellular uptake was observed using fluorescence detection filters for Sytox green™ (ex/em 504⁄523 nm) and mTHPC (ex/em. 420/ 652 nm). The scale bar represents 20 µm scale.

3.1.4.4 *In vitro* genotoxicity assessment

The comet assay is a cytogenic technique used mainly in the field of toxicological studies. Recently, it has also been employed in the assessment of the genotoxicity that can be caused by

the photodynamic treatment of the cells. The alkaline version of the comet assay is a simple and rapid *in vitro* screening method for analyzing and measuring the DNA single-strand breaks (SSB) or alkali labile sites [93]. The principle of the comet assay is based on the fact that DNA strands which occur as a negatively charged supercoiled structure in the nucleus can be fragmented due to the exposure to the toxins or drug treatments. These DNA SSBs are drawn towards anode under the influence of the electric field and appear as the olive tail. The measure of this tail moment is identified as the index of DNA damage. Due to the fact that photosensitizers upon administration may also accumulate into the normal tissue and may cause complications under low light dose or normal light (i.e. room or sunlight) [94]. Form Fig.24, it can be observed that no direct DNA strand breakage was caused by photodynamic treatment of mTHPC encapsulated liposomes as observed from the olive tail moment data. From the data, it was inferred that irradiation of the SK-OV-3 cells after treatment with a low drug or light dose (0.05 Jcm^{-2}) did not cause any significant DNA damage and there was no apparent increase in the olive tail. Also, it was observed that there was no DNA damage in the absence of light (data not shown). From the above-mentioned results, it can be assumed that mTHPC can be used clinically with no or minimum incidence of genetic toxicity [68].

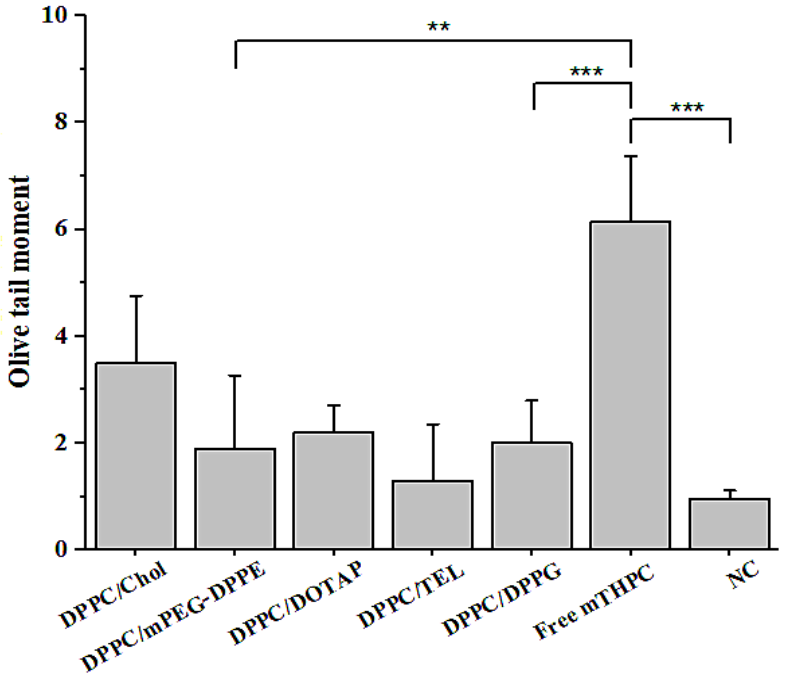

Figure 24. Distribution of comet tail moment (genotoxicity) to SK-OV-3 cells obtained from alkaline comet assay. The cells were incubated with mTHPC loaded liposomes for 2 h at an equitoxic dose to produce 80% cell viability to avoid false-positive response. Irradiation was performed at a light dose of 0.05 Jcm^{-2}. Each value is represented as the mean ± SD for three

independent experiments. For the statistical analysis, the comparison was done against the dark treatment. P values ($p < 0.05$) were considered significant and denoted as '****' ($p< 0.0001$) and '**' ($p< 0.01$).

3.1.4.5 Hemocompatibility studies

Hemocompatibility studies serve as a critical link between *in vitro* and *in vivo* studies because the data obtained from these studies can be used to tailor the dosage form for the *in vivo* experiments [95]. Hemolysis assay was used to investigate the extent of erythrocyte destruction induced by the liposomal formulations and was conducted by estimating the amount of hemoglobin released after erythrocyte damage. This hemoglobin is then converted to oxyhemoglobin in the presence of atmospheric oxygen. The oxyhemoglobin can be detected and measured spectrophotometrically. This assay can be used to determine the safe concentrations that can be administered intravenously [58]. In our study, it was observed that all the mTHPC loaded liposomal formulations exhibit very low hemolytic properties as compared to the free drug (Fig. 25). The hemolysis potential expressed by all the formulation was below 10% while the free drug showed a relatively higher hemolytic effect (i.e. 25%). Activated partial thromboplastin time (aPTT) was performed to evaluate the effect of liposomal formulation on the coagulation time. The coagulation time of all the formulations was found to between 30-40 s which was well under the standard range. aPTT values above 50 s are clinically significant while the value above 70 s indicates the continuous bleeding and hemorrhage. The free drug exhibited a higher coagulation time of 47 s (Fig. 25). These findings suggested that our mTHPC loaded liposomal formulations are non-toxic as well as highly biocompatible for i.v. injection.

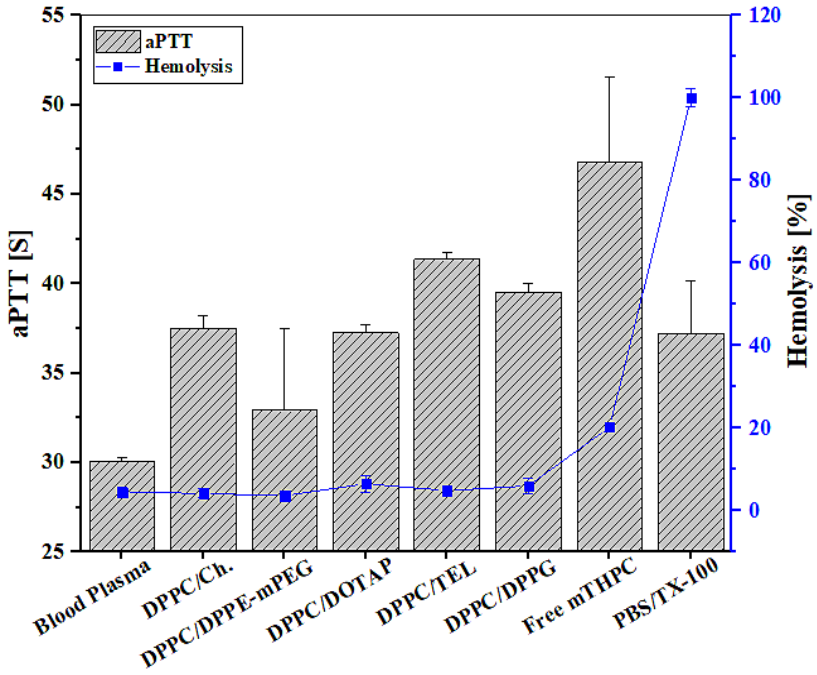

Figure 25. Hemocompatibility assay: aPTT test (left) & Hemolysis assay (right) of mTHPC loaded liposomes. All the formulations were tested at 10 x concentrations. Blood plasma and Triton™ X-100 were used as negative and positive control respectively. All the samples were measured in triplicate and the values were expressed as mean ± SD (n=3).

3.1.4.6 Photo-thrombic activity of mTHPC liposomes (CAM assay)

CAM is an alternative to *in-vivo* experiments that can be used to evaluate the efficacy of the delivery system. Vascular targeted photo-destruction of CAM is an important connection towards the targeting of tumor microvasculature thereby destroying the tumor tissue. To determine the extent of damage to the vasculature, PDT to the CAM was performed. In our experiments, it was observed that injection of the empty liposomes or normal saline only, produced no changes to the vasculature. Also, the additional application of the light dose to the CAM without prior treatment did not affect the integrity and profusion of the vasculature. To distinguish the changes in blood flow within CAM, 100 µl of mTHPC loaded liposomes were injected intravenously followed by irradiation of the injection site. It was observed the drug-light interval (DLI) plays a vital role in the photo-destruction of CAM vessels. Short DLI (e.g. 15 or 30 min) did not produce any effect and CAM vasculature remained intact. But when the irradiation was performed 1 h post liposomes injection, delayed local destruction of CAM vasculature was observed within the irradiated area. Typical stereographs of CAM at different time periods after i.v injection based on mTHPC loaded liposomes are demonstrated in Fig. 26 and 27. Nevertheless, all the formulations showed mild closure of smaller capillaries that onset at t_{post}= 10 min (data not shown), the larger vessels still

remain uninjured and intermittent blood flow was observed. The effect was more pronounced in liposome comprising of DPPC/DPPE-mPEG$_{5000}$ followed by DPPC/DPPG liposome. At t_{post}= 60 min, a complete occlusion of large vessels with the characteristic decline in blood flow was visible. These findings were in line with the previous observations regarding *in-ovo* PDT [96]. Ultimately at t_{post}= 24 h, a complete destruction of CAM vasculature at the irradiated area was evident. Scar formation due to the effective closure of all the blood vessels was observed in the CAM after 24 h of the treatment while the embryo still survived. There was a mild or no effect observed when free mTHPC (dissolved in PBS/ DMSO) was injected. This could be attributed to the dimerization of drug molecules that resulted in the reduction of its efficacy.

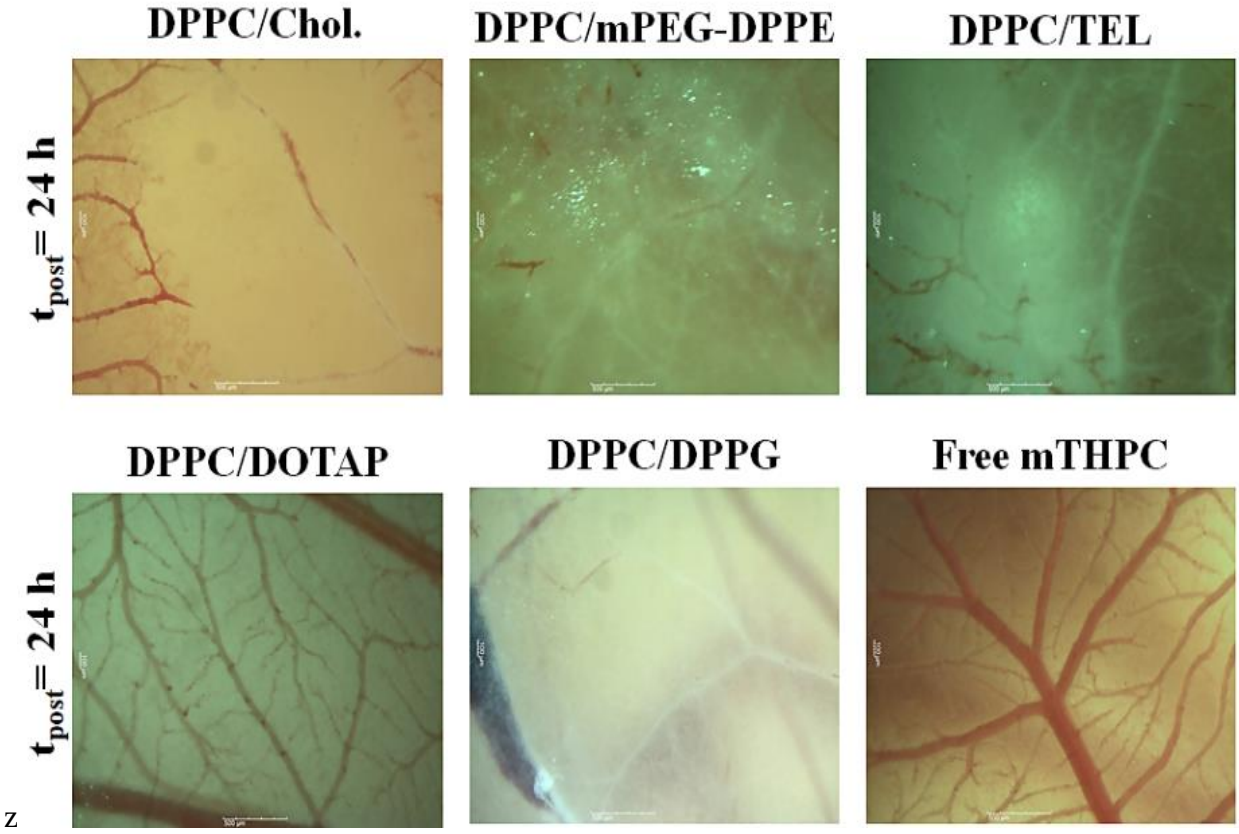

z

Figure 26. Stereomicrographs of CAM representing PDT mediated scar formation due to the effective closure of CAM vasculature at the irradiated area. The observations were continued till 48 h after that experiment was terminated. The embryo still survived the treatment indicating the local destruction of the vasculature. The irradiation was performed at a light dose of 4.8 Jcm^{-2} using a red laser diode (652 nm, 40 mW) with Weber needle. The scale bar represents the 500 µm scale.

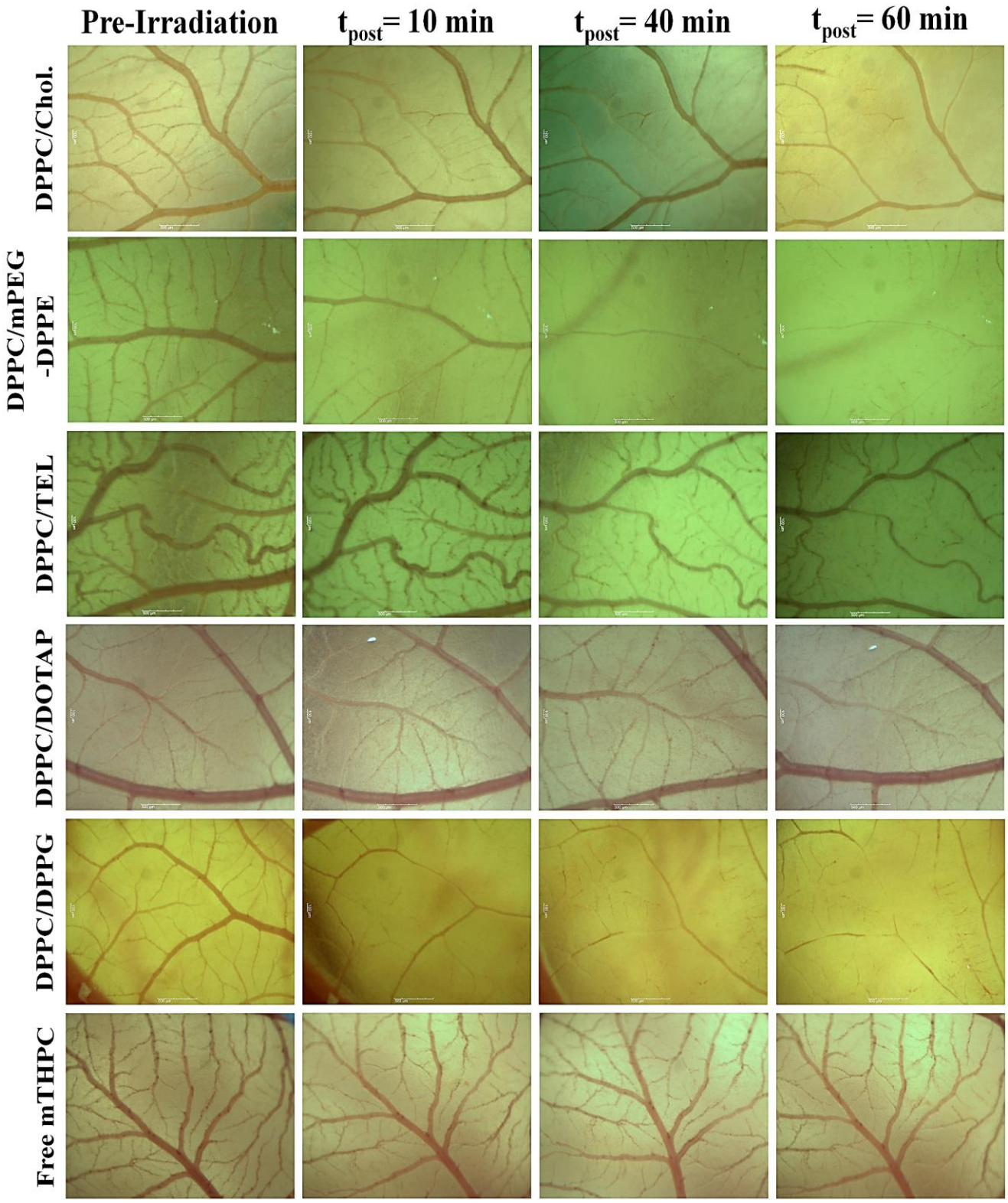

Figure 27. Typical stereomicrographs of CAM representing PDT mediated occlusion of CAM vasculature. Images were acquired before (dark), immediately after irradiation (t_{post} = 0 min) and at t_{post} 10, 40- and 60-min post i.v injection of mTHPC loaded liposomes 0.5mg mTHPC/10mg of lipids). Irradiation was performed at a light dose of 4.8 Jcm^{-2} using a red laser diode (652 nm, 40 mW) with Weber needle. The scale bar represents the 500 µm scale.

3.2 Lipid coated polymeric nanoparticles:

3.2.1 Physicochemical characterizations:

In the current study, PLGA nanoparticles were prepared utilizing emulsion solvent evaporation technique. Two different sizes of THP loaded PLGA nanoparticles (i.e. 200nm and 400nm) were prepared to compare their physicochemical properties and efficacy against the cancer cells. After the pilot study, the PVA concentrations were optimized to be 1% and 0.3% to produce 200nm and 400nm particles respectively, while maintaining all the other parameters constant. The particle size distribution and their surface charges are exhibited in Table 1. It can be observed that THP NP showed a narrow size distribution of 194.9 ± 2.7 nm and a low polydispersity index of 0.08 ± 0.02 as compared to PIR NP. This was due to the presence of a higher concentration of the emulsifier in THP NP causing the formation of stable emulsion with smaller and uniform droplet size, leading to the formation of smaller sized nanoparticles with low polydispersity index. The lower concentration of PVA in PIR NP not only produced a higher particle size of 373.4 ± 8.8 nm but the polydispersity index was also high indicating a bimodal distribution of particles (i.e. 0.23 ± 0.02) [52]. The addition of the THP in the nanoparticle formulations produced a slight increase in the particle size (10-15nm approximately) and size distribution. All the nanoparticle formulations exhibited a positive surface charge ranging from 8.3 ± 1.6 mV to 10.5 ± 1.7mV, owing to the presence of a small amount of chitosan in the formulations.

The composition of prepared liposomes and their physicochemical properties are presented in Table 4. The hydrodynamic diameter was determined to be 100.5 ± 3.4 nm with a PDI of 0.19 ± 0.06 representing the narrow monomodal distribution of liposomal vesicles. mTHPC loaded liposomes showed a slightly higher hydrodynamic diameter and PDI. This could be due to the fact that mTHPC orientate itself in the bilayer membrane and interacts with the polar heads of lipids through the hydrogen bonding leading to a slight increase in vesicle size [85]. Liposomal formulation possessed an overall negative zeta potential (-12.9 ± 0.5 mV). The lipid enveloped nanoparticle was produced by coating the THP NP with the mTHPC loaded PEGylate liposome (i.e. DPPC/DPPG /mPEG-DPPE-$_{5000}$). The hydrodynamic diameter of LCNP was found to be 208.6 ± 2.2 nm with no significant increase in the PDI. A small increase in the hydrodynamic diameter (i.e. 4 nm) of the LCNP was observed when compared to uncoated PLGA NP. Assuming the thickness of the lipid membrane to be about 4-5 nm, our results were in line with the previous experiments done by our workgroup [54].

Table 4. Physicochemical properties of THP loaded PLGA nanoparticles, mTHPC loaded liposomes, and lipid-coated nanoparticles (LCNP). Each THP loaded PLGA nanoparticle contains 2 mg of THP and 100 mg of PLGA. Each liposome consists of 0.5 mg of mTHPC in 10mg of total lipids. Hydrodynamic diameter is expressed as a function of particle size distribution by intensity. Values are expressed as mean ± S.D for three independent measurements (n=3).

Formulations	Diameter [nm]	PDI	ζ Potential [mV]
PLGA NP	194.9 ± 2.7	0.08 ± 0.02	8.3 ± 1.6
THP NP	204.7 ± 3.4	0.10 ± 0.03	7.6 ± 1.6
NP-Blank	373.4 ± 8.8	0.23 ± 0.02	8.6 ± 1.4
PIR NP	405.7 ± 10.0	0.23 ± 0.06	10.5 ± 1.7
LP-Blank	100.5 ± 3.4	0.19 ± 0.06	-12.9 ± 0.5
mTHPC-LP	108.8 ± 2.1	0.21 ± 0.02	-12.7 ± 1.2
LCNP	208.6 ± 2.2	0.11 ± 0.01	5.9 ± 1.1

3.2.2 Encapsulation efficiency:

The encapsulation efficiency of the THP loaded PLGA nanoparticles and mTHPC loaded liposomes were determined using the solvent extraction method. For this purpose, unentrapped drugs from the nanoparticles and liposomes were removed using centrifugation and ultracentrifugation technique respectively. A direct method of dissolving the nanoparticle or liposomal drug pellet was used and ultimately the actual amount of THP in PLGA nanoparticles and mTHPC in liposomes was measured. Being a highly lipophilic molecule, mTHPC tends to align itself in the hydrophilic milieu of the liposome and showed an overall high drug loading of 80.5 ± 5.1 % [83, 85]. Similarly, the optimized nanoparticle formulations also showed a relatively high encapsulation efficiency (EE) with THP NP showing an EE of 86.5 ± 4.5% and PIR NP showing EE of 74.3 ± 5.4%. This higher EE can be explained due to the fact that both, the THP and PLGA are soluble in ethyl acetate employed for the nanoparticle preparation [53].

3.2.3 Morphological characterizations:

3.2.3.1 Atomic force microscopy (AFM)

Morphological characterizations were conducted using atomic force microscopy (AFM) and transmission electron microscopy (TEM). AFM studies were carried out using intermittent contact mode and images were acquired in height measured trace, lock in amplitude as well as lock in-

phase mode. Fig. 28 shows the typical AFM monographs of mTHPC loaded liposomes, THP loaded nanoparticles and lipid-coated polymeric nanoparticles. The AFM micrographs manifested perfectly round shaped mTHPC liposomes as well as THP loaded nanoparticles. The height measured view was used to analyze the size distribution parameters of the nanocarriers. Some irregularly shaped liposomes also tend to spread on the silicon surface like a sheet of lipid monolayer that might be due to the liposomal disruption during the preparation of samples. The AFM size investigations were in correlation with the hydrodynamic diameter obtained from DLS studies. A uniform distribution of the THP nanoparticles (Fig. 28A-a) with a smooth surface can be seen which represents the unimodal distribution of the nanoparticles in the formulation [59, 97]. Whereas, PIR NP showed a tendency to aggregate forming clusters. This explains the broad range of particle sizes and the high polydispersity observed. This agglomeration tendency was likely due to insufficient steric stabilization by the PVA (Fig 28A-b). The lipid layer on the nanoparticle surface can also be visualized with AFM images (Fig. 28B). In some places, the nanoparticles are not completely covered with the lipid bilayer and show some gaps in between the coating. The thickness of the absorbed lipid bilayer was determined from these gaps and was found to be in the range (i.e. 4-5nm) [54].

3.2.3.2 Transmission electron microscopy (TEM)

Transmission electron microscopy (TEM) is the most widely used technique to study the size, shape, and morphology of the carrier system. TEM allows the imaging of the liposomes and nanoparticles in their original form, without further need of the sample modification (e.g. labeling, fixation, etc.). The samples were negatively stained using 2% uranyl acetate. Fig. 29 shows the representative TEM micrographs of the mTHPC loaded liposomes (Fig. 29a), THP loaded PLGA nanoparticles (Fig. 29b) and lipid-coated nanoparticles (Fig. 29e). TEM observations revealed mostly circular unilamellar lipid vesicles [58]. In addition, some irregularly shaped liposomes can also be seen in the formulation which could be caused by the quick drying of the liposomes during the staining process as the PEG conjugated DPPE and DPPC were stained using this dye to enhance electron density and improve the image contrast.

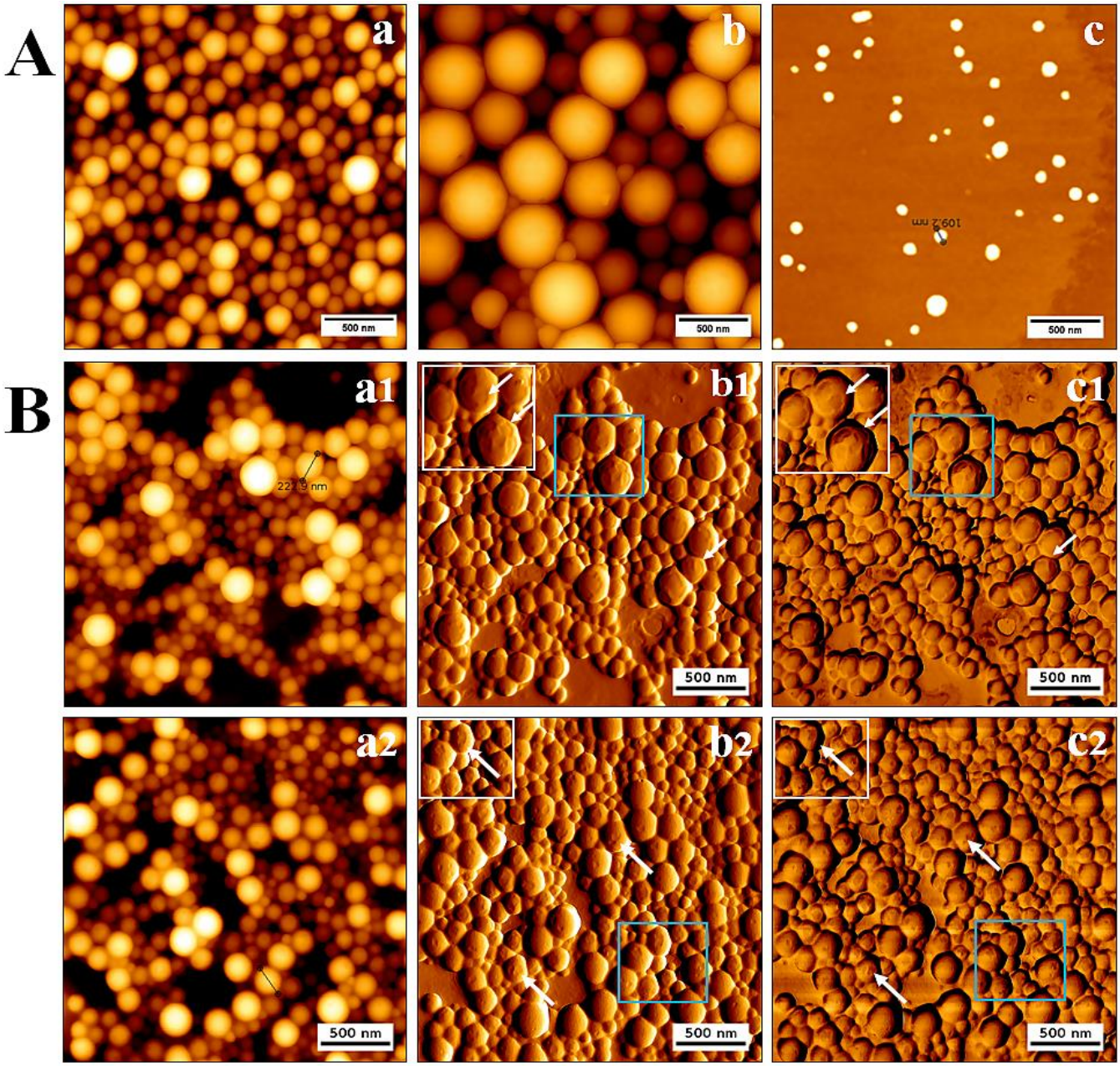

Figure 28. Illustration of surface morphology of **A)**: THP NP a); PIR NP b) and mTHPC- LP using AFM. Pane **B)** represents the AFM micrographs of lipid-coated nanoparticles a1-2) height measured view; b1-2) lock-in amplitude view and c1-2) lock-in phase view. HQ: NSC14/AL_BS cantilevers tips were used for liposomes while HQ: NSC16/AL_BS cantilevers were used for the uncoated and coated nanoparticles. The scale bar represents 500 nm scale.

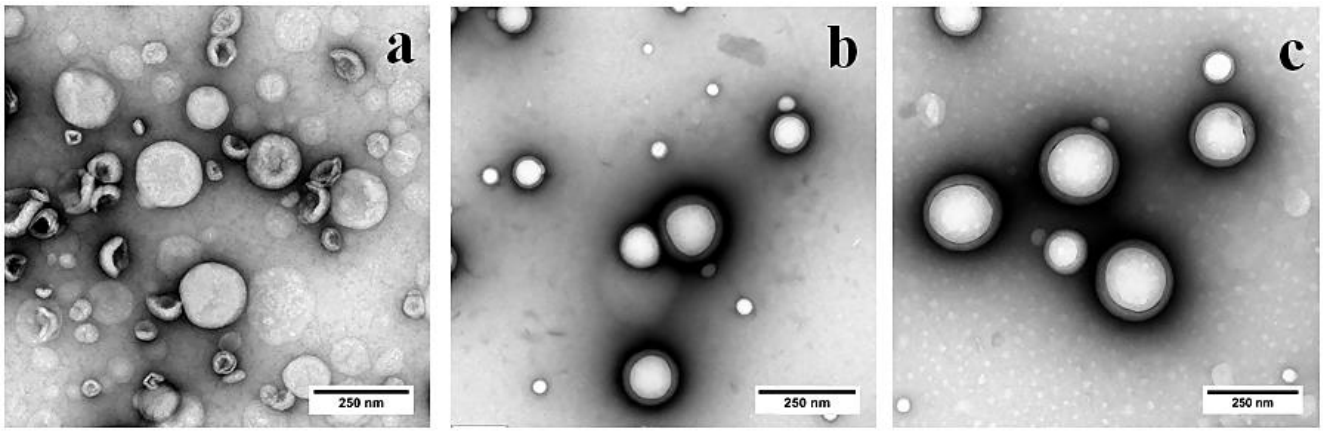

Figure 29. Typical TEM micrographs of nanoformulations including a) mTHPC-LP; b) THP NP and c) LCNP. The samples were stained with 2% uranyl acetate for 5min prior to imaging. The scale bar represents a 250 nm scale.

Furthermore, polymeric nanoparticles with a lipid layer adsorbed on their surface as a dim ring surrounding the polymeric core-shell of hybrid carriers can also be observed clearly [98]. This lipid coating is the result of the non-covalent weak electrostatic attractions between the lipid bilayer and polymeric nanoparticles. The size of these liposomes and lipid-coated vesicles obtained by TEM micrographs was in good agreement with the size distribution obtained by particle size analyzer [98, 99].

3.2.4 *In vitro* drug release profile:

The in vitro drug release from the pirarubicin loaded PLGA nanoparticles was conducted in PBS (pH 7.4) containing 1% tween 80. Tween 80 is a commonly used nonionic emulsifier used to enhance the solubilization of the hydrophobic drug by the formation of the micelles. Because of the very low aqueous solubility of pirarubicin, the addition of this solubility enhancing component was necessitated to ensure the sink conditions and to achieve detectable UV/VIS concentrations during the release studies [53]. The drug release mechanisms are important as the drug-polymer formulation because of the proposed application in sustained drug delivery. Different drug release mechanisms from PLGA nanoparticles have been reported including: (a) the desorption of the drug absorbed to the particle surface, (b) diffusion through the nanoparticle matrix, (c) erosion of nanoparticle matrix and (d) combination of diffusion and erosion. In order to manipulation the drug release from the polymer matrix, a complete understanding of these mechanisms is required [100]. The drug release from the PLGA nanoparticles is shown in Fig. 30. It is evident that the pirarubicin loaded PLGA nanoparticles followed a typical biphasic drug release pattern from the nanoparticle matrix with an initial burst release of 40% for THP-NP and 32% for PIR-NP within

first 24 h. This burst release was followed by a sustained release of the drug from polymer matrix over the period of 7 days. This initial phase of drug release is mainly attributed to desorption or diffusion of the drug located at the large surface of the nanoparticles or loosely bound with the polymer matrix. The remaining unreleased drug was assumed to be tightly associated with PLGA molecules and/or well entrapped within the nanoparticle matrix and occurs mainly by diffusion or erosion of the matrix under sink conditions. If the diffusion of a drug is faster than matrix erosion the mechanism of release is largely controlled by a diffusion process [101]. It was also observed that PIR-NP (i.e. 400nm) showed a lower cumulative drug release of 57% till the end of the experiment contrary to the THP-NP (i.e. 200 nm) which showed a relatively higher cumulative release of 72%. This could be explained by the fact that in case of smaller nanoparticles, the greater surface area produces a higher number of drug molecules at the surface of nanoparticles ready for faster release [102].

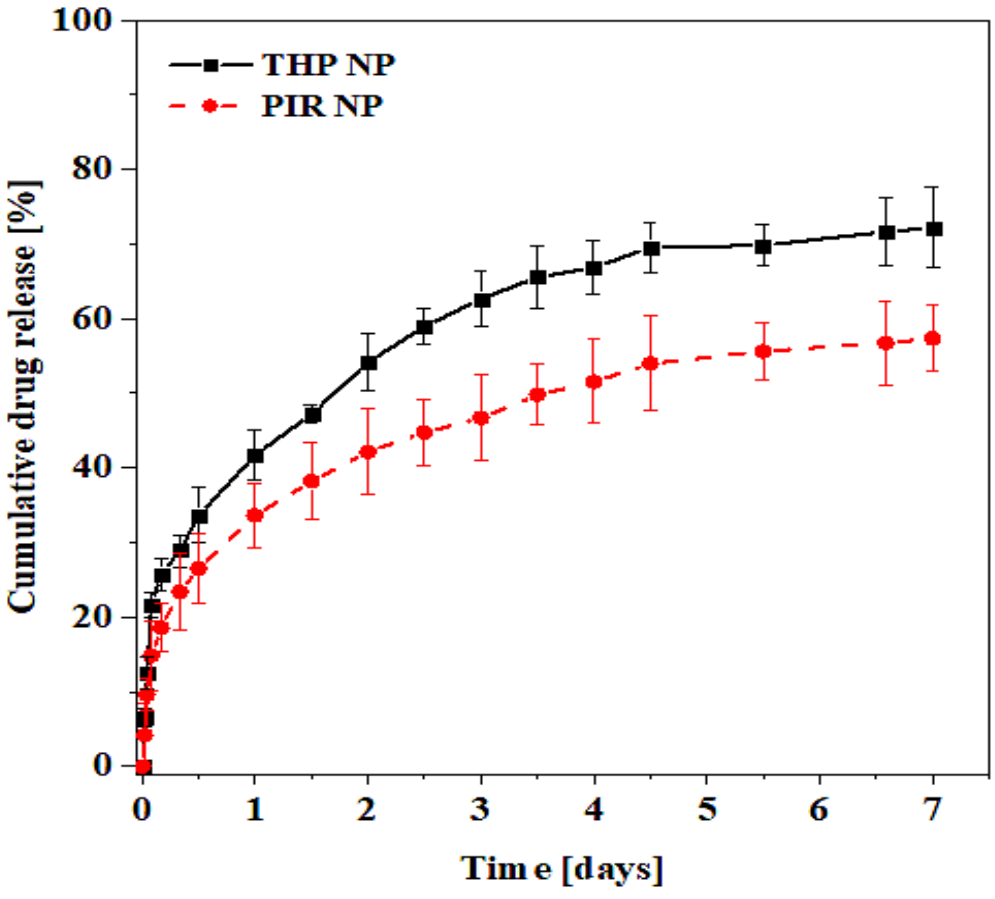

Figure 30. Cumulative drug release [%] of pirarubicin from PLGA nanoparticles (THP-NP & PIR-NP) in PBS (pH 7.4) buffer containing 1 % v/v tween 80% to assure sink conditions. The samples were withdrawn at specified time intervals were analyzed spectrophotometrically. The results are expressed as mean ± SD for three independent experiments (n=3).

3.2.5 *In vitro* cytotoxicity synergism

The in-vitro cytotoxicity synergism of LCNPs, as well as the cell viability of the SK-OV-3 cells after being treated with THP, loaded PLGA nanoparticles, mTHPC loaded liposomes, and free THP/mTHPC (dissolved in DMSO) was determined using MTT assay. It was done by incubating the cells in the presence of different concentrations of the nanoformulations as well as of the free drugs for 4 h. This was followed by subsequent irradiation of the cells at λ=652 nm (except for free THP and THP loaded nanoparticles). The results of the cytotoxicity assay are expressed in Fig. 31. It is evident from the results that the presence of free THP or THP loaded biodegradable nanoparticles caused a reduction in the SK-OV-3 cell viability with the highest reduction observed at the dose of 100μM (Fig. 31A). The highest cytotoxicity was produced by the free THP (72.26 ± 5.40%) followed by THP NP (62.14 ± 3.13%). The least effect was observed with PIR NP with the cell viability still recorded at 52.56 ± 5.50%. This can be attributed to the slower uptake of the larger particles (i.e. 400 nm) as the particle size ranging from 100-200 nm are appropriate for effective cellular uptake and consequently for the higher anticancer activity. It was also observed that free THP dissolved in the DMSO showed higher cytotoxicity, which could be referred to as the controlled release properties of PLGA nanoparticles as the rate-limiting step.

The treatment of the cells with free mTHPC (dissolved in 0.1% DMSO) without subsequent irradiation resulted in a slight reduction of cell viability (18.51± 1.87%). This dark toxicity was evident only at the highest mTHPC concentration (i.e. 5 μM) (Fig. 31B). Contrary to this, mTHPC did not show any dark toxicity when encapsulated in a liposomal formulation suggesting the safety of the formulation (Fig. 31C). These findings were also in accordance with the previous studies conducted by our research group. It is also evident that with the increase in light fluence, the cell viability continuously decreased ending up at 18-20% at 350 $mJcm^{-2}$ [89]. Similar results were obtained when the mTHPC encapsulated liposome was coated over THP loaded PLGA nanoparticles. The LCNPs without succeeding irradiation exhibited cell viability of 32.2± 1.3% which was relatively less as compared to the THP nanoparticles alone (i.e. 37.8± 3.1%). This effect can be attributed to higher cellular uptake of the lipid-coated particles as compared to the uncoated nanoparticles [103]. The dose-response cell viability curves obtained from the LCNPs treated cells manifested higher cell destruction as compared to mTHPC liposomes or THP nanoparticles alone (Fig. 31D). This higher anticancer effect can be credited to the synergistic effect produced by both the drugs combined in one nanocarrier system [79]. The half-maximal inhibitory concentration (IC_{50}) of the formulations was also reduced proportionally, as the light or drug dose into the cells was increased. The statistical evaluation using two-way ANOVA with

Dunnett's multiple comparisons showed that the PDT effect produced by different light fluences differed significantly ($p<0.0001$) to the unirradiated samples.

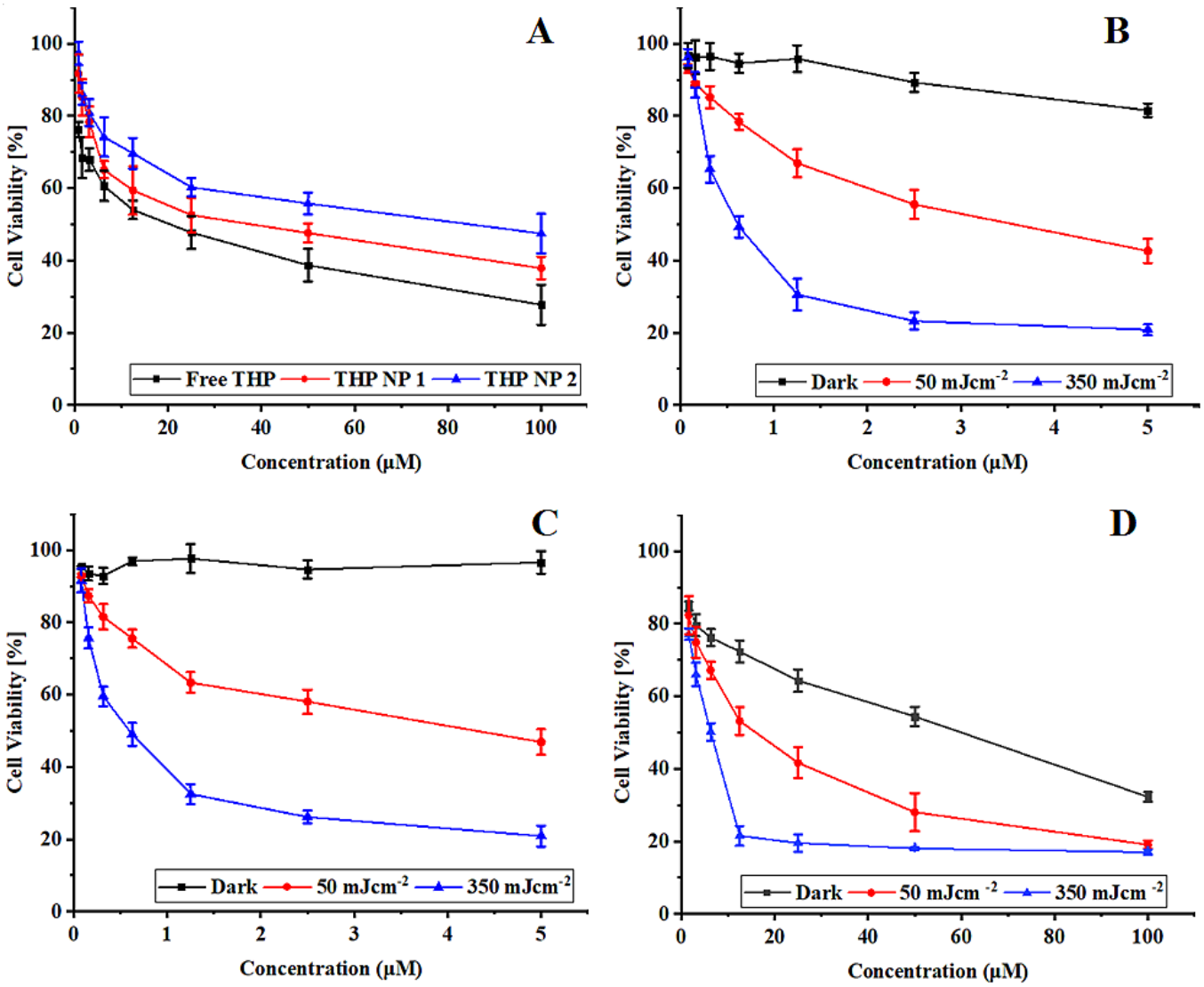

Figure 31. Dose-response curves representing cell viability of SK-OV-3 carcinoma cells. Cytotoxicity induced by THP loaded nanoparticles and free THP (A); dark and photo cytotoxicity induced by free mTHPC (B); mTHPC-LP (C); and lipid-coated nanoparticles (LCNP) (D). In all cases, the free drug was dissolved in 0.1% DMSO. The cells were incubated for 4 h with the formulations at 37˚C and then irradiated (except A) with radiation fluence of 50 $mJcm^{-2}$ and 350 $mJcm^{-2}$ at λ=652 nm. Dark was used as the negative control and represents cells without irradiation. The half-maximal inhibitory concentration (IC_{50}) was calculated by non-linear curve fitting. Each value is represented as the mean ± SD for three independent experiments (n=3).

Table 5. The half-maximal inhibitory concentration (IC50) values of the MTT assay induced by Pirarubicin loaded PLGA nanoparticles and photo-cytotoxicity induced by the THPC loaded

liposomes, free mTHPC (dissolved in DMSO) as well as LCNPs in SK-OV cells. The IC50 values were calculated by non-linear curve fitting from the graphs and tabulated for the respective radiation doses (fluences).

Formulations	Light Dose [mJ/cm^2]	IC_{50} [µM]
Free THP (dissolved in DMSO)	-	6.750
THP PLGA NP-1	-	14.37
THP PLGA NP-2	-	27.51
Free mTHPC (dissolved in DMSO)	50	1.962
	350	0.422
DPPC/DPPG/mPEG-DPPE$_{5000}$	50	1.947
	350	0.349
LCNP	50	0.414
	350	0.187

3.2.6 Assessment of reactive oxygen species (ROS):

The production of ROS has a very crucial effect on the results of combination therapy as the high production of ROS induces significant damage to the biomolecules (i.e. nucleic acids, proteins, etc.) in the cancer cells. In order to determine the effect of combination therapy on the intracellular ROS production in the SK-OV-3 cells, the ROS assay was performed. For this purpose, one of the commonly used molecular probe H2DCF was used. Esterified form of this dye is non-fluorescent and cell-permeable, thus can enter the cells freely. Inside the cell, it gets deacetylated into the cell impermeable dye by the action of cell-bound esterases and then gets oxidized by intracellular ROS into a green fluorescent DCF [104]. The fluorescence intensity corresponds to the ROS production is then detected using fluorescence microscopy. The data obtained from the production of ROS after being treated with formulations and free drugs is shown in Fig. 32. In our experiments, the irradiated liposomal formulation or free drug (dissolved in DMSO) produced increased levels of intracellular ROS as compared to non-irradiated one (dark). These findings were in line with the cytotoxicity experiments in which unirradiated formulations or free drug did not produce a significant reduction in cell viability [65]. The highest amount of ROS was produced by PEGylated liposomes coated over the THP loaded nanoparticles giving a synergistic effect for the production of ROS. The reason for higher ROS production by the lipid-coated nanoparticles can be explained by the higher cellular uptake of these particles as compared to uncoated particles

[103]. The fact that the highest damage to the cancer cells was done by lipid-coated THP nanoparticles could be explained by this higher ROS production. As expected, the amount of ROS produced by uncoated THP nanoparticles and free THP, before and after irradiation remained the same and no significant difference in the ROS levels was observed.

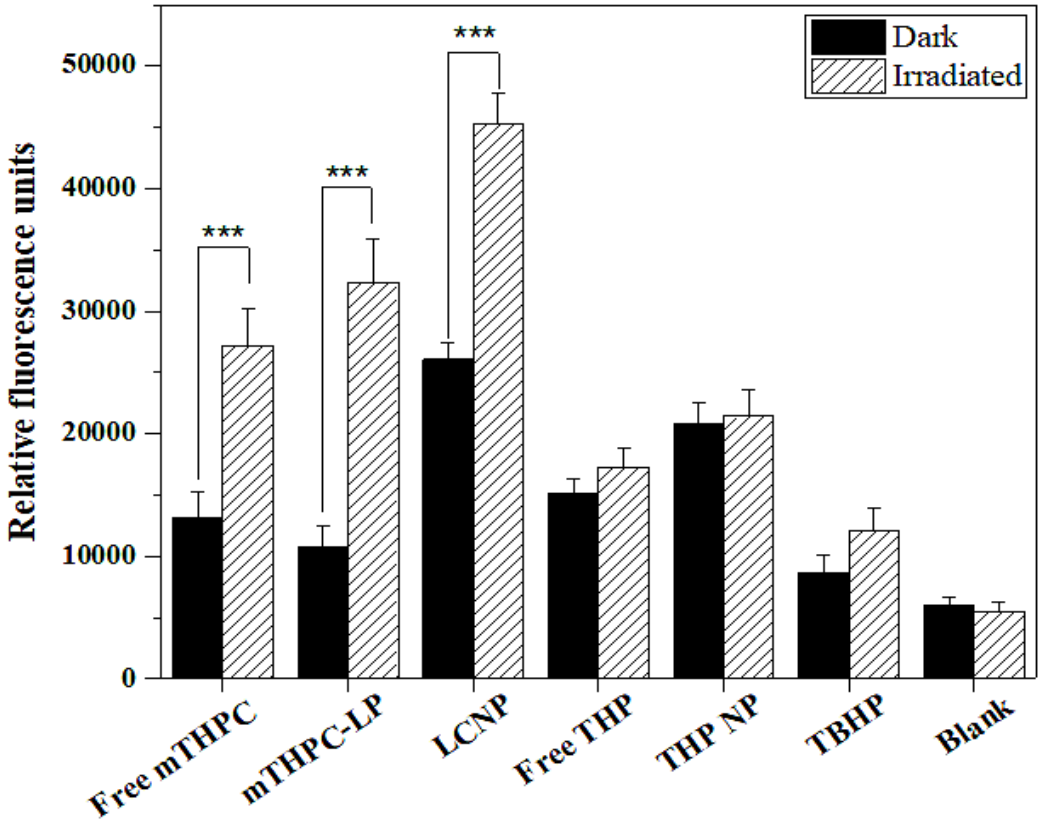

Figure 32. Production of ROS in response to mTHPC loaded liposomes, free mTHPC, THP loaded PLGA nanoparticles, free THP and Lipid coated polymeric nanoparticles (LCNP). DCFDA (25 μM) was used as a free radical quenching fluorescent dye. The cells were incubated with the formulations or free drug for 4 h at 37 ºC. Subsequent radiation was performed at a light dose of 0.5 J/cm^2 (λ = 652 nm). Blank represents the untreated cells whereas TBHP (50 μM) was used as a positive control. All the measurements were performed in triplicate and values were expressed as mean ± S.D (n=3). For the statistical analysis, the comparison was done against the blank group. P values ($p < 0.05$) were considered significant and denoted as '***' ($p< 0.001$), '**' ($p< 0.01$) and '*' ($p<0.1$).

3.2.7 Hemocompatibility assay

Hemocompatibility of the synthesized nano-formulations is a significant criterion for pharmaceutical and biomedical applications. It involves the necessary evaluation of the hemolytic potential of drug formulations with blood components which would, in turn, determine their

therapeutic efficacy and *in vivo* fate. These studies also serve as a critical link between *in vitro* and *in vivo* studies because the data obtained from these studies can be used to tailor the dosage form for the *in vivo* experiments**.** The hemolytic potential of our drug formulations was assessed to evaluate their safe concentrations that can be administered intravenously. It was done by estimation of the hemoglobin release after erythrocyte damage caused by drug formulations. The atmospheric oxygen then converts this hemoglobin into oxyhemoglobin which can be detected spectrophotometrically [105]. The results of the hemocompatibility studies are expressed in Fig. 33. In our study, it was observed that both of the free drugs showed a relatively higher hemolytic effect (i.e. 14% and 20% for free mTHPC and THP respectively) even at a lower dose, while the degree of hemolytic toxicity exhibited by all the formulations was less than 10% including lipid-coated nanoparticles (i.e. 8.93 %). This indicates that our formulations were less hemotoxic and had improved biocompatibility with the blood components. The aPTT test was performed to evaluate the effect of nanoformulations on the coagulation time of blood. An increase in aPTT time was observed in the case of free drugs (127.7 s and 60.2 s for free THP and mTHPC respectively). It is important to consider that the aPTT values above 50 s are clinically significant while the value above 70 s indicates the continuous bleeding and hemorrhage. Contrary to the free drugs, the coagulation time depicted by the nanoformulations was found to between 39.5 s – 46.8 s which was well under the standard range [106, 107]. The aPTT values exhibited by the drug formulations were also comparable to that of the blank (i.e. 37.2 s). These findings suggested that our nanoformulations were biocompatible as well as non-toxic for i.v. injection.

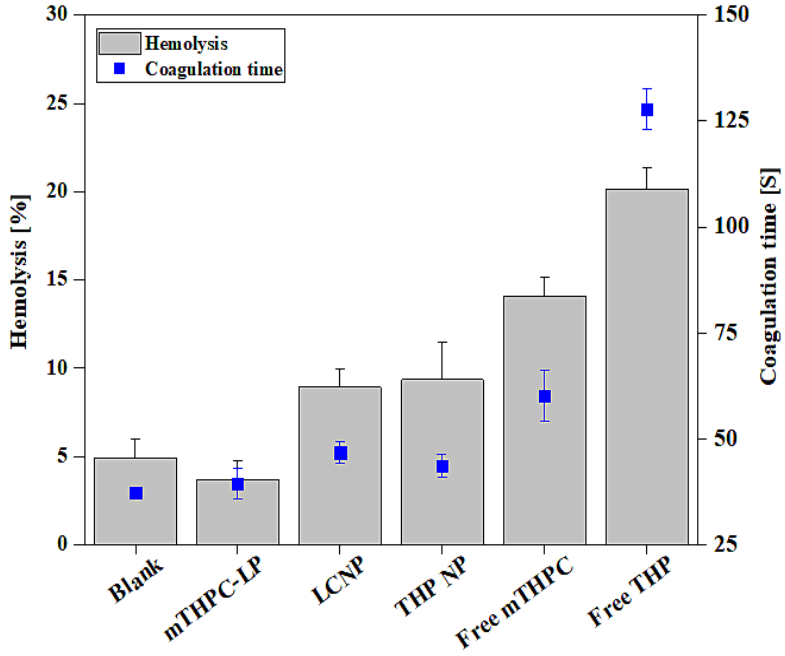

Figure 33. Hemocompatibility assay A) aPTT assay & B) Hemolysis assay of mTHPC loaded liposomes, THP loaded PLGA nanoparticles, Lipid-coated nanoparticles (LCNP) and free

mTHPC/ free THP (dissolved in DMSO). Triton X-100 was used as a positive control for hemolysis assay was considered as 100% hemolysis. Blood plasma was considered as blank in the case of hemolysis assay while erythrocytes were considered as blank in the aPTT test. All the samples were measured in triplicate and the values were expressed as mean ± S.D (n = 3).

3.2.8 Alkaline comet assay

Single-cell gel electrophoresis (SCGE) is a simple, sensitive and most extensively used technique for assessing DNA damage (DNA strand breaks) in eukaryotic cells. It has achieved the status of a standard test to explore the safety of the drug formulations. This test is based on the fact that the integrity of the cellular components gets compromised on exposure to genotoxic chemicals. DNA chromosomes get damaged on long term exposure and after segregation, they move towards the anode under the influence of electricity. This movement is detected by fluorescence microscopy and regarded as the tail moment [68, 93]. The measure of this tail moment is indexed as the degree of DNA damage. The results of the comet assay are shown in Fig. 34. It is evident from the results obtained that the highest genotoxicity was caused by the free drugs (free THP and mTHPC) when exposed to the SK-OV-3 cells but still categorized in the class II damage (i.e. 5-20%; low damage). On the other hand, none of the formulations, including the lipid-coated nanoparticles induced any direct DNA damage and were classified under class-I (i.e. 0-5%; no DNA damage) as observed from the olive tail moment data [108]. From the data, it was concluded that irradiation of the SK-OV-3 cells after treatment with a low drug or light dose did not cause any significant DNA fragmentation and there was no apparent increase in the olive tail. Tail lengths of different comets were statistically analyzed using one-way ANOVA. Dunnett's post hoc test with multiple comparisons against control (blank) was used to compare the results. The results were significant when compared to control with a p-value of < 0.05. The % DNA in the comet tail was almost the same as one of the negative controls, even although a statistically significant effect was observed. In conclusion, the present study clearly indicated that the lipid-coated PLGA nanoparticles can be used clinically with no or minimum incidence of genetic toxicity if accumulated in peripheral organs in a small amount.

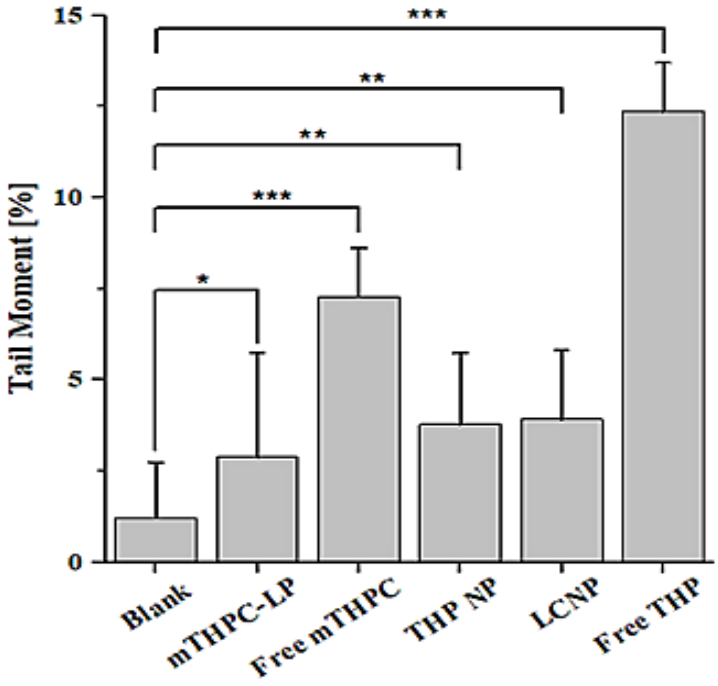

Figure 34. Distribution of comet tail moment representing the genotoxicity to SK-OV-3 cells obtained from alkaline comet assay. The cells were incubated with mTHPC loaded liposomes, THP loaded PLGA nanoparticles, LCNP and free mTHPC/ free THP (dissolved in 0.1% DMSO) for 4 h at an equitoxic dose. Irradiation was performed at a light dose of 0.05 J/cm^2. Each value is represented as the mean ± S.D for three independent experiments. For the statistical analysis, the comparison was done against the untreated cells. P values ($p < 0.05$) were considered significant and denoted as '***' ($p< 0.001$) and '**' ($p< 0.01$).

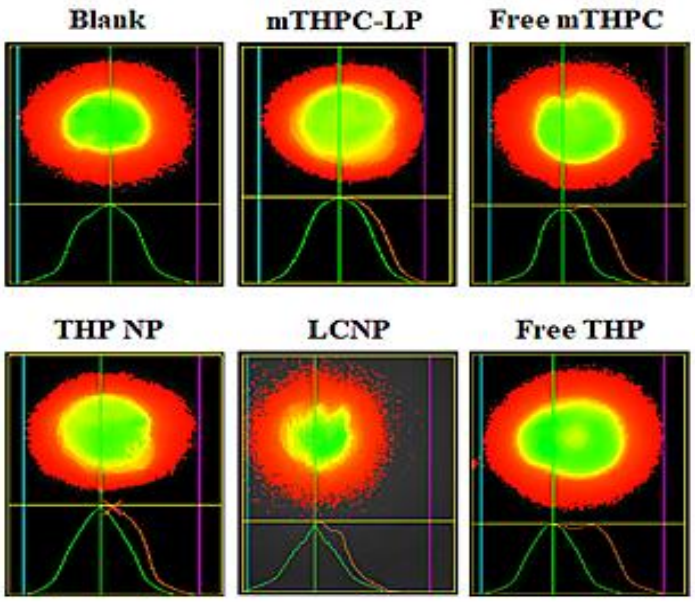

Figure 35. Representative fluorescence micrographs genotoxicity to SK-OV-3 cells obtained from alkaline comet assay

3.2.9 Cellular uptake pathway analysis

To study the internalization mechanism of nanoformulations in the SK-OV-3 cells, the inhibitors of the cellular uptake pathways were used. Two major pathways utilized for the internalization of the nanocarriers includes the clathrin-dependent endocytosis and caveolin dependent pathway. Clathrin dependent endocytosis is selectively obstructed by Chlorpromazine which acts by inhibiting the formation of clathrin-coated vesicles that are formed by the clathrin-coated pits leading to the formation of endosomes which ultimately fuse with the lysosomes. Chlorpromazine is also supposed to interfere with the intracellular processing of the clathrin. Caveolin dependent mechanism is inhibited by Filipin-III. It is a macrolide antibiotic derived from the *Streptomyces filipensis* and acts by interfering with cholesterol mediated endocytic functions thereby inhibiting the lipid raft or caveolae endocytosis [53]. Fig.36 demonstrates that the incubating the cells without nanoformulations and/or with inhibitors only did not cause any decline in the cell viability. Whereas, the cells incubated with nanoformulations without any inhibition showed a substantial reduction in cell viability. Furthermore, when the cells were preincubated with chlorpromazine, a considerable increase in the cell viability was observed due to the inhibition of clathrin-dependent uptake pathway. Additional incubation with Filipin-III showed relatively less inhibition of nanoformulations uptake. This inference leads to the presumption that nanoformulations uptake occurred mainly through clathrin-mediated endocytosis. None of the inhibitors was able to minimize the uptake of the free mTHPC and/or free THP (dissolved in DMSO). This result leads to the inference that the free drugs were not internalized by any of the said mechanisms. Instead, they were taken up by the cells through the diffusion process. These findings were in agreement with the earlier studies elaborating that the lipid particles are mainly internalized via clathrin-dependent pathways and are highly dependent on cell type [57, 109].

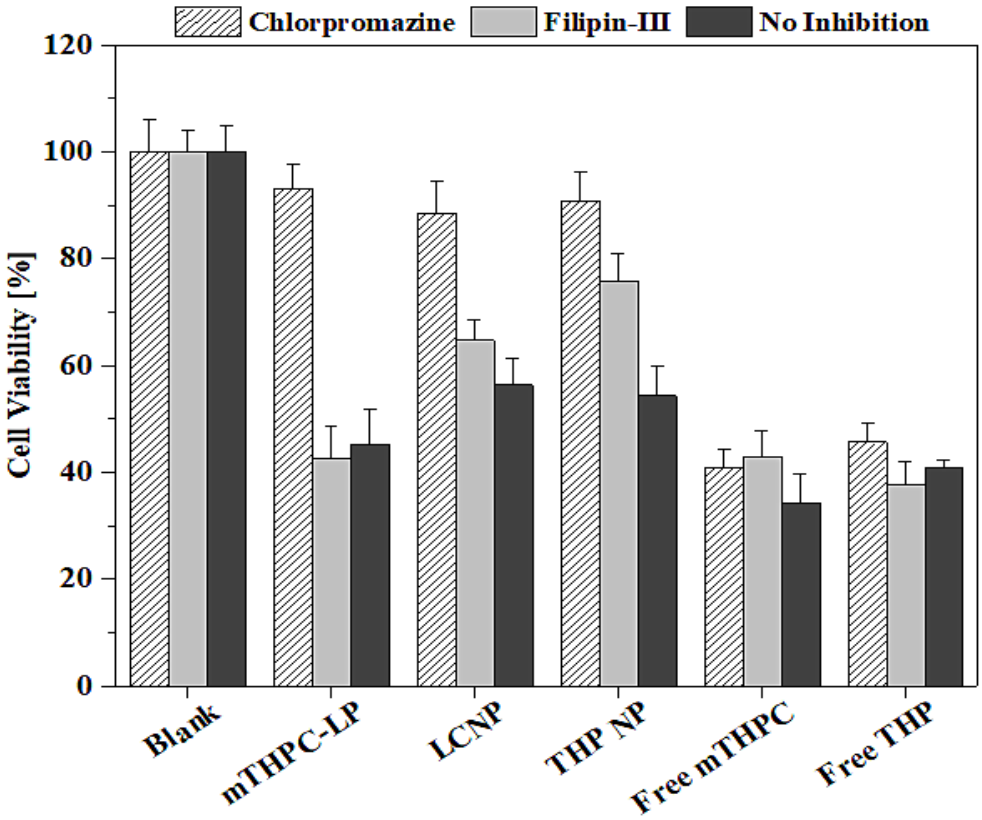

Figure 36. Cellular uptake mechanism of the nanoformulations in SK-OV-3 cells in the presence of specific inhibitors (i.e. 15 µM Filipin III and 30 µM Chlorpromazine). After pre-incubation with the inhibitors, the cells were then incubated with mTHPC loaded formulations (mTHPC-LP & LCNP) or free mTHPC (dissolved in DMSO) at a concentration of 1.5 µM as well the THP loaded formulations (THP-NP & LCNP) or free THP (dissolved in DMSO) at a concentration equivalent to 50 µM for 4 h. The irradiation was performed at a light dose of 0.5 Jcm^{-2} (for mTHPC loaded formulations). The viability of untreated cells was considered as 100%. Blank represents cells without any inhibitor. values are represented as the mean ± SD for three independent experiments.

3.2.10 Apoptosis assay using flow cytometry

Apoptosis also known as programmed cell death, is a normal process of the health and development of multicellular organisms. Unlike necrosis, which is considered as accidental or traumatic cell death and is mainly caused by acute cellular injury, apoptosis is a well-regulated and controlled process and gives advantages during the life cycle. It is mainly characterized by the morphological and biochemical changes including the compaction and fragmentation of the nuclear chromatin, cell surface blebbing, shrinkage of the cytoplasm and the loss of membrane asymmetry [110, 111]. In order to evaluate the synergistic apoptosis by flow cytometry (Fluorescence-activated cell sorting: FACS), one group of the cells was treated mTHPC loaded

liposomes and group two was treated with free mTHPC (dissolved in DMSO). Similarly, the 3rd group was treated with the THP loaded PLGA nanoparticles while group four was treated with the free THP (dissolved in DMSO). For the synergistic effect, group five was treated with the lipid-coated nanoparticles. The cells without any treatment but with the sequential irradiation as that of the other groups were considered as negative control. The results of the apoptosis assay are expressed in Fig. 37 represents the typical FACS micrographs of the flow cytometry. It was noticed that combining the cell treatment in the form of LCNPs had a pronounced apoptotic effect in the SK-OV-3 cells as compared to treatment with a nanocarrier having only one drug. The results also demonstrated that the cells which were treated with free mTHPC, mTHPC-LP, free THP or THP-NP manifested 54.57%, 39.37%, 58.22% and 54.39% apoptotic cells (early + late apoptosis; Q1+Q2) respectively. On the other hand, a synergistic treatment subsequently increased the cell apoptosis i.e. 70.71% which was comparable to the combined cellular apoptosis produced by the mTHPC-LP and THP-NP treatment. This could be attributed to the fact that increased amount of ROS generated due to combined chemo-photodynamic effect of LCNPs induced a synergistic apoptotic effect in the cells [112, 113]. These results were also in a good correlation with the results obtained from the quantitative ROS assessment and cell viability data obtained previously.

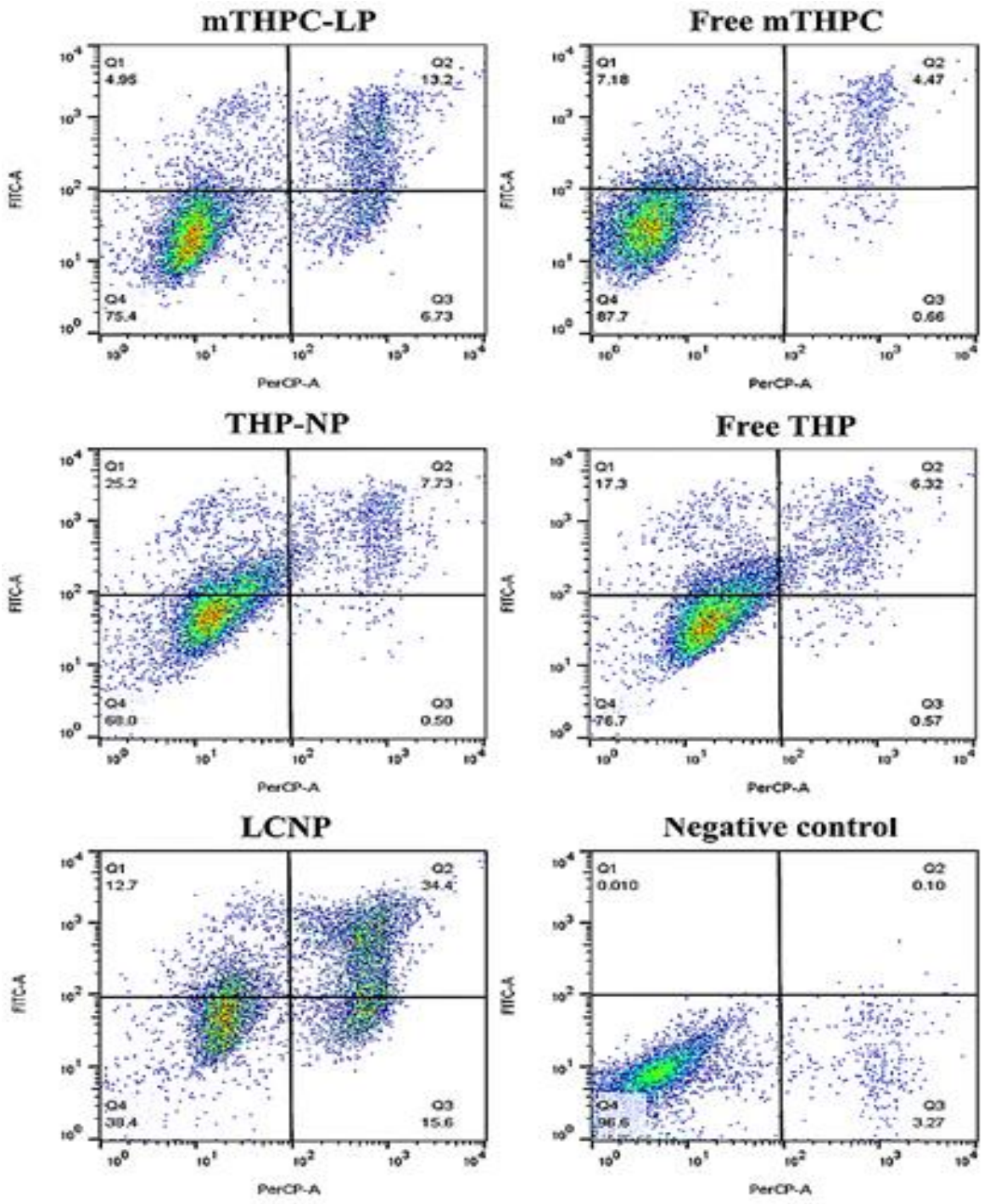

Figure 37. Apoptosis assay (FACS micrographs) in SK-OV-3 cell line by nanoformulations (mTHPC-LP, THP-NP and LCNP) as well as with free mTHPC/THP treatment. Here the top left (Q1) = early apoptotic cells, top right (Q2) = late apoptotic cells, bottom right (Q3) = d dead cells, and bottom left (Q4) = represents the healthy cells. The cells irradiated with equivalent light dose and without any treatment were considered as the negative control.

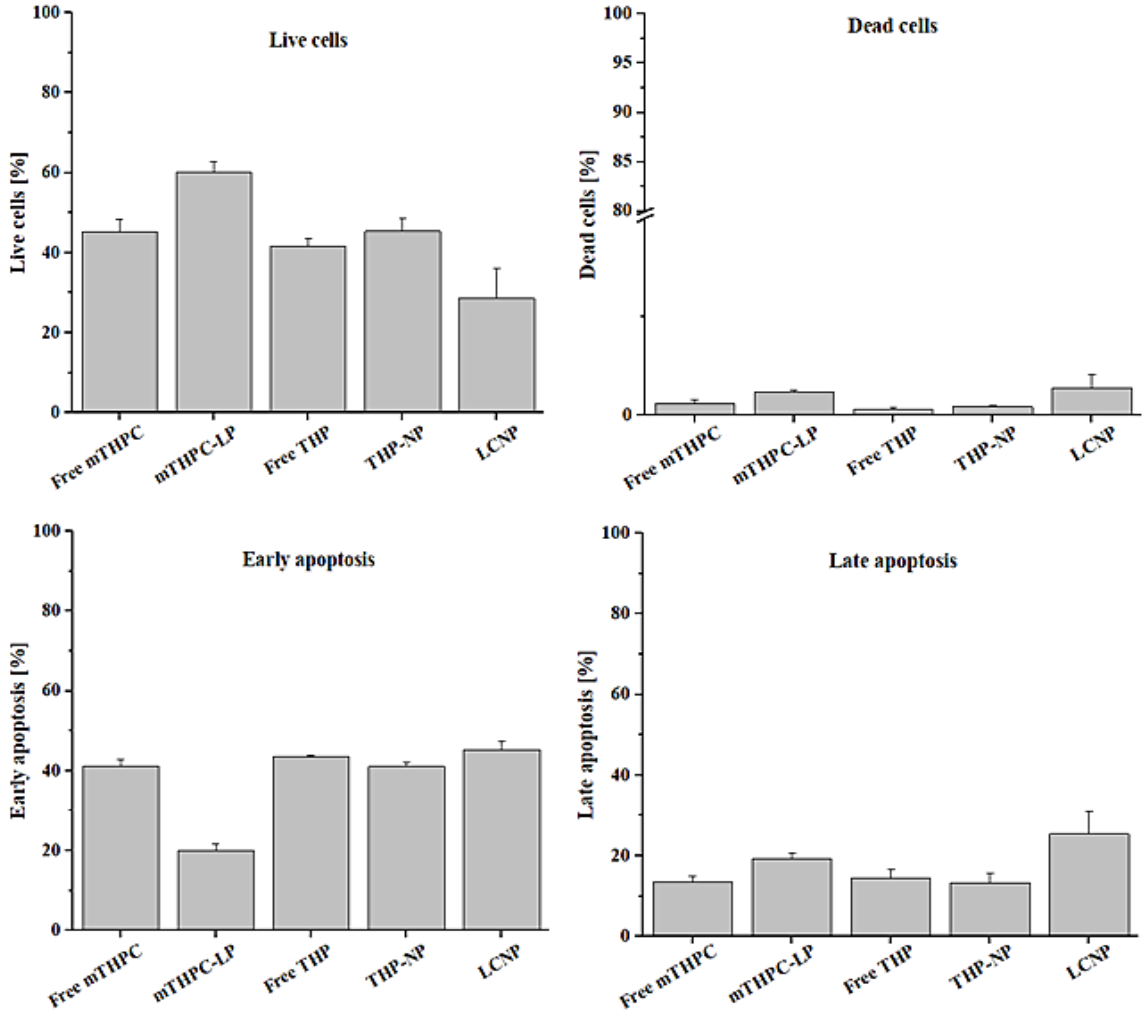

Figure 38. Apoptosis assay (graphical representation) by flow cytometry in SK-OV-3 cell line by nanoformulations (mTHPC-LP, THP-NP, and LCNP) as well as with free drugs (mTHPC/THP; dissolved in DMSO). Graphical representation of % positive cells (live, dead, early apoptotic and late apoptotic, respectively).

3.2.11 Stability studies in simulated conditions

Serum stability studies were performed to check the effect of serum protein on the formulations. The stability of the particles is based not only on the physical characteristics of the encapsulated agent and the carrier system but also on the biological environment with which they are placed. The adsorption of serum proteins on the formulations was estimated by DLS and LDA analysis. In order to simulate the physiological conditions, the formulations were incubated with 60% FCS and PBS (pH 7.4) in a shaking incubator at 37°C. The results manifested a reduction in the particle size of all the formulations (i.e. THP NP, mTHPC-LP and LCNP) after being incubated in the serum for 24 h (Table 7). This could be attributed to the release of surface-bound THP resulting in the reduction of nanoparticle size [114]. Furthermore, the decrease in the hydrodynamic

diameter of the particles could be due to the fact that serum proteins interact with the particles via osmotic forces which causes the shrinkage of the particle size [115]. Interestingly, the zeta potential of THP NP and lipid-coated PLGA particles was negative when placed in 60% serum, suggesting the adsorption of serum proteins. This result could be attributed to the fact that the serum is composed of negatively charged proteins which tend to adsorb more on the surface of the charged particle as compared to the neutral ones resulting in the reduction of the surface charge [116]. The increase in the PDI of the particles can be attributed to the reduction of the homogeneity of formulations. The changes in PDI were independent of the particle size.

Table 6. The changes in the physicochemical parameters of nanoformulations (THP loaded PLGA nanoparticles, mTHPC encapsulated liposomes, and lipid-coated nanoparticles). The formulations were incubated with PBS (pH 7.4; without Ca^{2+}/Mg^{2+}) at 37ºC for 24 h in a shaking incubator. Hydrodynamic diameter is expressed as particle size distribution by intensity. The results are expressed as mean ± SD (n=3).

Formulation	Time [h]	Diameter [nm] ± SD	PDI ± SD	ζ Potential [mV] ± SD
THP NP	0	204.7 ± 3.4	0.10 ± 0.03	7.60 ± 0.34
	1	212.4 ± 3.4	0.12 ± 0.02	6.18 ± 0.19
	4	220.2 ± 7.4	0.13 ± 0.03	5.27 ± 0.19
	24	202.7 ± 3.5	0.08 ± 0.02	6.28 ± 0.24
mTHPC-LP	0	108.8 ± 2.1	0.19 ± 0.06	-12.90 ± 0.5
	1	105.4 ± 9.5	0.21 ± 0.07	-12.60 ± 1.0
	4	115.0 ± 9.3	0.23 ± 0.01	-15.50 ± 3.4
	24	122.7 ± 8.9	0.22 ± 0.01	-14.00 ± 2.7
LCNP	0	208.6 ± 2.2	0.11 ± 0.01	5.90 ± 0.90
	1	212.6 ± 4.8	0.15 ± 0.04	4.24 ± 0.37
	4	220.5 ± 7.1	0.17 ± 0.02	4.63 ± 0.59
	24	205.3 ± 3.7	0.13 ± 0.04	4.39 ± 0.23

Table 7. The changes in the physicochemical parameters of THP loaded PLGA nanoparticles, mTHPC encapsulated liposomes, and lipid-coated nanoparticles. All the formulations were incubation with FCS (60%) at 37ºC for 24 h in a shaking incubator. Hydrodynamic diameter is expressed as particle size distribution by intensity. The results are expressed as mean ± SD (n=3).

Formulation	Time [h]	Diameter [nm] ± SD	PDI ± SD	ζ Potential [mV] ± SD
THP NP	0	204.7 ± 3.4	0.10 ± 0.03	7.60 ± 1.4
	1	195.5 ± 4.3	0.21 ± 0.02	-10.41 ± 1.2
	4	191.8 ± 4.7	0.22 ± 0.04	-15.42 ± 1.2
	24	179.3 ± 3.8	0.22 ± 0.01	-15.92± 1.3
mTHPC-LP	0	108.8 ± 2.1	0.19 ± 0.06	-14.68 ± 1.4
	1	113.2 ± 2.6	0.25 ± 0.01	-13.22 ± 0.5
	4	105.5 ± 4.5	0.27 ± 0.03	-15.05± 0.8
	24	101.7 ± 3.4	0.32 ± 0.03	-15.73 ± 0.9
LCNP	0	208.6 ± 2.2	0.11 ± 0.01	5.90 ± 0.9
	1	191.6 ± 9.8	0.22 ± 0.02	-14.61 ± 1.1
	4	180.5 ± 3.1	0.19 ± 0.02	-15.75 ± 1.0
	24	176.5 ± 1.9	0.21 ± 0.01	-15.31 ± 0.7

3.2.12 *In vivo* experiments

3.2.12.1 *In vivo* acute toxicity assessment

The safety and tolerability of the nanoformulations were tested relative to the treatments in mice with weight loss, serum biochemical analysis and histopathological examinations used as assessment parameters for the in vivo toxicity studies. The formulations were administered intravenously via tail vein to Swiss albino mice at a dose of 5 mg/kg and 0.150 mg/kg of body weight for THP and mTHPC respectively [117, 118]. During 48 h of observation, the mice did not show any sign of toxicity as examined from the behavioral patterns, skin, urine color, respiration, and sleep patterns. The same parameters were monitored every day to examine any signs of toxicity. Throughout the course of the study, no mortality or any significant change in the body weight was observed confirming the safety of our nanoformulations. Post 7 days, the blood was collected and the mice were euthanized to remove the body organs for histopathological studies [77].

3.2.12.2 Body visceral index

Body visceral index is considered as one of the effective indicators of chemically induced changes to the organs. The comparison of organ weight between the untreated and treated animal groups

can be used to evaluate the toxicity profile of the drug formulations [118]. Post 7 days treatment, the organ to body weight ratios (visceral indices) of vital body organs including liver, kidney, lungs, and heart were determined. After euthanizing the animals, the organs were removed carefully and washed with normal saline prior to weighing. Fig. 39 represents the visceral body index of the test animals after necropsy. It was observed that there was a slight increase in liver weight when compared to the control group. The highest increase was marked in the case of free THP which can be credited to the THP treatment-related hepatocellular hypertrophy. The kidneys also showed a slight increase in the organ weight especially in the case of free THP, THP nanoparticles as well as in the case of free mTHPC. This increase can be attributed to the tubular hypertrophy and may be associated with renal toxicity. The heart and lungs did not show any significant weight change and remained unaffected with all the treatments, which proposes the non-toxicity and biocompatibility of the formulations.

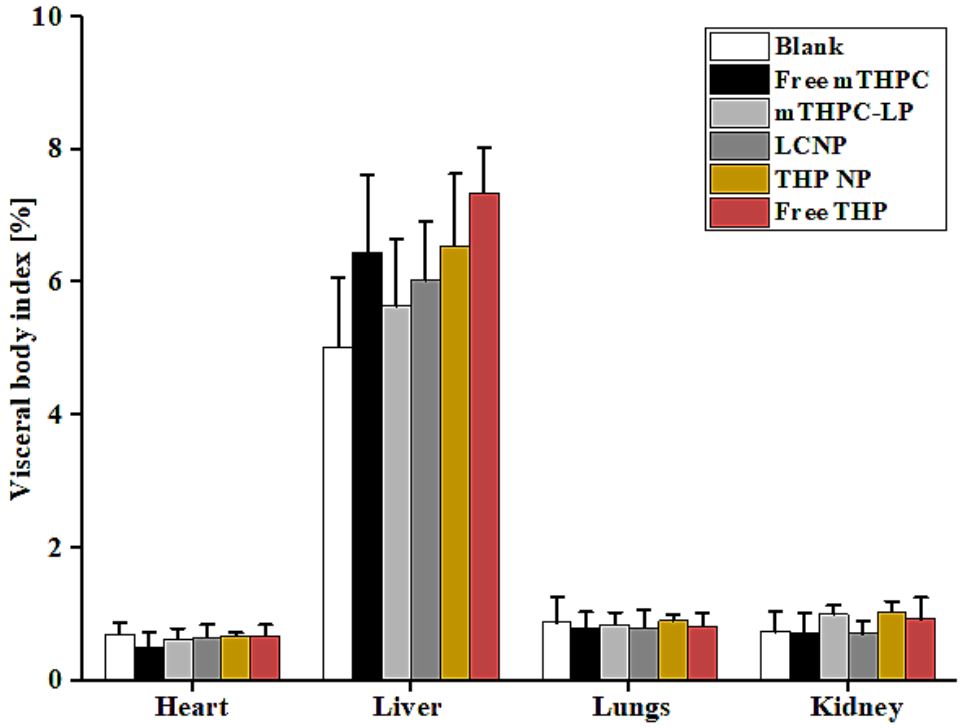

Figure 39. The visceral body index (%) of untreated group (normal saline) and treated groups (free mTHPC, mTHPC-LP, LCNP, THP NP and free THP) performed after sacrificing the animals (swiss albino mice) by cervical dislocation. Values are represented as mean ± S.D.

3.2.12.3 Biochemical analysis

Biochemical indices are highly sensitive biomarkers to determine the clinical symptoms produced by the biological treatments (i.e. formulations). Among these biomarkers, the liver function tests (LFTs) and renal function tests (RFTs) are the major indicators of proper liver and kidney

functioning respectively. The results of the biochemical analysis of mice blood after being treated with formulations are shown below. Aminotransferases are the standard measure of the hepatotoxicity. In case of any cellular damage to hepatocytes, alanine aminotransferase (ALT) and aspartate aminotransferase (AST) tend to leak out into the blood circulation resulting in the increase systemic levels of these enzymes. AST was observed in the highest level in the mice treated with free THP and THP loaded PLGA nanoparticles as compared to the mTHPC-LP and lipid-coated nanoparticles. The AST level was also slightly higher in the case of free mTHPC treated group when compared with the control group but statistically less significant as compared to free THP and THP loaded PLGA nanoparticles (Fig. 40). ALT level was also increased in free mTHPC and free THP treated groups. These higher levels of both enzymes could be an indication of detoxification of the foreign particles and possible liver inflammation. In all other treatment groups, no significant change of ALT level was observed. Alkaline phosphatase (ALP) level was also significantly increased in all the treatment groups with the highest increase observed in the free THP treated group. This could possibly be the indicator of non-alcoholic fatty liver and cardiac problems [119].

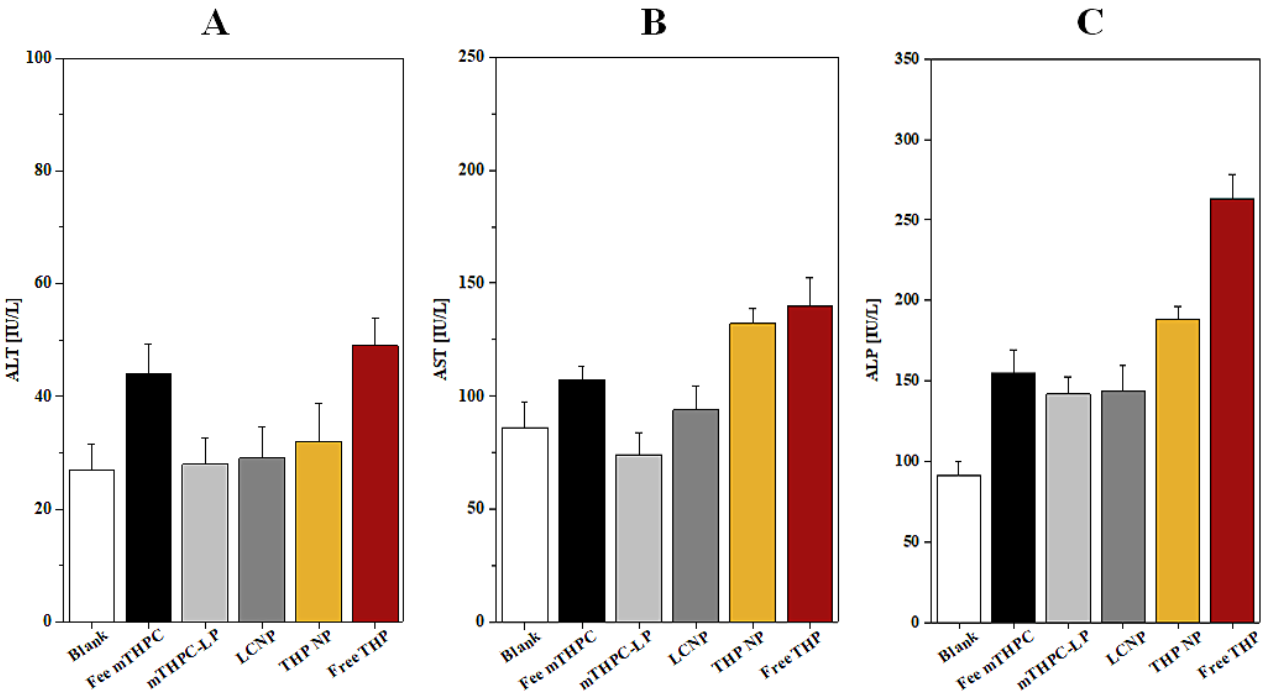

Figure 40. Typical liver function tests (LFTs) parameters including (A) ALT, (B) AST and (C) ALP levels after being treated with the nanoformulations intravenously. Values are represented as mean ± S.D (n=3).

The results of RFTs (Fig. 41) manifested that the level of uric acid was moderately increased in the case of free THP as compared to the controlled group. Contrary to this, the uric acid level was

slightly decreased in mTHPC-LP but fell within limits. Moreover, in all other treatment groups, the change in the level of these biomarkers remained statistically insignificant. The creatinine level was increased with free THP and free mTHPC when compared to the control, yet found within the limits. This slight increase in the level of these biomarkers could be a cause of renal hypertrophy and poor kidney functioning. With all other treatment groups, there was no significant variation in the creatinine level. The results also depicted that the bilirubin level with formulations was not altered significantly except for the free THP and mTHPC. The bilirubin level was slightly higher in these treatments as compared to the control group but still fell within the acceptable limits [120]. The effect of the formulations was also investigated on serum lipid profile and total protein level (Fig. 42). There was a significant increase in the cholesterol level with all the treatment groups except for mTHPC loaded liposomes but remained well within the normal range [121]. The triglycerides level was also found within the normal limit in all the treatment groups and no significant changes were observed. There was a slight increase in total protein level with free THP, THP NP and free mTHPC treatment but no significant difference with mTHPC-LP and LCNP treatment. All these results of the biochemical analysis were also in line with the body visceral indices.

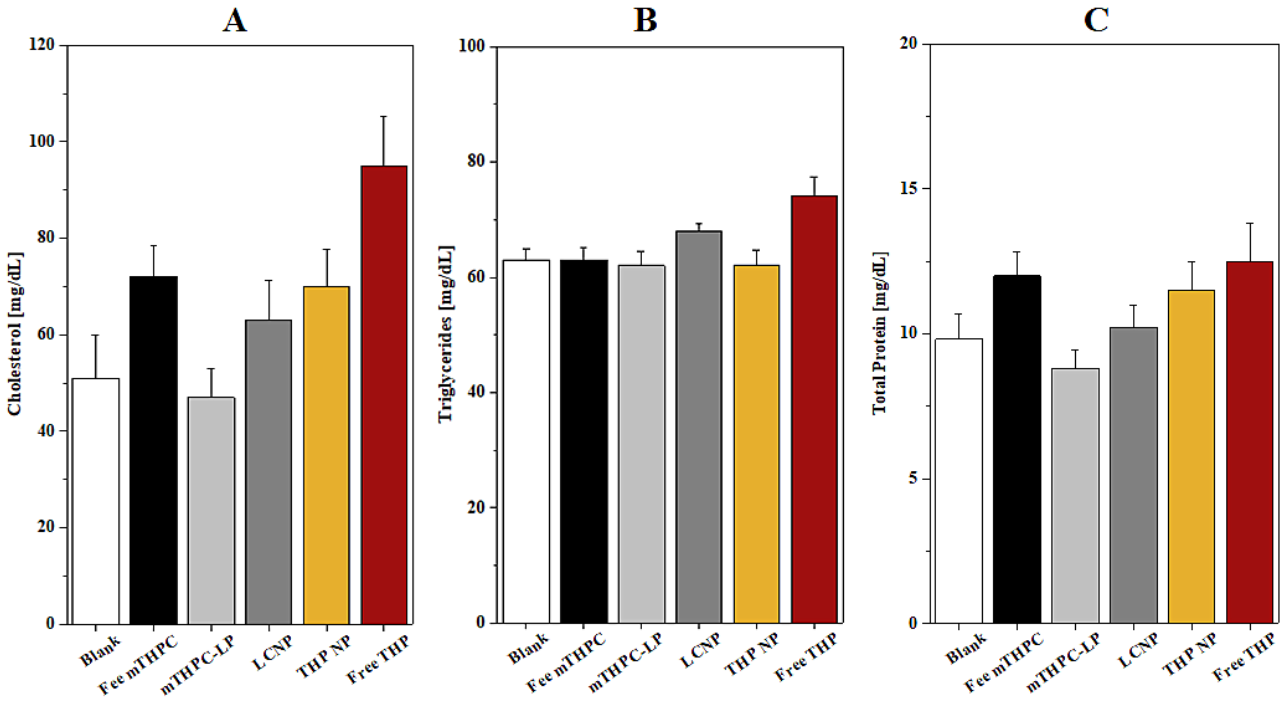

Figure 41. Typical renal function tests (RFTs) parameters including (A) creatinine, (B) Bilirubin and (C) uric acid levels in mice after being treated with the nanoformulations intravenously. Values are represented as mean ± S.D (n=3).

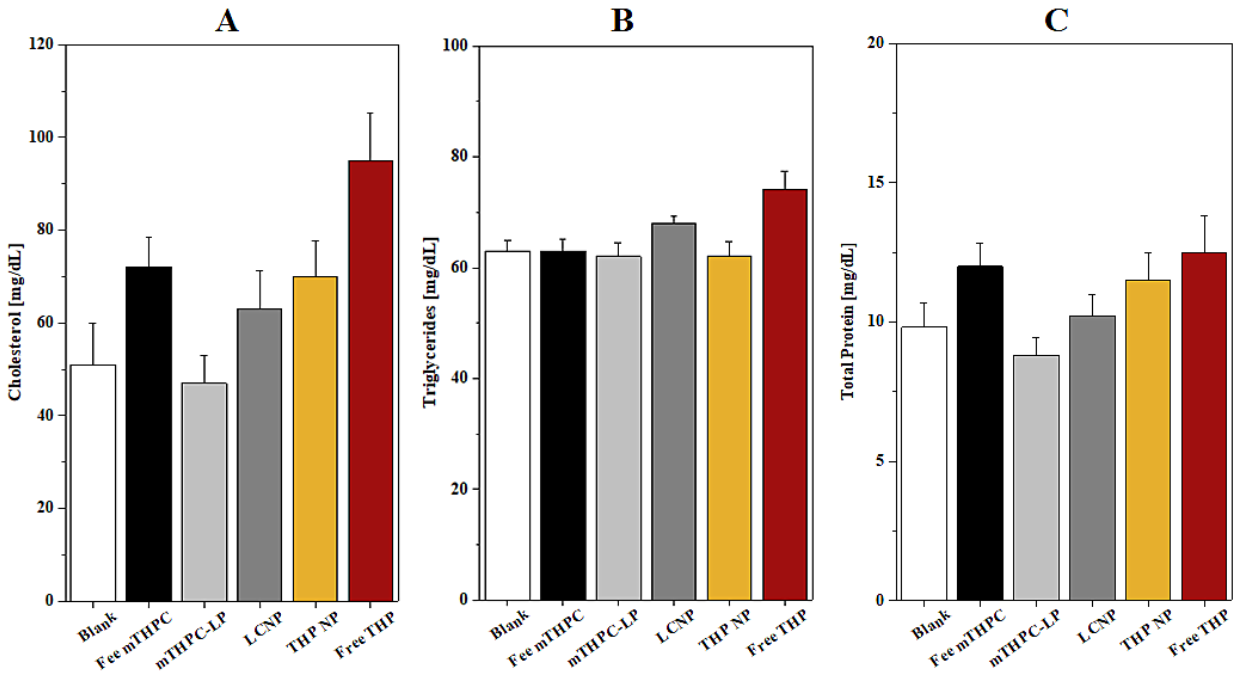

Figure 42. Typical lipid profile including (A) cholesterol, (B) triglycerides as well as (C) total protein levels after being treated with the nanoformulations intravenously. Values are represented as mean ± S.D (n=3).

3.2.12.4 Hematological analysis

Any foreign material including drug formulations when coming in contact with blood components may induce an acute inflammatory response resulting in complications to the pharmacotherapy. This necessitates the complete exploration of the possible toxicity potential of drug formulations and their carrier systems on the blood profile [79]. The effect of our nanoformulations on the mice's blood and its components was also evaluated through complete blood count (CBC). The results for the hematological analysis are presented in Table 8. The results demonstrated that free THP damaged the RBCs integrity resulting in decreased total erythrocyte count (TEC) which resulted in the reduction of hemoglobin (Hb) level in the blood. TEC and Hb levels were also reduced in free mTHPC treated group but less profound as compared to free THP. However, mTHPC-LP, LCNP, and THP NP did not significantly affect the RBCs level when compared with the control (blank) group. These observations were also in accordance with the previous results obtained during the ex vivo hemolysis assay. Total leukocyte count (TLC) was also remarkably affected during treatment with free THP which can lead to neutropenia [121]. This may be caused by bone marrow suppression resulting in a delayed inflammatory response. Free mTHPC also reduced the TLC but the effect was less intense as compared to free THP. These results call for the encapsulation of the free THP/mTHPC into relatively nontoxic carrier systems. The mTHPC-

LP, THP NP and LCNP did not show a significant effect on WBCs. Other parameters including mean corpuscular volume (MCV), Hematocrit (HCT), mean corpuscular hemoglobin (MCH), mean corpuscular hemoglobin concentration (MCHC), platelets count and mean platelet volume (MPV) were also monitored and it was observed that all these parameters remained more or less unchanged in all the nanoformulations, depicting the safety of these formulations.

Table 8. The changes in biochemical parameters in the blood serum of albino mice after intravenous administration of free mTHPC, mTHPC loaded liposomes, LCNP, THP PLGA nanoparticles, free THP, and normal saline into the tail vein. After 7 days of treatment, blood was withdrawn from the mice and complete blood count was performed. The values are expressed as mean ± S. D (n = 3).

Biomarker	Free mTHPC	mTHPC-LP	LCNP	THP NP	Free THP	Blank
TEC (10^{12}/L)	5.9 ± 1.6	7.0 ± 1.6	6.4 ± 1.7	6.2± 1.2	5.4 ± 1.8	6.7 ± 1.9
Hb (g/dL)	10.2 ± 1.8	10.5 ± 2.1	10.7 ± 1.6	10.7 ± 2.2	9.8 ± 1.9	10.9 ± 1.8
MCV (fL)	52.3 ± 5.4	54.7 ± 4.8	59.6 ± 5.4	55.5 ± 6.0	51.2 ± 5.5	58.3 ± 4.2
HCT (%)	31.6 ± 4.6	33.5 ± 5.3	32.1 ± 5.1	31.5 ± 3.9	30.8 ± 6.0	32.4 ± 5.6
MCH (pg)	16.5 ± 2.3	17.4 ± 2.6	16.8 ± 3.5	17.6 ± 2.7	18.4 ± 3.4	16.3 ± 4.1
MCHC (%)	34.7 ±2.8	33.8 ± 3.1	33.1 ± 1.7	34.6 ± 2.6	30.1 ± 2.9	33.6 ± 3.6
TLC (10^9/L)	8.7 ± 2.4	9.2 ±3.7	9.7 ± 3.9	8.9 ± 2.5	8.2 ± 2.7	9.4 ± 3.5
Platelets (10^9/L)	705 ± 19	714 ± 27	738 ± 21	726 ± 28	693 ± 22	758 ± 25
MPV (fL)	8.0 ± 1.6	7.7 ± 2.0	7.6 ± 1.8	7.9 ± 2.1	8.4 ± 2.1	7.5 ± 1.9

3.2.12.5 Erythrocyte adhesiveness /aggregation test (EAAT)

The erythrocyte aggregation assay is a sensitive biomarker to detect the presence of low grade, smoldering and subclinical inflammation. The degree of erythrocyte adhesiveness/aggregation correlated significantly with the presence of enhanced concentrations of the inflammation-sensitive plasma proteins (i.e. fibrinogen) which are directly involved in the erythrocyte aggregability. In our study, EAAT was carried out to check the ex vivo behavior of the nanoformulations on the red blood cells (RBCs) (Fig. 43). It was evident from the assay that the RBCs treated with free drugs (i.e. free mTHPC and free THP) as well as THP loaded nanoparticles showed slight changes in the overall structure and morphology in the erythrocytes. However, the changes were not to an extent to damage the RBCs morphology completely. In contrast to the free drugs, mTHPC-LP and LCNP did not induce any aggregation effect. These results were in correlation with the results of the hematological analysis which showed a small decrease in the erythrocytes counts when treated with free mTHPC, free THP or THP loaded PLGA nanoparticles. Based on these observations, it was inferred that our nanoformulations have very

slightly affected the erythrocytes and can be considered a biocompatible as the EAAT index was still within the acceptable limits [81, 122].

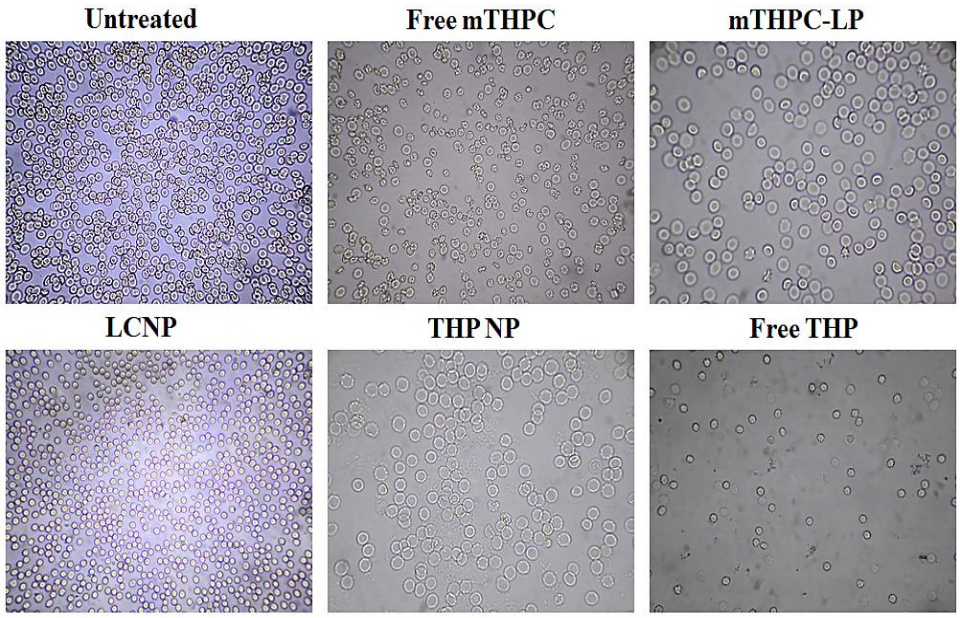

Figure 43. Ex vivo erythrocytes aggregation assay after treatment with the nanoformulations (free mTHPC and mTHPC liposomes at a dose equivalent to 0.150 mg kg-1 body weight; free THP and THP NP at a dose equivalent to 5 mg kg-1 body weight, while the LCNP was a administered at a combined dose of both mTHPC/THP) with 100 µl of erythrocytes suspension (2% v/v) compared to untreated cells.

3.2.12.6 Histopathological examinations

One of the major problems associated with the clinical use of the anticancer agents (e.g. chemotherapeutics and photosensitizers) is the injuries on the peripheral tissues which can lead to multiple organ toxicity [48]. In order to examine any toxicity to mice organs after being treated with our nanoformulations, the biochemical analysis was accompanied by histological studies. The histological slide of vital organs (i.e. heart, liver, kidney, and lungs) was prepared through the rotary microtome. The tissue sectioned were fixed on glass slides, stained with H&E stain and observed under the microscope (Fig. 44). For the H & E staining, the cell nucleus was stained blue with hematoxylin while the cell cytoplasm and extracellular matrix were stained pink by eosin. Normal cells appeared polygonal in shape with blue nuclei in spherical or spindle shape. The cytoplasm of the necrotic cells became pink amorphous material with their nucleus disappeared. Whereas the apoptotic cells shrank and turned round with the nucleus condensed and became darker [123]. The images of the tissue sections are presented in Fig. 44. From the figure, it can be observed that heart samples from all treatment groups appear to be completely normal.

There are no visible signs of inflammation, necrosis or hyperthermia. The structure of the liver was also found to be normal and no changes in fat tissues were seen except for free THP. The free THP treated group showed some signs of the apoptotic cells with fibrosis, pyknosis and hepatic lesions [124]. No evidence of the necrotic bodies or hydrophobic degradation was found in any of the treatment groups. Kidney showed the signs of necrosis, apoptosis, as well as congestion of the renal tissue in the free THP and THP NP, treated groups while other treatment groups remained unaffected. Moreover, small changes in the lung's histology with the breakage of the lung's fiber were also noticeable in free THP and THP NP treated groups [123]. In all the other treatment groups, normal alveolar and arteriolar structures were observed. These findings confirmed the safety of our lipid coated particles as no evidence of the toxicity was visible in any of histological studies.

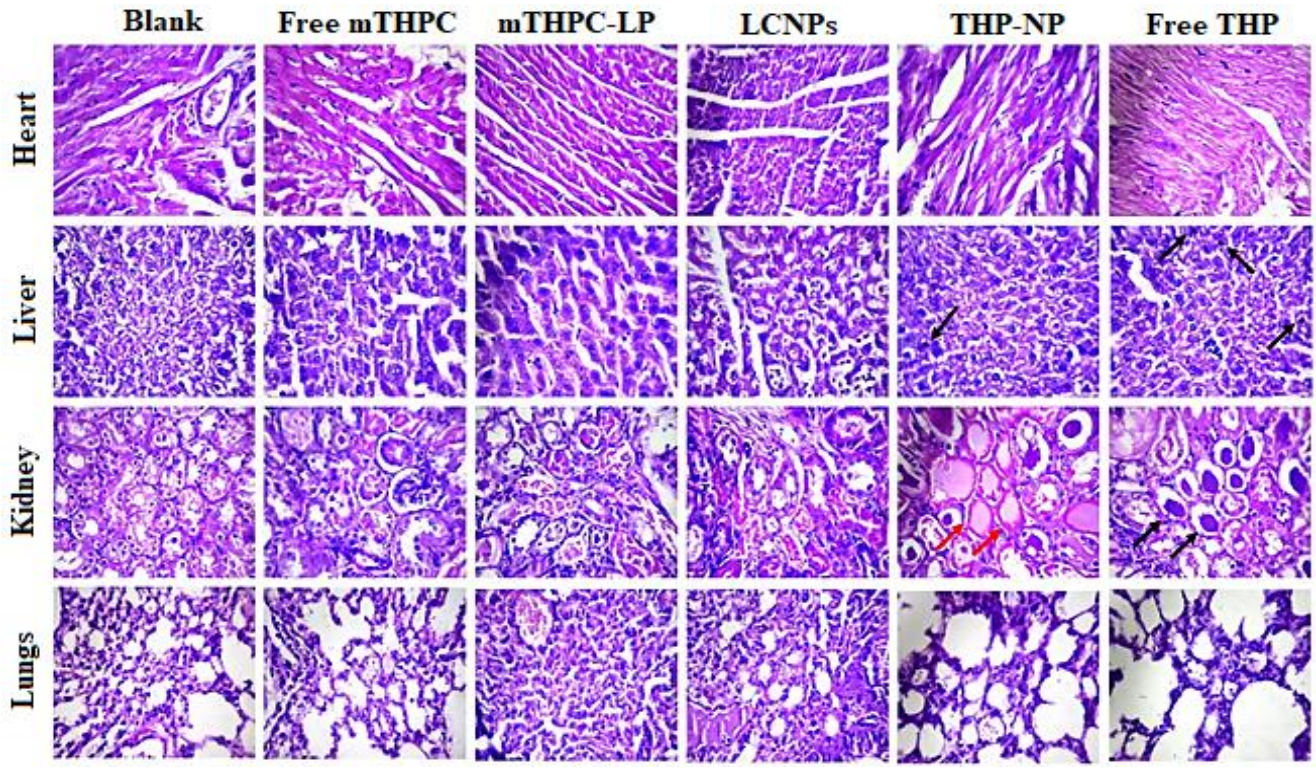

Figure 44. Histopathological analysis of various organs after treatment with free mTHPC, mTHPC-LP, THP NP, LCNPs and free THP. The animals treated with normal saline were taken as control (Blank). The tissues were stained with hematoxylin/eosin to assess the potential effects of treatments on the organ's morphology and cellular damage.

Chapter IV: Summary and Outlook

4.1 Summary and outlook

The main theme of the present work was the development of a novel nanocarrier system that can deliver two different therapeutics modalities to the cancer cells. Such a nanocarrier is superior to conventional drug delivery system as it combines two different approaches (i.e. chemotherapy and photodynamic therapy) within one carrier system to treat the cancer. In this work, we were interested in lipid enveloped biodegradable nanoparticles termed as lipoparticles in which two hydrophobic drugs could be encapsulated in separate compartments, a chemotherapeutic agent (Pirarubicin, THP) in the nanoparticle core and a photosensitizer (Temoporfin, mTHPC) in the lipid bilayer shell. Such a system not only increases the therapeutic efficacy, circulating time and bioavailability of the drugs but also reduce the drug leakage and side effects to the other body tissues.

In the introduction part of the thesis deals with back ground of the basic principles and detailed mechanism of the photodynamic therapy. The ideal properties of the photosensitizers were discussed. This was followed by a brief insight into the nanocarriers including the liposomes, polymeric nanoparticles and lipid-polymer hybrid nanoparticles. Different methods to prepare the lipoparticles have also been discussed.

The methodology section of the thesis deals with the preparation of mTHPC loaded liposomes, THP loaded nanoparticles and consequently the lipid enveloped polymeric nanoparticles. The formed nanoformulations were then evaluated in terms of physicochemical characterizations, *in vitro*, *in ovo*, *in vivo* as well as the biocompatibility studies.

In results section, the encapsulation of mTHPC, a potent 2nd generation PS in the liposomes was discussed. For this purpose, a broad range of lipid combination was explored. The physicochemical characterizations including size distribution, zeta potential and encapsulation efficiency was performed. Surface morphological studies using the at atomic force microscopy and cryogenic transmission electron microscopy was conducted. The results obtained from these studies were found to be in accordance with the previous results obtained from the zeta sizer measurement. Further investigations including quantitative assessment of the reactive oxygen species and cellular photodynamic therapy at different wavelengths and different light doses have been discussed. In order to minimize the unethical use of the animals, chick chorioallantoic membrane model (*in ovo*) as an alternative *in vivo* model was elaborated for the vascular targeted photodynamic therapy. The intracellular uptake studies using confocal laser scanning microscopy was performed and an effective cellular uptake in the perinuclear region have been shown.

In the next chapter of the results, the encapsulation of THP loaded PLGA nanoparticles have been discussed. Two different size of nanoparticles (200nm and 400nm) were prepared in order to have a comparative evaluation of the nanoparticles size, polydispersity index as well as the cell viability using dynamic light scattering and MTT assay respectively. In vitro drug release in simulated conditions revealed a biphasic drug release pattern with initial burst release phase followed by the sustained released pattern for the following days. The THP nanoparticles with smaller size (200nm) showed a higher drug release as compared to 400nm THP NP which was attributed to the larger available surface area for drug diffusion in the earlier case.

Further in the results section, the preparation of the lipoparticles have been discussed. Based on the preliminary studies, two best performing liposomes DPPC/mPEG-DPPE$_{5000}$ and DPPC/DPPG were combined to form a single liposome i.e. DPPC/DPPG/mPEG-DPPE$_{5000}$ and was coated over the 200nm THP nanoparticles. The formed lipoparticles were also subjected to physicochemical characterizations. An increase in the lipoparticles size of 4-5 nm as compared to uncoated nanoparticles was perceived which was also confirmed with the surface morphological studies using AFM and TEM. The determination higher therapeutic efficacy of the lipoparticles by in vitro cytotoxicity synergism and ROS assay has also been described. The lipoparticles did not show any genotoxicity has been elaborated using single cell gel electrophoresis (comet assay). The stability of the lipoparticles was established in simulated physiological conditions (60% serum & PBS 7.4) and small reduction in particles size owing to the presence of protein corona was demonstrated.

Biocompatibility studies were also performed to validate the compatibility of the lipoparticles with the blood components. Hemolysis assay, activated partial thromboplastin time and erythrocyte aggregation assay confirmed the non-toxic and biocompatible nature of the lipoparticles. After the evidencing the biocompatibility of the lipoparticles, the acute in vivo toxicity assessment was performed using BALB/c mice. No significant changes in the body visceral index and serum biomarkers was observed. Also, no significant changes in the tissue histopathology was observed.

On the basis of all of these finding, it can be concluded that development of such a novel nanocarrier system can be employed for simultaneous delivery of the multiple drugs to the cancer cells with minimum toxicity. Future pharmacokinetic profiling with *in vivo* biodistribution and *in vivo* tumor models with targeting ligands (e.g. antibodies, aptamer etc.) attached on the lipoparticles can serve as a critical link for the pre-clinical studies.

4.2 Zusammenfassung und Ausblick

Das Hauptthema der vorliegenden Arbeit war die Entwicklung eines neuartigen Nanocarrier-systems, das zwei verschiedene Therapieansätze zur Krebsbehandlung vereint. Ein solcher Nanocarrier ist dem herkömmlichen Drug Delivery System überlegen, da er verschiedene Ansätze (z.B. Chemotherapie und photodynamische Therapie) innerhalb eines Trägersystems kombiniert. In dieser Arbeit lag der Fokus auf Lipid umhüllte, biologisch abbaubare Nanopartikel, die als „Lipopartikel“ bezeichnet werden. Hierbei ist es möglich, zwei hydrophobe Arzneistoffe in getrennten Bereichen des Trägersystems zu verkapseln: ein Chemotherapeutikum (Pirarubicin, THP) im Nanopartikelkern und ein photoaktiver Stoff (Temoporfin, mTHPC) in der Lipid-Doppelschicht. Ein solches System erhöht nicht nur die therapeutische Wirksamkeit, die Blutzirkulationszeit und die Bioverfügbarkeit der Arzneimittel, sondern reduziert auch den frühzeitigen Austritt des Arzneistoffes sowie Nebenwirkungen auf andere Gewebe.

In der Einleitung der Arbeit werden die Grundprinzipien und der detaillierte Mechanismus der photodynamischen Therapie dargestellt. Das Eigenschaftenprofil wie auch deren Optimierung solcher photoaktiven Stoffe, der sogenannten „Photosensitizer“, standen hier im Vordergrund der Diskussion. Im Anschluss erfolgte eine systematische Präsentation nanoskaliger „drug delivery“ Systeme, einschließlich Liposomen, polymerer Nanopartikel und Lipid-Polymer-Hybrid-Nanopartikel. Verschiedene Methoden zur Herstellung der modernen Lipopartikel wurden ebenfalls dargestellt und diskutiert.

Der experimentelle Teil der Dissertation umfasst die Herstellung mTHPC-beladener Liposomen, THP-beladener Nanopartikel und Lipid umhüllter Polymernanopartikel. Die Charakterisierung der hergestellten parenteralen Formulierungen erfolgte mit Hilfe von physikalisch-chemischen Methoden, in vitro, in ovo, in vivo sowie mit toxikologischen Biokompatibilitätsstudien.

Der Ergebnisteil beschreibt ausführlich die verwendeten Methoden und Analyse der Verkapselung von mTHPC, dem verwendeten potenten Photosensitizer der 2. Generation, in Liposomen. Zu diesem Zweck wurde ein breites Spektrum an Lipidkombinationen getestet und mit physikalisch-chemischen Methoden einschließlich Größenverteilung, Zetapotenzial sowie deren Verkapselungseffizienz untersucht. Durch Rasterkraftmikroskopie (AFM) und Gefrier-Transmissionselektronenmikroskopie konnte die Teilchengröße wie auch deren Oberflächenmorphologie analysiert werden. Die Ergebnisse dieser Studien bestätigten die Ergebnisse der PCS-Messungen. Weitere Untersuchungen wie die quantitative Bewertung der während der biologischen Untersuchungen entstandenen reaktiven Sauerstoffspezies sowie die Wirkung der in Zellkultur durchgeführten photodynamischen Therapie, bei verschiedenen Wellenlängen und Lichtstärken, wurden diskutiert. Um die unethische Nutzung von Versuchstieren zu minimieren, erfolgte die Untersuchung der gezielten antivaskulären (antiangiogenese Therapie) photodynamischen Therapie an dem chorioallantoischen Membranmodell (CAM, *in ovo*), das eine Alternative zum *in vivo* Modell darstellt. Die Aufnahme der Wirkstoffträger in die Zellen erfolgte mit Hilfe der konfokalen Laserscanning-Mikroskopie und verdeutlichte eine effektive zelluläre Aufnahme in den perinukleären Bereich.

Das folgende Kapitel des Ergebnisteils beschäftigt sich mit der Verkapselung von THP in PLGA-Nanopartikel. Zwei verschiedene Größen von Nanopartikeln (200nm und 400nm) wurden hergestellt, um eine vergleichende Bewertung der Größe der Nanopartikel und des Polydispersitätsindex auf das Zellüberleben zu erhalten. Diese Daten konnten mittels dynamischer Lichtstreuung bzw. MTT-Assay erhalten werden. Die *in vitro* Freisetzung des Arzneistoffes unter simulierten Bedingungen ergab ein zweiphasiges Freisetzungsprofiel, mit einer anfänglichen Burst-Freisetzungsphase, gefolgt von einer über die folgenden Tage anhaltenden kontinuierlichen Freisetzung. Die THP-Nanopartikel mit geringerer Größe (200 nm) zeigten dabei eine höhere Wirkstofffreisetzung pro Zeiteinheit im Vergleich zu 400 nm großen THP Nanopartikeln, was als eine Folge der größeren verfügbaren Oberfläche für die Wirkstoffdiffusion diskutiert werden kann.

Basierend auf den Voruntersuchungen wurden im nächsten Kapitel die beiden leistungsstärksten Liposomen zu einem einzigen Liposom mit der Zusammensetzung DPPC/DPPG/mPEG-DPPE5000 kombiniert. Diese Liposomen sind anschließend zur Beschichtung der 200nm großen THP-Nanopartikel verwendet worden. Diese wurden eingehend physikalisch-chemisch charakterisiert. Die Lipopartikelgröße nimmt um etwa 4-5 nm im Vergleich zu unbeschichteten Nanopartikeln zu, was auch die oberflächenmorphologischen Studien mit AFM und TEM bestätigten. Die Bestimmung der höheren therapeutischen Wirksamkeit der Lipopartikel durch Zytotoxizitätsstudien wurde *in vitro* betätigt. Der Nachweis der erhöhten Produktion reaktiver Sauerstoffspezies erfolgte ebenfalls. Die Einzelzellgelelektrophorese (Comet-Assay) gab keinerlei Hinweise auf eine Genotoxizität der Lipopartikel. Die Untersuchung der Stabilität der Lipopartikel fand unter simulierten physiologischen Bedingungen (60% Serum, PBS 7,4) statt und zeigte eine geringe Vergrößerung des Partikeldurchmessers durch das Vorhandensein einer Proteinkorona.

Durch Biokompatibilitätsstudien war es möglich, die Verträglichkeit der Lipopartikel mit Blutkomponenten zu validieren. Die Bestimmung der aktivierten Teilthromboplastinzeit und Erythrozytenaggregationstests bestätigten die Verträglichkeit und Biokompatibilität der Lipopartikel. Anschließend konnte die *in vivo* Toxizität der Lipidpartikel an BALB/c-Mäusen stattfinden. Es wurden keine signifikanten Veränderungen im viszeralen Index der Mäuse und in den Serum-Biomarkern beobachtet. Die Gewebehistopathologie zeigte ebenfalls keine signifikanten Veränderungen.

Auf der Grundlage all dieser Ergebnisse kann der Schluss gezogen werden, dass es möglich ist, solche neuartigen Nanocarriersystems für die gleichzeitige Abgabe verschiedener Arzneistoffe an Krebszellen mit minimaler Toxizität prinzipiell einzusetzen. Die zukünftige Erstellung des pharmakokinetischen Profils einschließlich der *in vivo* Biodistribution und die Überprüfung der Effektivität der Lipopartikel an *in vivo* Tumormodellen können als kritisches Bindeglied für präklinische Studien dienen. Auch durch eine Kopplung von Liganden (z.B. Antikörpern, Aptameren etc.) kann eine weitere Steigerung der Effizienz erreicht werden.

Chapter IV: Appendix

5.1 Research output

5.1.1 Publications:

Sajid Ali, Muhammad Umair Amin, Muhammad Yasir Ali, Imran Tariq, Shashank Reddy Pinnapireddy, Lili Duse, Nathalie Goergen, Christian Wölk, Gerd Hause, Jarmila Jedelská, Jens Schäfer and Udo Bakowsky; Wavelength dependent photo-cytotoxicity to ovarian carcinoma cells using temoporfin loaded tetraether liposomes as efficient drug delivery system. *Submitted manuscript.*

Sajid Ali, Muhammad Umair Amin, Imran Tariq, Farhan Sohail, Muhammad Yasir Ali, Shashank Reddy Pinnapireddy, Lili Duse, Jarmila Jadelská, Jens Schäfer and Udo Bakowsky; Lipid enveloped biodegradable nanoparticles for synergistic delivery of temoporfin and pirarubicin to ovarian carcinoma cells; *in vitro* and *in vivo* evaluations. *Ready for submission.*

Sajid Ali, Muhammad Umair Amin, Imran Tariq, Farhan Sohail, Muhammad Yasir Ali, Shashank Reddy Pinnapireddy, Jarmila Jadelská, Jens Schäfer and Udo Bakowsky; Temoporfin loaded biodegradable polymeric nanoparticles for the photodynamic therapy of ovarian carcinoma cells; *in vitro* and *in vivo* toxicity profile. *Manuscript in preparation*

Muhammad Umair Amin, **Sajid Ali**, Imran Tariq, Muhammad Yasir Ali, Shashank Reddy Pinnapireddy, Christian Wölk, Richard D. Harvey, Gerd Hause, Jana Brüßler, Udo Bakowsky; Ultrasound-responsive smart drug delivery system of lipid coated mesoporous silica nanoparticles. *Ready for submission*

Muhammad Umair Amin, **Sajid Ali**, Muhammad Yasir Ali, Imran Tariq, Shashank Reddy Pinnapireddy, Udo Bakowsky, and Jana Brüßler; Lipid coated mesoporous silica nanoparticles for enhanced delivery and cellular uptake of Doxorubicin. *Ready for submission*

Muhammad Umair Amin, **Sajid Ali**, Dominik C. Fuhrmann, Imran Tariq, Muhammad Yasir Ali, Jana Brüßler, Bernhard Brüne, Udo Bakowsky; Lipid supported mesoporous silica nanoparticles for co-delivery of carbonic anhydrase IX inhibitor and Doxorubicin to address chemoresistance in hypoxia. *Manuscript in preparation*

Imran Tariq, Shashank Reddy Pinnapireddy, Lili Duse, Muhammad Yasir Ali, **Sajid Ali**, Muhammad Umair Amin, Nathalie Goergen, Jarmila Jedelská, Jens Schäfer and Udo Bakowsky; Lipodendriplexes: A promising nanocarrier for enhanced gene delivery with minimal cytotoxicity, European journal of pharmaceutics and biopharmaceutics, 135 (2019) 72-82.

Imran Tariq, Muhammad Yasir Ali, Muhammad Farhan Sohail, Muhammad Umair Amin, **Sajid Ali**, Nadeem Irfan Bukhari, Abida Raza, Shashank Reddy Pinnapireddy, Jens Schäfer and Udo Bakowsky; A comprehensive biodistribution and toxicity profile of PAMAM based lipid triblock nanocarriers after system delivery. *Ready for submission.*

Imran Tariq, Muhammad Yasir Ali, Harshvardhan Janga, **Sajid Ali**, Muhammad Umair Amin, Uzma Ali, Ghazala Ambreen, Shashank Reddy Pinnapireddy, Jens Schäfer and Udo Bakowsky; Downregulation of *MDR* 1 gene contributes to caspase-dependent apoptosis in colon carcinoma: A gravity to space investigation. *Ready for submission.*

Muhammad Yasir Ali, Imran Tariq, **Sajid Ali**, Muhammad Umair Amin, Shashank Reddy Pinnapireddy, Lili Duse, Konrad Engelhardt, Jens Schäfer, and Udo Bakowsky; Targeted ErbB3 cancer therapy: A synergistic approach to effectively combat cancer. International journal of pharmaceutics, 575 (2019) 118961.

Muhammad Yasir Ali, Imran Tariq, Muhammad Farhan Sohail, Muhammad Umair Amin, **Sajid Ali**, Shashank Reddy Pinnapireddy, Asad Ali, Jens Schäfer, and Udo Bakowsky; Selective anti-ErbB3 aptamer modified sorafenib microparticles: *In vitro* and *in vivo* toxicity assessment. European journal of pharmaceutics and biopharmaceutics, 145 (2019) 42-53

5.2 Presentations

Photodynamic mediated anticancer therapy using Temoporfin loaded liposomes- *Oral Presentation*: **Sajid Ali**, Umair Amin, Jens Schäfer, Jarmila Jedelská and Udo Bakowsky; 12th World Drug Delivery Summit (Conference series LLC Ltd) 24-26 September 2018, Chicago, Illinois, USA.

5.2.1 Poster Presentations

Temoporfin liposomes as an efficient delivery system for antimicrobial photodynamic therapy- *Poster Presentation*: **Sajid Ali**, Umair Amin, Imran Tariq, Yasir Ali, Shashank Reddy Pinnapireddy, Jarmila Jedelská, Jens Schäfer and Udo Bakowsky; 23nd Annual Meeting of Controlled Release Society, German Local Chapter (Functional Biomaterials and Release of Nucleic Acid Drugs) 7-8 March, 2019, Leipzig, Germany.

Photodynamic mediated anticancer therapy using Temoporfin loaded liposomes- *Poster Presentation*: **Sajid Ali**, Umair Amin, Jens Schäfer, Jarmila Jedelská and Udo Bakowsky; 12th

World Drug Delivery Summit (Conference series LLC Ltd) 24-26 September 2018, Chicago, Illinois, USA.

Lipid enveloped PLGA nanoparticles for synergistic photo-chemotherapy- *Poster Presentation*: **Sajid Ali**, Jens Schäfer, Jarmila Jedelská, Umair Amin and Udo Bakowsky; 21st Annual Meeting of Controlled Release Society, German Local Chapter (Future Trends in Nanomedicine) 2-3 March 2017, Marburg, Germany

5.3 Curriculum Vitae

PERSONAL INFORMATION

Name	**Sajid Ali**
Address (1)	Zimmer 02-02 Geschwister Scholl Str. Maxkade wohnheim 11C, 35039 Marburg, Germany
Address (2)	House No. 47, Street No. 09, Main Bazar Gulshan Park MughalPura, Lahore, Pakistan
Telephone	Mobile: +49 152 06491522
Email	sajid.ali@pharmazie.uni-marburg.de sajidalichishti@gmail.com
Aufenthalstitel	YOFZOYLL3
Nationality	Pakistani
Date of Birth	02.02.1986

WORKING EXPERIENCE

Lecturer **1st July 2011 till to date**
Faculty of Pharmacy
The University of Lahore, Lahore Pakistan

Production Pharmacist **1st March 2010 - 30th June 2011**
SEARLE Pakistan Pvt. Ltd

EDUCATION AND CERTIFICATES

Matriculation (BISE, Lahore)	**2001**	**78.94%**
F.Sc. (BISE, Lahore)	**2004**	**77.09%**
Pharm-D The Faculty of Pharmacy Bahauddin Zakariya University, Multan, Pakistan	**2010**	**60.30%**

M. Phil Pharmaceutics **2013** **3.6 CGPA**
The Faculty of Pharmacy
The University of Lahore, Lahore, Pakistan

PhD Scholar **1st March 2016 to 30th March 2020**
Department of Pharmaceutics and Biopharmaceutics
Philipps University Marburg, Marburg, Germany

ORGANIZATIONAL GOAL

To achieve responsible, challenging and career growth-oriented position in the organization and want to work more efficiently by harnessing the potentials of honesty, hard work, dedication, and professional skills

CONFERENCES

- 23rd Annual Meeting of Controlled Release Society, German Local Chapter (Functional Biomaterials and Release of Nucleic Acid Drugs) 7-8 March 2019, Leipzig, Germany.
- 12th World Drug Delivery Summit (Conference series LLC Ltd) 24-26 September 2018, Chicago, Illinois, USA.
- 21st Annual Meeting of Controlled Release Society, German Local Chapter (Future Trends in Nanomedicine) 2-3 March 2017, Marburg, Germany.

INSTRUMENT HANDLING

- Atomic force microscope, JPK Instruments, Germany
- Zeta sizer, Malvern Instruments, Germany
- UV/VIS spectrophotometer, Shimadzu UV-1240, Japan
- Fluostar optima plate reader, BMG Labtech, Germany
- Fluorescence microscopy, Olympus, Germany
- Dissolution apparatus, Erweka DT-700, Germany
- Freeze Dryer, Christ
- Rotary evaporator, Heidolph, Japan

REFERENCES

Prof. Dr. Udo Bakowsky
ubakowsky@aol.com
0049 (6421) 2825881

Dr. Jens Schafer
j.schaefer@staff.uni-marburg.de
0049 (171) 1219000

5.4 References:

1. Krishnamurthy, S., et al., Lipid-coated polymeric nanoparticles for cancer drug delivery. Biomaterials science, 2015. 3(7): p. 923-936.
2. Chow, E.K.-H. and D. Ho, Cancer nanomedicine: from drug delivery to imaging. Science translational medicine, 2013. 5(216): p. 216rv4-216rv4.
3. Moore, C.M., D. Pendse, and M. Emberton, Photodynamic therapy for prostate cancer—a review of current status and future promise. Nature Reviews Urology, 2009. 6(1): p. 18.
4. Spikes, J.D., Photodynamic action: from paramecium to photochemotherapy. Photochemistry and Photobiology, 1997. 65: p. 142S-147S.
5. Triesscheijn, M., et al., Photodynamic therapy in oncology. The oncologist, 2006. 11(9): p. 1034-1044.
6. Ledoux-Lebards, C., Action de la lumiere sur la toxicite de l'eosine et de quelques autres substances. Ann. l'Institut. Pasteur, 1902. 16: p. 587-593.
7. Dolmans, D.E., D. Fukumura, and R.K. Jain, Photodynamic therapy for cancer. Nature reviews cancer, 2003. 3(5): p. 380.
8. Robertson, C.A., D.H. Evans, and H. Abrahamse, Photodynamic therapy (PDT): a short review on cellular mechanisms and cancer research applications for PDT. Journal of Photochemistry and Photobiology B: Biology, 2009. 96(1): p. 1-8.
9. Castano, A.P., T.N. Demidova, and M.R. Hamblin, Mechanisms in photodynamic therapy: part one—photosensitizers, photochemistry and cellular localization. Photodiagnosis and photodynamic therapy, 2004. 1(4): p. 279-293.
10. Detty, M.R., S.L. Gibson, and S.J. Wagner, Current clinical and preclinical photosensitizers for use in photodynamic therapy. Journal of medicinal chemistry, 2004. 47(16): p. 3897-3915.
11. Allison, R.R., et al., Photosensitizers in clinical PDT. Photodiagnosis and photodynamic therapy, 2004. 1(1): p. 27-42.
12. Peer, D., et al., Nanocarriers as an emerging platform for cancer therapy. Nature nanotechnology, 2007. 2(12): p. 751.
13. Hans, M.L. and A.M. Lowman, Biodegradable nanoparticles for drug delivery and targeting. Current Opinion in Solid State and Materials Science, 2002. 6(4): p. 319-327.
14. Soppimath, K.S., et al., Biodegradable polymeric nanoparticles as drug delivery devices. Journal of controlled release, 2001. 70(1-2): p. 1-20.
15. Daraee, H., et al., Application of liposomes in medicine and drug delivery. Artificial cells, nanomedicine, and biotechnology, 2016. 44(1): p. 381-391.

16. Gregoriadis, G. and A.T. Florence, Liposomes in drug delivery. Drugs, 1993. 45(1): p. 15-28.
17. Sercombe, L., et al., Advances and challenges of liposome assisted drug delivery. Frontiers in pharmacology, 2015. 6: p. 286.
18. Riaz, M.K., et al., Surface functionalization and targeting strategies of liposomes in solid tumor therapy: A review. International journal of molecular sciences, 2018. 19(1): p. 195.
19. Mandal, B., et al., Core–shell-type lipid–polymer hybrid nanoparticles as a drug delivery platform. Nanomedicine: Nanotechnology, Biology and Medicine, 2013. 9(4): p. 474-491.
20. Zhang, L., et al., Self-assembled lipid− polymer hybrid nanoparticles: a robust drug delivery platform. ACS nano, 2008. 2(8): p. 1696-1702.
21. Cheow, W.S. and K. Hadinoto, Factors affecting drug encapsulation and stability of lipid–polymer hybrid nanoparticles. Colloids and Surfaces B: Biointerfaces, 2011. 85(2): p. 214-220.
22. Klopfer, K. and T. Vanderlick, Isotherms of dipalmitoylphosphatidylcholine (DPPC) monolayers: features revealed and features obscured. Journal of colloid and interface science, 1996. 182(1): p. 220-229.
23. Wang, M., et al., The effect of temperature on supported dipalmitoylphosphatidylcholine (DPPC) bilayers: Structure and lubrication performance. Journal of colloid and interface science, 2015. 445: p. 84-92.
24. Bedu-Addo, F.K., et al., Effects of polyethyleneglycol chain length and phospholipid acyl chain composition on the interaction of polyethyleneglycol-phospholipid conjugates with phospholipid: implications in liposomal drug delivery. Pharmaceutical research, 1996. 13(5): p. 710-717.
25. Sandström, M.C., E. Johansson, and K. Edwards, Structure of mixed micelles formed in PEG-lipid/lipid dispersions. Langmuir, 2007. 23(8): p. 4192-4198.
26. Terp, M.C., et al., Differential efficacy of DOTAP enantiomers for siRNA delivery in vitro. International journal of pharmaceutics, 2012. 430(1-2): p. 328-334.
27. Inglut, C.T., et al., Predictors and Limitations of the Penetration Depth of Photodynamic Effects in the Rodent Brain. Photochemistry and photobiology, 2019.
28. Jõemetsa, S., et al., Molecular Lipid Films on Microengineering Materials. Langmuir, 2019. 35(32): p. 10286-10298.
29. Engelhardt, K.H., et al., Transfection studies with colloidal systems containing highly purified bipolar tetraether lipids from sulfolobus acidocaldarius. Archaea, 2017. 2017.

30. Ulrih, N.P., D. Gmajner, and P. Raspor, Structural and physicochemical properties of polar lipids from thermophilic archaea. Applied microbiology and biotechnology, 2009. 84(2): p. 249-260.
31. Swain, M., et al., Identification of β-l-gulose as the sugar moiety of the main polar lipid of Thermoplasma acidophilum. Biochimica et Biophysica Acta (BBA)-Lipids and Lipid Metabolism, 1997. 1345(1): p. 56-64.
32. Jeworrek, C., et al., Structure and phase behavior of archaeal lipid monolayers. Langmuir, 2011. 27(21): p. 13113-13121.
33. Nogueira, E., et al., Design of liposomal formulations for cell targeting. Colloids and Surfaces B: Biointerfaces, 2015. 136: p. 514-526.
34. Crook, K., et al., Inclusion of cholesterol in DOTAP transfection complexes increases the delivery of DNA to cells in vitro in the presence of serum. Gene therapy, 1998. 5(1): p. 137.
35. Laouini, A., et al., Preparation, characterization and applications of liposomes: state of the art. Journal of colloid Science and Biotechnology, 2012. 1(2): p. 147-168.
36. Ansary, R.H., M.B. Awang, and M.M. Rahman, Biodegradable poly (D, L-lactic-co-glycolic acid)-based micro/nanoparticles for sustained release of protein drugs-A review. Tropical Journal of Pharmaceutical Research, 2014. 13(7): p. 1179-1190.
37. Nair, L.S. and C.T. Laurencin, Biodegradable polymers as biomaterials. Progress in polymer science, 2007. 32(8-9): p. 762-798.
38. Patel, B. and S. Chakraborty, Biodegradable polymers: emerging excipients for the pharmaceutical and medical device industries. Journal of Excipients and Food Chemicals, 2016. 4(4): p. 1010.
39. Mäder, K., RESOMER®—Biodegradeable Polymers for Sutures, Medical Devices, Drug Delivery Systems and Tissue Engineering. Polymers for Advanced Architectures, 2011: p. 62.
40. Koide, S., Chitin-chitosan: properties, benefits and risks. Nutrition research, 1998. 18(6): p. 1091-1101.
41. Sudarshan, N., D. Hoover, and D. Knorr, Antibacterial action of chitosan. Food Biotechnology, 1992. 6(3): p. 257-272.
42. Chandy, T. and C.P. Sharma, Chitosan-as a biomaterial. Biomaterials, artificial cells and artificial organs, 1990. 18(1): p. 1-24.
43. Nilsen-Nygaard, J., et al., Chitosan: gels and interfacial properties. Polymers, 2015. 7(3): p. 552-579.

44. Sahoo, S.K., et al., Residual polyvinyl alcohol associated with poly (D, L-lactide-co-glycolide) nanoparticles affects their physical properties and cellular uptake. Journal of controlled release, 2002. 82(1): p. 105-114.
45. DeMerlis, C. and D. Schoneker, Review of the oral toxicity of polyvinyl alcohol (PVA). Food and chemical Toxicology, 2003. 41(3): p. 319-326.
46. Mitra, S. and T.H. Foster, Photophysical Parameters, Photosensitizer Retention and Tissue Optical Properties Completely Account for the Higher Photodynamic Efficacy of meso-Tetra-Hydroxyphenyl-Chlorin vs Photofrin¶. Photochemistry and photobiology, 2005. 81(4): p. 849-859.
47. Senge, M.O., mTHPC–A drug on its way from second to third generation photosensitizer? Photodiagnosis and Photodynamic Therapy, 2012. 9(2): p. 170-179.
48. Zhou, J., et al., Novel lipid hybrid albumin nanoparticle greatly lowered toxicity of pirarubicin. Molecular pharmaceutics, 2013. 10(10): p. 3832-3841.
49. Nakamura, H., et al., Comparison between linear and star-like HPMA conjugated pirarubicin (THP) in pharmacokinetics and antitumor activity in tumor bearing mice. European Journal of Pharmaceutics and Biopharmaceutics, 2015. 90: p. 90-96.
50. Mahmoud, G., et al., Stabilized tetraether lipids based particles guided prophyrins photodynamic therapy. Drug delivery, 2018. 25(1): p. 1526-1536.
51. Schäfer, J., et al., Liposome–polyethylenimine complexes for enhanced DNA and siRNA delivery. Biomaterials, 2010. 31(26): p. 6892-6900.
52. Kumar, M.R., U. Bakowsky, and C. Lehr, Preparation and characterization of cationic PLGA nanospheres as DNA carriers. Biomaterials, 2004. 25(10): p. 1771-1777.
53. Duse, L., et al., Photodynamic Therapy of Ovarian Carcinoma Cells with Curcumin-Loaded Biodegradable Polymeric Nanoparticles. Pharmaceutics, 2019. 11(6): p. 282.
54. Schäfer, J., et al. A new drug vehicle-lipid coated biodegradable nanoparticles. in Advances in Science and Technology. 2008. Trans Tech Publ.
55. Baghdan, E., et al., Lipid coated chitosan-DNA nanoparticles for enhanced gene delivery. International journal of pharmaceutics, 2018. 535(1-2): p. 473-479.
56. Plenagl, N., et al., Hypericin Loaded Liposomes for Anti-Microbial Photodynamic Therapy of Gram-Positive Bacteria. physica status solidi (a), 2018. 215(15): p. 1700837.
57. Plenagl, N., et al., Photodynamic therapy–hypericin tetraether liposome conjugates and their antitumor and antiangiogenic activity. Drug delivery, 2019. 26(1): p. 23-33.

58. Duse, L., et al., Low level LED photodynamic therapy using curcumin loaded tetraether liposomes. European Journal of Pharmaceutics and Biopharmaceutics, 2018. 126: p. 233-241.
59. Sitterberg, J., et al., Utilising atomic force microscopy for the characterisation of nanoscale drug delivery systems. European Journal of Pharmaceutics and Biopharmaceutics, 2010. 74(1): p. 2-13.
60. Seitz, B.S., et al., Nanoparticles and liposomes for the surface modification of implants: a comparative study of spraying and dipping techniques. physica status solidi (a), 2018. 215(15): p. 1700847.
61. Agel, M.R., et al., Curcumin loaded nanoparticles as efficient photoactive formulations against gram-positive and gram-negative bacteria. Colloids and Surfaces B: Biointerfaces, 2019. 178: p. 460-468.
62. Janich, C., et al., Structures of malonic acid diamide/phospholipid composites and their lipoplexes. Soft matter, 2016. 12(27): p. 5854-5866.
63. Ali, M.Y., et al., Selective anti-ErbB3 aptamer modified sorafenib microparticles: In vitro and in vivo toxicity assessment. European Journal of Pharmaceutics and Biopharmaceutics, 2019. 145: p. 42-53.
64. N'Diaye, M., et al., Hybrid lipid polymer nanoparticles for combined chemo-and photodynamic therapy. Molecular pharmaceutics, 2019. 16(9): p. 4045-4058.
65. Duse, L., et al., Preparation and characterization of curcumin loaded chitosan nanoparticles for photodynamic therapy. physica status solidi (a), 2018. 215(15): p. 1700709.
66. Yow, C., et al., Cellular uptake, subcellular localization and photodamaging effect of temoporfin (mTHPC) in nasopharyngeal carcinoma cells: comparison with hematoporphyrin derivative. Cancer letters, 2000. 157(2): p. 123-131.
67. McNair, F.I., et al., A comet assay of DNA damage and repair in K562 cells after photodynamic therapy using haematoporphyrin derivative, methylene blue and meso-tetrahydroxyphenylchlorin. British journal of cancer, 1997. 75(12): p. 1721.
68. Yow, C., et al., Photocytotoxic and DNA damaging effect of temoporfin (mTHPC) and merocyanine 540 (MC540) on nasopharyngeal carcinoma cell. Toxicology letters, 2000. 115(1): p. 53-61.
69. Raschpichler, M., et al., In situ intravenous photodynamic therapy for the systemic eradication of blood stream infections. Photochemical & Photobiological Sciences, 2019. 18(2): p. 304-308.

70. Pinnapireddy, S.R., et al., Composite liposome-PEI/nucleic acid lipopolyplexes for safe and efficient gene delivery and gene knockdown. Colloids and Surfaces B: Biointerfaces, 2017. 158: p. 93-101.
71. Tariq, I., et al., Lipodendriplexes: A promising nanocarrier for enhanced gene delivery with minimal cytotoxicity. European Journal of Pharmaceutics and Biopharmaceutics, 2019. 135: p. 72-82.
72. Mahmoud, G., et al., Bipolar tetraether lipids derived from thermoacidophilic archaeon Sulfolobus acidocaldarius for membrane stabilization of chlorin e6 based liposomes for photodynamic therapy. European Journal of Pharmaceutics and Biopharmaceutics, 2015. 95: p. 88-98.
73. Özcetin, A., A. Aigner, and U. Bakowsky, A chorioallantoic membrane model for the determination of anti-angiogenic effects of imatinib. European Journal of Pharmaceutics and Biopharmaceutics, 2013. 85(3): p. 711-715.
74. Bonté, F. and R. Juliano, Interactions of liposomes with serum proteins. Chemistry and physics of lipids, 1986. 40(2-4): p. 359-372.
75. Oecd, OECD Guidelines for the Testing of Chemicals. 1994: Organization for Economic.
76. Saleem, U., et al., Is folklore use of Euphorbia helioscopia devoid of toxic effects? Drug and chemical toxicology, 2016. 39(2): p. 233-237.
77. Sohail, M.F., et al., Cell to rodent: toxicological profiling of folate grafted thiomer enveloped nanoliposomes. Toxicology research, 2017. 6(6): p. 814-821.
78. Vandebriel, R.J., et al., Immunotoxicity of silver nanoparticles in an intravenous 28-day repeated-dose toxicity study in rats. Particle and fibre toxicology, 2014. 11(1): p. 21.
79. Sohail, M.F., et al., Polymeric nanocapsules embedded with ultra-small silver nanoclusters for synergistic pharmacology and improved oral delivery of Docetaxel. Scientific reports, 2018. 8(1): p. 13304.
80. Gautam, M. and R. Goel, Toxicological study of Ocimum sanctum Linn leaves: hematological, biochemical, and histopathological studies. Journal of toxicology, 2014. 2014.
81. Rotstein, R., et al., The erythrocyte adhesiveness/aggregation test (EAAT): A new biomarker to reveal the presence of low grade subclinical smoldering inflammation in individuals with atherosclerotic risk factors. Atherosclerosis, 2002. 165(2): p. 343-351.
82. Hoebeke, M., et al., Fluorescence, absorption and electron spin resonance study of bacteriochlorin a incorporation into membrane models. Biochimica et Biophysica Acta (BBA)-Biomembranes, 1999. 1420(1-2): p. 73-85.

83. De Vetta, M., L. González, and J.J. Nogueira, Hydrogen Bonding Regulates the Rigidity of Liposome-Encapsulated Chlorin Photosensitizers. ChemistryOpen, 2018. 7(6): p. 475-483.
84. Dragicevic-Curic, N., et al., Assessment of fluidity of different invasomes by electron spin resonance and differential scanning calorimetry. International journal of pharmaceutics, 2011. 412(1-2): p. 85-94.
85. Li, Y. and L. Yang, Driving forces for drug loading in drug carriers. Journal of microencapsulation, 2015. 32(3): p. 255-272.
86. Ruozi, B., et al., AFM, ESEM, TEM, and CLSM in liposomal characterization: a comparative study. International journal of nanomedicine, 2011. 6: p. 557.
87. Almgren, M., K. Edwards, and G. Karlsson, Cryo transmission electron microscopy of liposomes and related structures. Colloids and Surfaces A: Physicochemical and Engineering Aspects, 2000. 174(1-2): p. 3-21.
88. Kuntsche, J., J.C. Horst, and H. Bunjes, Cryogenic transmission electron microscopy (cryo-TEM) for studying the morphology of colloidal drug delivery systems. International journal of pharmaceutics, 2011. 417(1-2): p. 120-137.
89. Reidy, K., et al., mTHPC-mediated photodynamic therapy is effective in the metastatic human 143B osteosarcoma cells. Photochemistry and photobiology, 2012. 88(3): p. 721-727.
90. Kiesslich, T., et al., Comparative characterization of the efficiency and cellular pharmacokinetics of Foscan®-and Foslip®-based photodynamic treatment in human biliary tract cancer cell lines. Photochemical & Photobiological Sciences, 2007. 6(6): p. 619-627.
91. Maytin, E.V., et al., Blue light versus red light for photodynamic therapy of basal cell carcinoma in patients with Gorlin syndrome: a bilaterally controlled comparison study. Photodiagnosis and photodynamic therapy, 2018. 22: p. 7-13.
92. Blanco, E., H. Shen, and M. Ferrari, Principles of nanoparticle design for overcoming biological barriers to drug delivery. Nature biotechnology, 2015. 33(9): p. 941.
93. Fairbairn, D.W., P.L. Olive, and K.L. O'Neill, The comet assay: a comprehensive review. Mutation Research/Reviews in Genetic Toxicology, 1995. 339(1): p. 37-59.
94. Penning, L.C., et al., Relationship between photodynamically induced damage to various cellular parameters and loss of clonogenicity in different cell types with hematoporphyrin derivative as sensitizer. Biochimica et Biophysica Acta (BBA)-Molecular Cell Research, 1994. 1221(3): p. 250-258.

95. Pinnapireddy, S., et al., Photo-enhanced delivery of genetic material using curcumin loaded composite nanocarriers. Clin. Oncol, 2017. 2(1323): p. 2019.
96. Mahmoud, G., et al., Photo-responsive tetraether lipids based vesicles for prophyrin mediated vascular targeting and direct phototherapy. Colloids and Surfaces B: Biointerfaces, 2017. 159: p. 720-728.
97. Schaefer, J., et al., Atomic force microscopy and analytical ultracentrifugation for probing nanomaterial protein interactions. ACS nano, 2012. 6(6): p. 4603-4614.
98. Sengel-Turk, C.T. and C. Hascicek, Design of lipid-polymer hybrid nanoparticles for therapy of BPH: Part I. Formulation optimization using a design of experiment approach. Journal of Drug Delivery Science and Technology, 2017. 39: p. 16-27.
99. Zhang, L. and L. Zhang, Lipid–polymer hybrid nanoparticles: synthesis, characterization and applications. Nano Life, 2010. 1(01n02): p. 163-173.
100. Kumari, A., S.K. Yadav, and S.C. Yadav, Biodegradable polymeric nanoparticles based drug delivery systems. Colloids and surfaces B: biointerfaces, 2010. 75(1): p. 1-18.
101. Magenheim, B., M. Levy, and S. Benita, A new in vitro technique for the evaluation of drug release profile from colloidal carriers-ultrafiltration technique at low pressure. International journal of pharmaceutics, 1993. 94(1-3): p. 115-123.
102. Dinarvand, R., et al., Preparation of biodegradable microspheres and matrix devices containing naltrexone. AAPS PharmSciTech, 2003. 4(3): p. 45-54.
103. Win, K.Y. and S.-S. Feng, Effects of particle size and surface coating on cellular uptake of polymeric nanoparticles for oral delivery of anticancer drugs. Biomaterials, 2005. 26(15): p. 2713-2722.
104. McLennan, H.R. and M. Degli Esposti, The contribution of mitochondrial respiratory complexes to the production of reactive oxygen species. Journal of bioenergetics and biomembranes, 2000. 32(2): p. 153-162.
105. Dobrovolskaia, M.A. and S.E. McNeil, Handbook of immunological properties of engineered nanomaterials. Vol. 1. 2013: World Scientific.
106. Lenahan, J.G., S. Frye, and G.E. Phillips, Use of the activated partial thromboplastin time in the control of heparin administration. Clinical chemistry, 1966. 12(5): p. 263-268.
107. Wintrobe, M.M., Wintrobe's clinical hematology. Vol. 1. 2008: Lippincott Williams & Wilkins.
108. Akhtar, M.F., et al., Textile industrial effluent induces mutagenicity and oxidative DNA damage and exploits oxidative stress biomarkers in rats. Environmental toxicology and pharmacology, 2016. 41: p. 180-186.

109. Rejman, J., A. Bragonzi, and M. Conese, Role of clathrin-and caveolae-mediated endocytosis in gene transfer mediated by lipo-and polyplexes. Molecular Therapy, 2005. 12(3): p. 468-474.
110. Darzynkiewicz, Z., et al., Cytometry in cell necrobiology: analysis of apoptosis and accidental cell death (necrosis). Cytometry: The Journal of the International Society for Analytical Cytology, 1997. 27(1): p. 1-20.
111. Allen, R.T., W.J. Hunter III, and D.K. Agrawal, Morphological and biochemical characterization and analysis of apoptosis. Journal of pharmacological and toxicological methods, 1997. 37(4): p. 215-228.
112. Simon, H.-U., A. Haj-Yehia, and F. Levi-Schaffer, Role of reactive oxygen species (ROS) in apoptosis induction. Apoptosis, 2000. 5(5): p. 415-418.
113. Liu, S.-Y., et al., Molecular mechanism of cell apoptosis by paclitaxel and pirarubicin in a human osteosarcoma cell line. Chemotherapy, 2010. 56(2): p. 101-107.
114. Nafee, N., et al., Relevance of the colloidal stability of chitosan/PLGA nanoparticles on their cytotoxicity profile. International journal of pharmaceutics, 2009. 381(2): p. 130-139.
115. Wolfram, J., et al., Shrinkage of pegylated and non-pegylated liposomes in serum. Colloids and Surfaces B: Biointerfaces, 2014. 114: p. 294-300.
116. Hasan, W., et al., Delivery of multiple siRNAs using lipid-coated PLGA nanoparticles for treatment of prostate cancer. Nano letters, 2011. 12(1): p. 287-292.
117. Kawano, K., et al., Preparation and pharmacokinetics of pirarubicin loaded dehydration–rehydration vesicles. International journal of pharmaceutics, 2003. 252(1-2): p. 73-79.
118. Sellers, R.S., et al., Society of Toxicologic Pathology position paper: organ weight recommendations for toxicology studies. Toxicologic pathology, 2007. 35(5): p. 751-755.
119. Javed, I., et al., Lecithin-gold hybrid nanocarriers as efficient and pH selective vehicles for oral delivery of diacerein—in-vitro and in-vivo study. Colloids and Surfaces B: Biointerfaces, 2016. 141: p. 1-9.
120. Shi, H.B., et al., Compound pollen protein nutrient increases serum albumin in cirrhotic rats. Gastroenterology research, 2010. 3(6): p. 253.
121. Adeyemi, O.S. and I. Adewumi, Biochemical evaluation of silver nanoparticles in wistar rats. International scholarly research notices, 2014. 2014.
122. Sharshun, Y., et al., Inflammation at a glance: erythrocyte adhesiveness/aggregation test to reveal the presence of inflammation in people with atherothrombosis. Heart disease (Hagerstown, Md.), 2003. 5(3): p. 182-183.

123. Yi, X., et al., Co-delivery of pirarubicin and paclitaxel by human serum albumin nanoparticles to enhance antitumor effect and reduce systemic toxicity in breast cancers. Molecular pharmaceutics, 2015. 12(11): p. 4085-4098.
124. Inomata, K., et al., A Pre-Clinical Large Animal Model of Sustained Liver Injury and Regeneration Stimulus. Scientific reports, 2018. 8(1): p. 14987.